# THE ROLE OF ADHESION STRENGTH IN HUMAN MESENCHYMAL STEM CELL OSTEOBLASTIC DIFFERENTIATION ON BIODEGRADABLE POLYMERS

by

Sylva Jana Krizan

A dissertation submitted in partial fulfillment
of the requirements for the degree of
Doctor of Philosophy
(Biomedical Engineering)
in The University of Michigan
2009

Doctoral Committee:

Professor David H. Kohn, Co-chair
Assistant Professor Kurt D. Hankenson, Co-chair, University of Pennsylvania
Professor Paul H. Krebsbach
Professor Peter X. Ma
Associate Professor Yvonne L. Kapila

To Ivan, for your understanding, your faith, your strength

**ACKOWLEDGEMENTS**

The road to this place has been long and full of surprises; two labs, two homes and a multitude of people who have supported me and my work in both locations.

It all started at the Orthopaedic Research Labs at the University of Michigan with a wonderful group of colleagues and friends. Special thanks to Connie Pagedas Soves and Jessica Knowlton for their technical expertise, tireless enthusiasm and friendship. Thanks as well to Jeff Meganck, Michael Pashcke, Ramon Ruberte, Danese Joiner and Erik Waldorff for making the lab environment such a good one.

The move to the University of Pennsylvania created an opportunity to interact with some excellent investigators and trainees. In particular, I'd like to thank David Boettiger for his support and insight, May Chan for her assistance with the work done in his lab, Lingli Zhang for invaluable help with confocal imaging, as well as Chris Chen for his generosity. I'd also like to acknowledge Dee Breger at Drexel University for training and assistance in using the Environmental SEM. I had the opportunity to mentor an exceptional Master's student, Jacqueline Wilhelmy, who directly contributed to the work in the Rho studies for which I am extremely thankful. Finally, I'd like to thank those members of the Hankenson lab, past and present who have made the ride worthwhile; Michael Friedman and Hailu Shitaye for their steadfast advice and quick wit and Bryan Marguiles who has helped to bring sober wisdom to this sometimes disorienting

process. A special thanks also goes out to Shawn Terkhorn for providing me with enough fuel for the journey by way of Tim Horton's coffee.

The complexity of dealing with two campuses was made easier with the support and advice of my committee, for which I am grateful. I would specifically like to thank Kurt Hankenson, my advisor, for his willingness (and patience!) in letting an engineer take up residence in his molecular biology lab for six years with only the rarest of complaints. I truly appreciate the opportunities and experiences I've had as a result.

I am grateful for the direct support of my research as made possible by several funding sources, including the Biomedical Engineering Department at the University of Michigan, the National Institutes of Health, and the National Science and Engineering Research Council of Canada.

I would also like to acknowledge my parents, Jan and Jana Krizan and brothers Jan and David Krizan for their encouragement when I needed it the most. Finally, I would like to thank my husband, Ivan Nagy, for supporting me unconditionally throughout every stage of my emotional and intellectual journey in graduate school, and for retaining a sense optimism and belief in myself and in us, despite the difficulties or the distance.

## TABLE OF CONTENTS

## LIST OF FIGURES

**Figure**

## LIST OF TABLES

## LIST OF ABBREVIATIONS

| | |
|---|---|
| hMSC | Human Mesenchymal Stem Cell |
| BDP | Biodegradable Polymers |
| FBS | Fetal Bovine Serum |
| ECM | Extracellular Matrix |
| GDL | D-(+)-Gluconic acid δ-lactone |
| PCL | Polycaprolactone |
| PLGA | Poly-lactide-co-glycolide |
| ePLGA | Ester-capped PLGA |
| a/mPLGA | PLGA with acid end groups |
| TCP | Tissue Culture Polystyrene |
| $\tau_{50}$ | 50% detachment force (adhesion strength) |
| BGP | β-Glycerol Phosphate |
| Dex | Dexamethasone |
| Ctrl | Control growth media, 2% FBS + doxycycline |
| OST | Osteogenic media, Control media + Ascorbic Acid + BGP + ITS + Dex |
| RGD | Arginine-Glycine-Aspartic Acid |
| FAK | Focal Adhesion Kinase |
| RhoV14 | Constitutively active Rho GTPase construct |
| RhoN19 | Dominant negative Rho GTPase construct |
| Y397 | Autophosphorylation Site of FAK, construct contains tyrosine to phenylalanine substitution |

| | |
|---|---|
| FRNK | Non-catalytic C-terminal domain of FAK |
| DTER | Truncation FAK mutant construct |
| Y27632 | Rho kinase (ROCK) Inhibitor |

ABSTRACT

THE ROLE OF ADHESION STRENGTH IN HUMAN MESENCHYMAL STEM CELL OSTEOBLASTIC DIFFERENTIATION ON BIODEGRADABLE POLYMERS

by

Sylva Jana Krizan

Co-chairs: David H. Kohn and Kurt D. Hankenson

Human mesenchymal stem cells (hMSC) are promising candidates for promoting bone growth on biodegradable polymer scaffolds however little is known about early hMSC-polymer interactions. Adhesion is highly dynamic and during adhesive reinforcement, numerous proteins form adhesion plaques linking the cell's cytoskeleton with the extracellular environment. These proteins are known to affect cellular function but their role in hMSC differentiation is less clear. Adhesion plaques are associated with adhesive force, still a detachment force of hMSC on polycaprolactone (PCL), poly-lactide-co-glycolide (PLGA) or alginate has never been described or shown to affect downstream function.

We demonstrate that hMSC attached to PCL, PLGA and alginate exhibit different adhesion strengths ($\tau_{50}$) as determined by both fluid shear and spinning disk systems, with PLGA demonstrating the greatest $\tau_{50}$. Elastic modulus and hydrophobicity were characterized for these surfaces and correlated positively with $\tau_{50}$ to an optimum. Attachment studies of hMSC showed that adhesion plateau timespans were

independent of cell line and surface but both morphology and focal adhesion expression varied by polymer type. Differentiation studies of hMSC on PLGA and PCL showed a strong association between markers of differentiation (alkaline phosphatase activity and mineral content) and $\tau_{50}$ within polymer groups, but a poor relationship was found between $\tau_{50}$ and differentiation across polymer groups, suggesting that other polymer properties may be important for differentiation.

Subsequently, we examined the role of focal adhesion kinase (FAK) and Rho-GTPase (RhoA) on hMSC adhesion and differentiation when plated onto PLGA. hMSC were retrovirally transduced with mutant constructs of FAK and RhoA cDNA. Alternatively, hMSC were treated with Rho-kinase inhibitor, Y27632. Both cells transduced with mutant RhoA or FAK constructs, or those treated with Y27632 displayed aberrant cell morphology and changes in focal adhesion number. Differentiation studies demonstrated that both constitutively active RhoA and mutants of FAK increase osteoblastic activity, while both dominant negative RhoA cells and hMSC treated with Y27632 exhibited a decrease in osteoblastic markers. Manipulating FAK or RhoA in hMSC resulted in greater modulations in osteogenesis on PLGA previously demonstrating maximal $\tau_{50}$. This suggests that hMSC differentiation on polymers exhibiting high adhesion strength depends on FAK and RhoA signaling.

# CHAPTER I

## THE NEED FOR A SYSTEMATIC UNDERSTANDING OF ADHESION IN BONE TISSUE ENGINEERING

### The need for tissue-engineered bone grafts

The field of orthopedic reconstruction and trauma devices has experienced significant financial and scientific growth in the past several years; the market was estimated at $5.4 billion in 2002 and is expected to grow to $14.2 billion by 2012 [1]. In association with this trend, there has been an intensification of research in the area of biodegradable polymers for critical gap repair and bone regeneration. Potential advantages of biodegradable implants include avoidance of donor site morbidity and insufficient material associated with bone autografts. Polymers have been actively pursued for this application as they are easily fabricated and customized for specific chemistry, degradation profile, wettability, surface charge, porosity, and mechanical properties. In addition, modifications such as plasma discharge, incorporation of hydroxyapatite mineral, adhesion peptides, and cytokines or drugs for delayed delivery lead to potentially limitless combinations of polymer properties.

Preliminary studies analyzing bone regeneration capacity of these polymers generally involve growing osteoblasts or multipotent mesenchymal stem cells (MSC) on 2D films or 3D scaffolds in vitro. Quantitative analyses of viability, attachment level, proliferation and terminal osteoblast differentiation are not consistently carried out in these studies.

In addition, many biomaterial-inherent factors contribute to a cell's acceptance of a substrate for growth and/or differentiation, and such analyses may further lead to varied results depending on cell maturity, stage of differentiation and species of origin. Some of these material-inherent factors include surface topography, substrate rigidity, roughness, charge density or surface energy.

Biodegradable polymers (BDP) for bone tissue engineering (TE)

Many hydrolytically unstable polymers have been suggested for use as degradable biomaterials, however few have been approved by the FDA for use in human clinical studies. Among those that are FDA-approved are PLGA poly(lactide-co-glycolide), PCL (poly-ε-caprolactone) and alginate.

PLGA is a co-polymer consisting of the rapidly degrading glycolic acid (PGA) and the slower degrading and more hydrophobic lactic acid (PLA). The ester bonds in the polymers are hydrolytically labile and degrade by non-enzymatic hydrolysis creating byproducts eliminated from the body in the form of carbon dioxide and water [2]. By controlling the relative amounts of either polymer, degradation characteristics can be tightly controlled, however, the relationship between lactic acid content and degradation rate of PLGA is not linear. PGA is a straight-chain aliphatic polyester which is highly crystalline and has a high melting point and low solubility in organic solvents. The hydrophobicity of PLA leads to a reduced rate of backbone hydrolysis relative to PGA. PLA contains the chiral lactic acid and exists in two stereoisomeric forms, however $_{L}$-PLA is generally used since hydrolysis yields $_{L}$-Lactic acid, which is the physiological stereoisomer of lactic acid. The crystallinity of PGA is rapidly lost in the PLGA copolymer, and both crystallinity and hydrophobicity affect the degradation rate of the PLGA. However, in the mid-range of LA/GA composition (50/50), the copolymer is

amorphous and crystallinity does not play a role [3]. Both PGA and PLGA have been used to create resorbable sutures and bone pins [4] as well as drug delivery devices such as Lupron Depot™ for treatment of prostate cancer [5].

PCL is a semi-crystalline aliphatic polyester, with high solubility, low melting point and is well-suited in forming blends. It degrades at a slower pace than PLA and can be used in devices that remain active for over a year and is generally considered non-toxic. Typically, the first stage of degradation involves non-enzymatic hydrolytic cleavage of ester groups, and the second stage involves intracellular digestion once the molecular weight is reduced, but degradation can also occur by enzymatic mechanisms or microorganisms [6, 7]. PCL has been approved for use in absorbable sutures [8], has been used in extended contraceptive delivery (Capronor III) [4] and recently has been shown to support mandibular bone regeneration [9].

Alginate is a natural biodegradable polysaccharide which is extracted from seaweed as alginic acid. It is an anionic copolymer hydrogel composed of β-D–mannuronate and α-L–guluronate. The physical and mechanical properties of alginate gel are strongly correlated with gelation rate [10] as well as the proportion and length of the polyguluronate block in the alginate chains [11]. Degradation of alginate differs in mechanism from PLGA or PCL. When in the presence of physiological fluids, cations cross-linking the polymer chains become replaced, disrupting the cross-linked structure. In order to create a decrease in molecular weight, an enzyme (such as alginase) must be used. Alginate is approved by the FDA for human use as a wound dressing, such as in Algicell™ or Silvercel™ [12], for biodegradable urethral stents, encapsulating cells [13] and sustained drug delivery [14].

These biodegradable polymers represent those most commonly used for bone tissue engineering, and all three have successfully promoted bone regeneration in animal models. Despite the fact that they demonstrate different cell attachment rates in vitro [15-17], few studies have directly compared degree of differentiation on these scaffolds, or the role of adhesion in this process.

Mesenchymal Stem Cells (MSC) and biodegradable polymers

Recently, MSC have been studied for use in bone regeneration as they are easily isolated, purified, and cultured from bone marrow aspirates. Further, MSC are able to differentiate into a variety of cell types, including osteoblasts and adipocytes. Use of cell-scaffold implants for bone regeneration has resulted in varying levels of success. To improve outcomes with MSC-based therapy, it is important to understand how an MSC interacts with its carrier substrate, in order to promote osteogenesis, and ultimately bone formation. A thorough investigation of the role of MSC adhesion to common biodegradable polymers on differentiation has not yet been attempted, as it is difficult to make substrate properties comparable, and studies are often more focused on finding a scaffold that works to promote osteogenesis in vitro, or bone formation in vivo, rather than performing rigorous comparisons. Instead, adhesion has been studied as being directly related to a controlled material property. To study effects of physical properties on adhesion, osteoblasts have been grown on metal alloys or ceramics [18-20], while polymers have been used to investigate surface chemistry or wettability effects [21], and more recently, mechanical properties [153]. Additionally, establishing a role for adhesion to BDP on differentiation based on the literature is difficult due to inconsistencies between studies, as cells of different commitment stages (MSC vs. pre-osteoblast vs. osteoblast) and species of origin (namely murine and human) are used.

This makes it difficult to compare these studies as different cells may adhere to the same polymer in a remarkably dissimilar fashion [17].

The need for a more mechanistic approach in assessing bone TE constructs

When presented with a substrate, a cell may regulate its expression of adhesion molecules, such as integrins, based on the various physical and chemical surface properties of the polymer. There has been a growing interest in the use of integrin binding sites to modify a variety of substrate surfaces to improve cell adhesion, and presumably osteogenesis. Consequently, there have been a multitude of investigations examining short peptide (often RGD (arginine-glycine-aspartic acid)) or extracellular matrix peptide (such as osteopontin, fibronectin or collagen) modification of biomaterials for bone tissue engineering [22-34]. However, although RGD is a common integrin ligand in ECM proteins, the effects of modification have not always been predictable [35], which may be due in part to peptide conformation and the need for synergy sites to make the peptide functional [27]. Additionally, the effects of these peptides may not translate directly to cells of differential commitment as it was recently found that while both linear and cyclic RGD peptides promote ostoegenesis in osteoblasts, hMSC only underwent osteogenesis on cyclic RGD [36]. This idea is further confirmed as subsequent studies showed that spatial organization of RGD peptides and substrate stiffness had a greater impact on osteoblast differentiation and stem cells were less sensitive to these cues [37]. Although these modifications do tend to alter some aspect of attachment or adhesion, greater understanding is needed in correlating how these modifications affect differentiation, and in whether those effects translate into an in vivo environment.

Adhesion and bone extracellular matrix (ECM)

There are four major steps that precede proliferation of cells on biomaterials: (1) protein adsorption, (2) cell-substrate contact, (3) attachment and (4) adhesion/spreading [38-40]. A classic description of this process is summarized in Figure 1.1 [38]. Protein adsorption is a complex process that occurs rapidly, on the order of seconds, and is affected by many factors such as charge density, as proteins tend to be negatively charged [41-43]. In the second stage, cells will come into contact with the surface as dictated by physicochemical forces such as van der Wals (attractive) and electrostatic (repulsive) interactions. As the cells pass through the secondary energy minimum (where these attractive and repulsive forces balance), cells begin to make physical contact with the surface. Current models suggest that for some cells, an early stage of attachment primarily involves the formation of a 1μm-thick gel-like hyaluronan coat keeping the cell at a distance of a few microns from the surface [44]. This has been shown to be true for MC3T3E1 osteoblasts [45], and further, manipulation of this glycocalyx can affect stem cell function [46]. Specific adhesion interactions described below then bring the cell to within approximately 15-50nm of the surface, the primary energy minimum. The probability of integrins participating in initial cell-substrate interactions is extremely low [44], and rather integrins take part in the adhesion phase. The adhesion phase occurs over a longer time frame and involves more specific adhesive interactions with extracellular matrix proteins, the cell membrane and cytoskeletal proteins [39]. Attached cells then typically take hours to slowly spread over the surface, and begin to produce their own matrix. It is in this stage that adhesion proteins are produced by cells leading to the production of focal complexes or adhesions. The steady-state adhesion plateau can be approximated by the classic thermodynamic DLVO theory of colloid stability of attractive forces and repulsive barriers, as well as the Dupre equation whereby the work of adhesion is the sum of

interfacial tensions between the substrate, cell and liquid; $W_{SC}=\gamma_{(cl)}+\gamma_{(sl)}-\gamma_{(sc)}$ [38] although recent evidence suggests that a better model for bond formation is that of specific receptor-ligand bonds [47]. Additionally, the time to reach the steady-state plateau can be approximated by $t_{max}$ (Figure 1.1).

Integrins are the predominant cell-surface receptors mediating adhesion to the extracellular matrix. Integrins are heterodimeric proteins composed of an alpha and beta subunit and they combine in more than 20 different transmembrane glycoprotein receptors. Following integrin-ligand binding, transduced signals regulate cytoskeletal organization, activate kinase signaling cascades and modulate cell cycle and gene expression. It has been suggested that integrins regulate cell adhesion through conformational activation in order to increase ligand affinity, and lateral clustering to increase avidity [48]. Signaling may also occur from the inside-out, as from the cytoskeletal protein talin to the cytoplasmic domain of the integrin, and by the less-studied proteins, kindlins which also interact at integrin cytoplasmic sites, acting as essential regulators of integrin activation and cytoskeletal reorganization [49].

The main adhesive ligands for integrins are the matrix proteins collagen, laminin and fibronectin, as well as adhesive plasma proteins such as vitronectin and thrombospondin. The extracellular matrix of bone is composed of 90% collagen and 10% non-collagenous proteins [39]. These proteins are synthesized by osteoblasts and most are involved in adhesion. In vitro, human osteoblasts adhere preferentially to fibronectin, a major component of blood serum as compared with type I and IV collagens and vitronectin, but adhere weakly to laminin and type V collagen [50]. hMSC adhesion to type I collagen, fibronectin, vitronectin and laminin also appear to be important for function [51, 52] with the greatest cell-binding affinity occurring for

fibronectin [53]. Additionally, heparin improves viability and spreading of hMSC in culture [54] which has been shown to affect MSC differentiation in other systems [55].

Integrin-mediated cell-substrate contact sites are heterogeneous and appear in the forms of focal complexes, focal adhesions and fibrillar adhesions. Focal adhesions represent the strongest cell-substrate contact, with the shortest gap distance. The sequential formation of cytoskeleton-associated focal complexes and later focal and fibrillar adhesions, is a hierarchical process involving the clustering of integrins and recruitment of specific proteins to the adhesion site [44, 56]. Vinculin, for example is involved in late focal complex and focal adhesion formation [44] and maintains a dynamic equilibrium between its focal-adhesion and cytoplasmic levels [57] while paxillin is involved in early focal complex formation and is found in the ventral half of focal adhesions [58]. The components of focal complexes and adhesions (such as vinculin, talin, integrins, cytoskeletal proteins, phosphatases and signaling molecules) may interact to induce signal transduction (through tyrosine and serine-threonine kinases, Rho family GTPases, and ion channels), promoting action of transcription factors thereby regulating gene expression and downstream cellular processes. Focal and fibrillar adhesions are distinct in the primary type of integrins they contain ($\alpha v\beta 3$ and $\alpha 5\beta 1$ integrins, respectively) as well as other adhesion proteins. Additionally, the morphology and function of adhesive complexes varies substantially as focal complexes are smaller and found in migrating and spreading cells, focal adhesions are larger enabling robust adhesion at the termini of actin filaments, while fibrillar adhesions are important for matrix remodeling, aligning alongside the actin filaments [44]. Further, paxillin tyrosine phosphorylation appears to regulate the transition between these adhesive structures [59]. While it is easier to categorize adhesion complexes in this

way, in reality, the larger picture is much more intricate as it was found that compiling all recent evidence, there are 90 direct and 66 peripheral components important for these structures, leading to 690 interactions [60].

Focal adhesion signaling

Focal adhesion kinase (FAK) is a key signaling component found in focal adhesions and its activation has been implicated in many cellular processes [61]. The N-terminal domain of FAK directs interactions with integrins and growth factor receptors, while the central catalytic domain contains Tyr397, which is an autophosphorylation site [62]. The non-catalytic C-terminal domain, (FAK-related non-kinase or FRNK), contains sites for protein-protein interactions and a focal adhesion targeting (FAT) region which binds paxillin [63]. FRNK and FAT are dominant-negatives of FAK, inhibiting cell spreading and migration as well as growth factor-mediated signals to mitogen-activated protein kinase [64, 65]. Y397F, a mutant of FAK, which contains a phenylalanine substitution for tyrosine at the autophosphorylation site, disrupts focal adhesion turnover [66], number and traction force [67]. DTER is an 18kDa carboxy-terminus truncation mutant of FAK which lacks a kinase domain and the ability to bind paxillin [68].

Focal adhesion formation is promoted by plating cells on fibronectin (via the central binding domain [69]) or vitronectin with serum. Growth factors also stimulate focal adhesion and stress fiber formation in a Rho-dependent manner [70]. In addition, the formation of focal adhesions is activated by local mechanical forces (either internal contractile forces or external perturbations), which are dependent on active RhoA and its downstream targets Rho kinase (ROCK) and mDia, as well as engagement of integrin receptors [71]. Rho kinase activates myosin-II driven cell contractility [72] and mDia is involved in regulation of actin and tubulin dynamics. While the actin

cytoskeleton is important in maintaining cell shape, when present in bundles associated with focal adhesions, it causes the formation of stress fibers which may transmit forces to the substrate through the adhesion sites [73]. Overall, focal adhesion formation depends upon both functionally active Rho family members and matrix proteins (including RGD sites) and neither is sufficient for focal adhesion formation alone [74]. Additionally, it has recently been found that the force transmitted in focal adhesions is dependent upon vinculin binding to both F-actin and integrins, which is modulated specifically at the vinculin-integrin interface [75]. In turn, these forces can lead to fibronectin fibrillogenesis by causing unfolding of fibronectin protein at RGD-binding sites, leading to cell detachment and fibronectin polymerization, which is an important part of extracellular matrix development and repair [76].

<u>α5β1 and αvβ3 integrins in osteogenesis</u>

α5 and β1 integrins have been found to be expressed in high quantities in primary hMSC [77] and in all cell types in human bone [78, 79]. α5β1 is important for, and colocalizes with fibronectin matrix assembly [77]. The β1 integrin is likely important for cells of the osteoblast lineage as it binds major bone ECM proteins such as type I collagen (α1β1, α2β1) and fibronectin (α3β1, α5β1 and α8β1) [80]. In cultured calvarial osteoblasts, interfering with β1 integrin-binding to collagen and fibronectin impairs differentiation [81]. In a transgenic mouse dominant-negative for β1 integrin, driven by the osteocalcin promoter, it was found that bone mass and bone formation were reduced [82]. Further, most marrow-derived MSC from transgenic β1 mice plated in vitro detached and did not display any alkaline phosphatase activity [83].
αv integrin is also abundantly expressed by cells of the osteoblast lineage in vitro [80], and in human bone [78], and αvβ3 is expressed by most hMSC [79]. αv is

codistributed with the terminal ends of actin and binds with vitronectin in vitro [77] through arginine-glycine-aspartic acid (RGD) [84]. Conflicting results have been reported for the role of αvβ3 integrin in osteoblast differentiation. In primary human osteoblasts, blocking αv integrin lead to decreased osteogenic marker protein levels and abrogated mineralization when cells were treated with BMP2 [85]. Conversely, MC3T3E1 cells overexpressing human αv and β3 integrin subunits showed inhibited mineralization and decreased expression of most bone marker proteins, while levels of FAK and vinculin activity were unaltered and β1 integrin levels decreased [86]. These inconsistencies may result from species-specific regulation of differentiation by αvβ3, differences in differentiation with or without BMP2, or biphasic effects of levels of αvβ3 expressed on the cell membrane. Also, the ratio of αvβ3 to β1 may be important for differentiation, however this was not reported in the former study. Most importantly, in the former study, the authors could not conclude as to which of the five αv integrins expressed by osteoblasts contributed the greatest effect.

Adhesion strength

While the understanding of biochemical aspects of integrin-mediated adhesion has dramatically increased over the past decade, the mechanical aspects of adhesion remain poorly understood [87, 88]. It is generally accepted that receptor recruitment, clustering, cytoskeletal interactions and focal adhesion assembly lead to increases in adhesion strength over time, but the relative contributions of each of these, as well as the role of specific structural and regulatory molecules is not well-understood.

Despite some advances, there is still a substantial gap in knowledge in this field, which is partially due to the limitations of common adhesion assays to provide reproducibility

and high detachment forces, as well as the difficulty of tracking the molecular, spatial and temporal complexities of adhesion. There are three categories of cellular detachment strength assays currently used; (1) micromanipulation, (2) centrifugation and (3) hydrodynamic force. In addition, traction forces of cells on substrates have been calculated using both elastic substrates, and more recently, combining these substrates with the principles of microfluidics [89]. Micromanipulation involves measuring normal or tangential detachment forces with a micropipette, microprobe, AFM cantilever, laser (optical) tweezers, or more recently, by laser spallation [90]. Real-time force displacements are measured in the pico-nanonewton range. Centrifugation assays involve applying a controlled detachment force via speed perpendicular to the adhesion area, however, only relatively low detachment forces are possible. Hydrodynamic flow systems may apply a wide range of detachment forces to a large cell population and provide the most reliable measurement of adhesion strength and likely the best means of quantifying relative numbers of adhesive bonds [91]. Adhesion strength is generally reported as shear stress at the flow chamber wall to produce a level of cell detachment (i.e. at 50% detachment, $\tau_{50}$ is reported). However, net force applied to the cell will be slightly different from shear stress due to applied hydrodynamic drag and torque, which are highly sensitive to cell-shape, size and adhesion contact points [92].

Two common devices that use hydrodynamic flow are parallel plate flow chambers and the spinning disk.

In the parallel plate flow chamber, fluid shear is delivered as static, cyclic or pulsatile flow via a programmable syringe pump [93]. Laminar flow between two parallel plates generates fluid shear on that surface due to friction at the fluid-plate interface.

Governing this principle is the equation: $\tau = 6\mu Q/bh$ where $\mu$ = media viscosity, Q = flow rate, b = channel width and h = channel height. Entrance length, which occurs before flow is purely laminar can be estimated as $EL=0.6Re_{max}h$ (where $Re_{max}= \rho Qh/\mu$ and $\rho$=density). Flow is generated by a programmable syringe pump and is controlled by an actuator which is an integrated servo motor and linear actuator controlled by the interface software package to control motor position and velocity to create precise flow waveforms.

The spinning disk device is a fluid-filled chamber containing a circular holder for the sample disk. By using electrochemical measurements with a ferric/ferricyanide redox reaction on a Pt electrode on the spinning disk, flow and mass transport generated can be approximated by those for a disk spinning in an infinite fluid [94]. Then for a given configuration, concentration and velocity boundary layers are independent of radial position at a given rotational speed, thereby rendering diffusion uniform over the surface of the disk with constant surface chemistry. Surface shear stress ($\tau$) linearly varies with radial position as dictated by the equation: $\tau = 0.800r\sqrt{\rho\mu\varpi^3}$, where r is the radial position relative to the disk center, $\rho$ is fluid density, $\mu$ is viscosity, and $\varpi$ is the angular disk speed. By running spin experiments at a constant speed (rpm) and time, cell detachment profiles may be quantified and compared.

Adhesion strength increases following initial adhesion and has been correlated with cell-substrate contact area (within 10-15nm of the substrate), thereby requiring an intact cytoskeleton [95, 95]. Using micropatterned elastic substrates, or substrates embedded with fluorescent beads, traction forces of cells may be calculated using substrate displacement vectors. Using elastic substrates, the adhesion strength of a

fibroblast focal adhesion has been reported to be approximately 30-70nN [96]. A recent advance in this field involved the use of atomic force microscopy and nanolithography with RGD-functionalized surfaces which demonstrated that adhesive reinforcement can occur in less than 5 minutes and detachment strength increases as long as the distance between integrin molecules is less than 70nm [97]. Further, a resultant model from similar work showed that integrin bond force, numbers and distribution along the contact area strongly modulate adhesion strength [98].

Adhesive interactions with fibronectin are important for osteoblast differentiation and bone formation [82, 99, 100]. In a study investigating adhesion strength of primary human MSC from bone marrow aspirates on tissue culture polystyrene (TCP) using a micropipette, it was found that although fibronectin-coated TCP initially had lower adhesion strength at less than 85min when compared with uncoated TCP, at up to 180min, adhesion strength was increased by over 100% ($7.96x10^{-2}$ dynes). Blocking with soluble β1 integrin monoclonal antibody decreased adhesion strength by 49% [101]. Although this study did not investigate a correlation between adhesion strength and differentiation, this does suggest that peak or delayed adhesion strength (at greater than 90min) may promote osteogenic differentiation of MSC.

A study using FRET to quantify MC3T3E1 traction forces on sodium alginate modified with fluorescent RGD peptides found that osteoblastic differentiation correlated inversely with gel stiffness and traction force (while proliferation correlated positively), but that clustering of adhesion ligands did not correlate with gel stiffness [102]. This suggests that clustering of adhesion ligands may not regulate differentiation in this model. Further, the gels that supported 50% greater focal adhesion formation showed diminished differentiation of cells, but focal adhesion content and distribution were not

explored. It is therefore possible that high numbers of focal adhesions may correlate with diminished differentiation, but it is unclear from this study whether integrin expression levels or focal adhesion distribution is important in this process, or whether these findings are applicable to hMSC.

Cell shape is important for MSC commitment to the osteoblastic vs. adipogenic lineage (which is mediated by a RhoA/ROCK mechanism) [103]. Cell shape, spreading and lamellipodia formation have been correlated with discrete patterns in traction force [104] and while traction force correlates with size and density of focal adhesions [105], the total area of focal adhesions formed is not dependent on total ECM amount but rather on spread cell area [106]. A cell's cytoskeletal organization undergoes changes during the process of spreading, however, it is unknown whether effectors of signaling by the cytoskeleton, such as the small GTPases, are an indicator of total adhesion state of MSC. A role for adhesion state in MSC differentiation is unclear, however the results of the studies previously mentioned suggest that focal adhesion area, number or distribution, and therefore adhesion strength, may be important for MSC differentiation.

Rho family GTPase signaling and adhesion

Rho family GTPases are a family of 20 small proteins (20-25kDa) that bind to and hydrolyze guanosine triphosphate (GTP), acting as molecular switches to help regulate a variety of cell responses by cycling through their inactive (GDP-bound), and active (GTP-bound) forms. Rho GTPases have profound effects on the cytoskeleton and when overexpressed contribute to contractility and focal adhesion and stress fiber formation while Rac GTPases regulate lamellipodia formation [107]. Rho GTPases can also regulate transcription [108], membrane trafficking and apoptosis [109] while FAK can temporarily inhibit Rho activity to promote focal adhesion turnover [110]. Recent in

vivo studies show that RhoB and RhoC knockout mice are viable, but RhoA knockouts have never been reported [111].

Integrins modulate the activity and localization of Rho-GTPases and their effector proteins [112, 113] and the small GTPases have been called key mediators of integrin signaling [112, 114, 115]. A current model by DeMali et al suggests that at early stages of adhesion with some integrins (10-30 minutes), the activity of Rho is transiently suppressed via c-Src and p190RhoGAP deactivating Rho, but that with other integrins, or at later timepoints (45-90 minutes) Rho is activated via RhoGEF through protein tyrosine phosphatase alpha (PTP$\alpha$) and Fyn [116]. Further, integrin-linked kinase (ILK) may be involved in this regulation of Rho [117]. However this may not be reflective of all cell types or species, and the applicability of these findings to hMSC is unknown.

Integrins can regulate Rho GTPases via two mechanisms, both by direct biochemical activation and by controlling the membrane binding sites needed for translocation of active GTPases to the plasma membrane. Biochemical regulation presumably takes place via conventional nucleotide exchange factors (GEFs), GTPase activating proteins (GAPs) and guanine nucleotide dissociation inhibitors (GDIs), although these mechanisms are not yet entirely clear. The second way that integrins regulate Rho GTPases is by promoting local membrane translocation of the GTPase. This is due to integrin effects on membrane binding sites in lipid rafts, so that the GTPase preferentially translocates to regions of the plasma membrane proximal to sites of integrin-mediated adhesion. Integrins regulate lipid raft availability by controlling their internalization (as has been shown in BMP-induced osteosarcoma migration [118]), but this mechanism is also not completely understood.

Integrins $\alpha5\beta1$ and $\alpha v\beta3$ specifically modulate RhoA-GTP loading, organization of cell matrix adhesions, and fibronectin fibrillogenesis in mouse embryonic fibroblasts [119] while $\beta1$ and $\beta3$ integrins have been shown to selectively modulate Rac and Rho activitiy, respectively, in CHO cells [120]. In this system, $\beta3$ over-expression enhances Rho activity and stress fiber formation while $\beta1$ over-expression enhances Rac activity (via PI3K and JNK activation) and lamellipodia formation, with the I-domain-like extracellular sequence of $\beta1$ playing a critical role in the process [120]. These studies demonstrate adhesion-dependent regulation of Rho and Rac, however the mechanisms still need to be elucidated. Possibly, the extracellular domains of $\beta$ subunits change conformation, affecting recruitment of signaling molecules at focal adhesions and the anchorage of the cytoskeleton, or Rho and Rac may be differentially regulated by integrin modulation of GEFs, GAPs or GDIs, changing the overall balance of regulators [120].

Rho-GTPase signaling can regulate cell commitment through Rho/p190B RhoGAP in myogenesis and adipogenesis in mouse embryo-derived fibroblasts [121], RhoA/ROCK in osteogenesis and adipogenesis in hMSC [103], RhoA/ROCK/myosin in embryonic stem cell renewal [122], and via Rho/ROCK in breast epithelial cell differentiation [123]. However, while the Rho/ROCK mechanism has been positively correlated with hMSC osteoblastic differentiation, a recent study found that Rho (stimulated by recombinant PMT toxin) strongly inhibited murine calvarial osteoblast differentiation, while Rho and ROCK inhibitors potently stimulated bone nodule formation as well as BMP2 and BMP4 mRNA levels [124]. Perhaps in osteogenesis, Rho acts in a contextual manner as it appears to do so in chondrogenesis of murine MSC grown in 2D or 3D environments [125, 126]. Recent evidence suggests that substrate stiffness influences calcium

oscillation levels in hMSC and that Rho modulation (either by RhoV14 or RhoN19 expression) negatively impacts these oscillations, which are mediated by a ROCK mechanism, however the link to differentiation is still unclear [127]. These inconsistencies in Rho signaling may possibly be due to species-specific regulation. Additionally, in the former study PMT may be influencing other signaling pathways as PMT promoted cell proliferation unlike C3-transferase (a Rho inhibitor).

Adhesion and differentiation of MSC on biodegradable polymer scaffolds

It is generally accepted that adhesion is important for success of tissue engineering scaffolds. Cells delivered in a scaffold must stay localized within the implant for proper function. However, as previously discussed, adhesion is a complex process and attachment is merely one early stage in this progression. As a result of this assumption, many groups have modified BDP to promote attachment and/or adhesion, however it is only recently that investigators have tried to understand how increased adhesion affects differentiation on BDP. As these studies have primarily been done with osteoblasts, work with both MSC and osteoblasts is discussed below.

Attachment and scaffold success: an unexplored assumption

There is a suggestion that improved attachment of cells on polymer substrates is indicative of greater function in vivo, but this has not yet been fully demonstrated. For instance, it was found that a PLGA/type I collagen woven sheet had superior cell attachment with murine osteoblasts in vitro compared with PLGA alone, and it also showed accelerated bone regeneration in a mouse calvarial defect compared with sheets not seeded with cells. However a relationship between degree of attachment in vitro and in vivo bone formation can not be suggested as the unmodified PLGA sheet was not used as a comparison in vivo [128].

Polymer substrate-attachment studies often fail to describe the subsequent effects on MSC or osteoblast differentiation [129-133]. This includes a study of rabbit MSC on polymer films in which PLGA (50:50, 75:25) showed approximately 76% adherence, which was significantly greater than PLA, PCL or PLA/PCL films [15], but no differentiation studies were done. Conversely, studies in which differentiation markers such as alkaline phosphatase activity, type I collagen or osteonectin expression are explored, attachment is often not addressed [134]. Furthermore, while gene expression may correlate with osteoblast maturation, terminal differentiation is best demonstrated by production and deposition of hydroxyapatite mineral.

Improving attachment via polymer modification: varied effects on differentiation

It has been suggested that a cell does not contact its substrate directly, but rather interacts with adsorbed proteins from serum [135]. As a result, some groups have sought to increase adsorption of serum proteins (like fibronectin and vitronectin) on polymers in order to improve attachment. However, some studies have shown that increased protein adsorption can lead to decreased attachment and proliferation, and increased osteogenesis in vitro. For instance two groups found that PLA-PEG or PLA films seeded with rat MSC showed decreased protein adsorption, attachment and cell proliferation, but increased mineral formation and alkaline phosphatase activity [136, 137]. Others have shown that increased fibronectin adsorption to surfaces of different charges relates to both surface roughness and charge and correlates well with detachment strength mediated by $\alpha 5\beta 1$ integrins [138].

Using integrin binding sites (such as RGD) to modify polymers is another way to manipulate cell attachment. For instance, rat MSC seeded on low molecular weight RGD-modified oligo-PEG-fumarate hydrogels showed increased attachment, however,

no differentiation studies were reported [139]. In another study, human osteosarcoma cells (MG63) seeded on an RGD-modified PLL-g-PEG-coated titanium surface showed increased cell number and decreased osteogenic properties (alkaline phosphatase and osteocalcin expression) [25]. This is in contrast to RGD-modified alginate studies with murine MC3T3E1 osteoblasts which show both improved attachment and differentiation in vitro, and support modest increases in bone formation in vivo [140]. Another study showed that RGD-modification of self-assembled monolayers with various peptide sequences led to insignificant changes in adhesion strength and minimal changes in mineralization of MC3T3E1 cells [138].

Understanding adhesion of MSC on BDP: an incomplete picture

More detailed investigations of cell adhesion to biodegradable polymers affecting differentiation have been carried out primarily with osteoblasts, and these results are discussed below in addition to recent work with hMSC.

Many groups have investigated integrin or focal adhesion expression of osteoblasts on biomaterials during adhesion, but comparative conclusions are difficult to make due to the use of various substrates and cell types (for example, on Na-alginate, human and rat MSC show vastly different rates of adhesion [17]). Overall, it can be concluded that different substrates and peptide/protein coatings can influence integrin expression and cell behavior. While integrin expression plays a role in cellular activities, it is unknown whether initial attachment and spreading of cells on biomaterials may predict long-term behavior, although recent evidence suggests that spatial patterning of hMSC on multicellular sheets can control the osteogenic or adipogenic phenotype [141].

The ratio of $\alpha 5\beta 1$ to $\alpha v\beta 3$ integrins expressed by cells may regulate consequent osteoblastic differentiation in vitro (as found in MC3T3E1 cells) [21], coinciding with findings that $\beta 1$ integrin is important for osteoblast-biomaterial interactions [39, 142]. While $\beta 1$ and $\alpha v\beta 3$ are important for hMSC differentiation, it is unclear how necessary they are relative to one another [143] although vitronectin, collagen I and fibronectin adsorption all appear to be important for differentiation on biodegradable polymers [144]. Further, integrin expression is affected by the conformation of coated-fibronectin expressed on the surface, which in turn is altered by surface chemistry [142, 145, 146]. However, in the Garcia group studies, integrin-blocking was initiated 24h after plating making it hard to determine whether earlier adhesion played a role in differentiation [21]. In addition, the adhesion strength and integrin binding affinity assays were done for only one time point (30min), such that dynamic changes in adhesion were not studied. A different timepoint (1h) was used to examine focal adhesion components and FAK phosphorylation, which was expressed more highly on surfaces promoting differentiation [145]. Even though these studies found that surfaces which modulated differentiation showed differences in adhesion, little correlation could be drawn overall.

Other attempts to describe adhesion on biomaterial substrates have examined both integrin and ECM protein expression. For instance, primary human osteoblasts seeded on PLGA vs. PLA films showed greater adherence to PLGA films from 3-12 hours. However, while PLGA-seeded cells had higher expression of osteocalcin and several integrin subunits at 72h, complete differentiation studies were not carried out, and importantly, values were not normalized to cell number, confounding the data [147]. Consequent studies found that osteoblasts on PLGA substrates demonstrated higher levels of ECM protein expression and a more developed actin network sooner than on

PLA [148], but while adhesion to both polymers was integrin-mediated, those integrins most important for adhesion were different for each polymer [149].

While some investigators have started to map adhesion of cells on polymers over time, there has been little attempt to explore how different aspects of the attachment and adhesion profile may affect differentiation. A detailed analysis of adhesion of an immortalized human fetal osteoblast line (hFOB 1.19) up to 180 minutes showed that $t_{1/2}$ (time to attain half the cell number of the plateau) on various materials ranged from 31 to 75 minutes, with maximum adhesion being between 8-72% on a variety of biomaterial substrates, including PLGA, PCL and their copolymers. Proliferation rates were not statistically different on these surfaces and it was found that alkaline phosphatase activity did not correlate with surface energy or chemical composition, however, no long term differentiation studies were carried out [16]. In a subsequent study, it was found that hFOB cells displayed well-developed actin-stress fibers on hydrophilic substrates relative to hydrophobic substrata, and that in the latter case, cells expressed lower levels of $\alpha$v and $\beta$3 integrins, but these variations in integrin expression were lessened over culture time. Vinculin protein expression also mimicked the expression of the integrins with respect to surface wettability [150]. However, these studies were carried out on surface-modified quartz and glass, and not on biodegradable polymers.

More recent studies of hMSC-biodegradable polymer interactions do appear to include preliminary study of cell adhesion, however a link between such studies has not yet been drawn. One of these studies did find that in an in vivo model, high molecular weight PLGA supported greater osteocalcin gene expression in comparison to low molecular weight PCL, and that in an in vitro model, PLGA demonstrated collagen I-

mediated adhesion of hMSC while on PCL, hMSC preferentially adhered via vitronectin [144]. While fibronectin was shown to adsorb to both surfaces, further study was not undertaken despite the fact that physiologically, fibronectin levels are far greater than that of serum, and could potentially be very important for understanding the relative osteoinductivity of PCL and PLGA. Further, a direct analysis of how adhesive mechanisms are different on these surfaces was not undertaken [144]. Another in vivo study used fibroblasts retrovirally transduced with the transcription factor Runx-2 as a cell model and demonstrated increased matrix formation on PLGA vs PCL scaffolds. Adhesion was only addressed as a cell seeding efficiency at 24hrs, the mechanism of which was not pursued [151]. Finally, a recent in vitro study demonstrating the effects of PCL-PLGA blends on primary hMSC differentiation showed that PCL dominant blends tended to promote chondrogenesis while those blends containing more PLGA showed an increased in osteogenic markers, although robust osteogenesis was not demonstrated on any surface studied, and adhesion was not addressed [152].

In the field of bone tissue engineering, there is an underlying assumption that high cellular attachment rate to polymer scaffolds is desirable for in vivo success. However, relative adhesion strength, focal adhesion formation and associated down-stream signaling, rather than attachment rate, may play an important role in MSC differentiation on polymer substrates. In tissue engineering, more attention needs to be paid to translation from in vitro studies to practical applications [135]. Understanding how initial adhesion affects MSC differentiation on polymer substrates may contribute knowledge to help maximize bone growth on cell-seeded scaffolds. Additionally, insight into the relationship between MSC adhesion and differentiation is important for understanding the regulation of MSC in vivo, in the marrow-environment.

Global Hypothesis and Specific Aims

Given the current understanding of MSC adhesion and differentiation, our global hypothesis for the following work is that:

The adhesion strength of hMSC to synthetic substrates affects differentiation. Specifically, biodegradable polymer substrates that promote high initial adhesion strength and form robust focal adhesions activate small GTPases leading to osteogenesis.

To address this global hypothesis we propose the following Specific Aims:

Aim I. Examine the significance of hMSC adhesion strength to biodegradable polymer substrates in osteoblast differentiation.

Hypothesis: Substrates that support high adhesion strength of hMSC have increased osteogenesis.

1a. Determine the adhesion strength of hMSC to substrates with various degrees of cellular attachment.

1b. Examine the relative degree of osteogenic differentiation of hMSC on polymers of differing adhesion strengths.

Aim II. Ascertain the importance of focal adhesion formation and GTPase activity on osteogenesis of hMSC on adhesive biodegradable substrates.

Hypothesis: Focal adhesion formation and RhoA/ROCK activation promote osteogenesis of hMSC on adhesive biodegradable substrates.

2a. Determine the quantity of hMSC focal adhesions (FA) and cellular morphology on adhesive polymer groups.

2b. Explore whether focal adhesion formation and activity on adhesive polymer groups promotes hMSC osteogenesis.

2c. Examine RhoA activity of hMSC throughout differentiation.

2d. Determine whether reduced RhoA signaling diminishes hMSC osteoblast differentiation on adhesive polymers.

2e. Determine whether RhoA activation is sufficient to promote greater osteoblast differentiation on adhesive substrates.

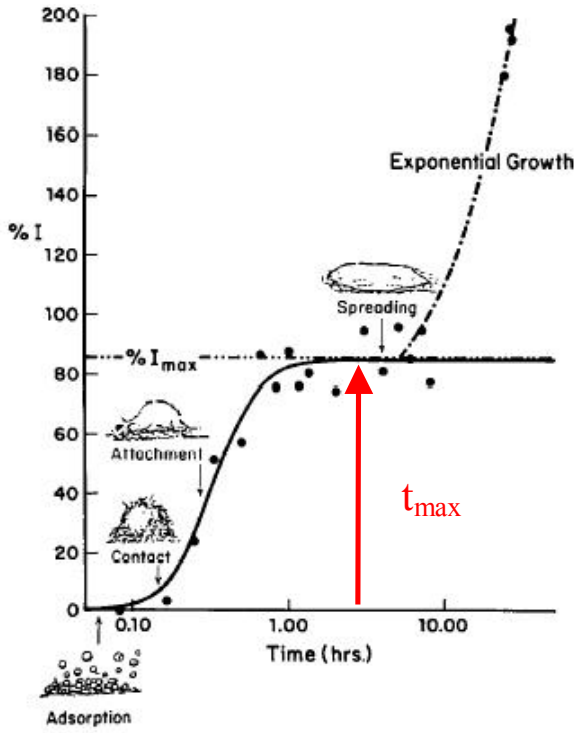


Figure 1.1. Time course of cell adhesion to tissue culture polystyrene. $t_{max}$ represents the half-way point between the initiation of exponential growth and completion of attachment on the adhesion plateau [38].

# CHAPTER II

## CHARACTERIZATION OF ADHESION STRENGTH AND OSTEOGENIC DIFFERENTIATION OF hMSC ON BIODEGRADABLE POLYMERS

### Introduction

Mesenchymal stem cells (MSC) are multipotent progenitor cells which have been widely studied for orthopaedic tissue engineering. While MSC are promising candidates for tissue engineering applications (as they are easily isolated from marrow and can promote bone, cartilage or fat regeneration), the delivery of these cells to sites of interest necessitates the use of a carrier substrate, whether synthetic or naturally-derived. Because cell-material interactions vary by both cell species and material characteristics, it is important to understand how human MSC (hMSC) interact with novel biomaterials. However, for those materials commonly used at present, there is still a narrow understanding of how early hMSC-material interactions (occurring prior to proliferation) affect downstream function.

Previous work with hMSC has shown that cell shape affects differentiation, as highly-spread cells tend to undergo osteogenesis while smaller rounded cells tend to undergo adipogenesis [103]. Further, it has been shown that substrate material characteristics such as stiffness can also affect differentiation of hMSC [153-155]. As a result, this suggests that cell adhesion may play an important role in the relative suitability of materials for supporting osteoblast differentiation. However, it is unclear as to what aspect of adhesion might be most important for this effect. Cell shape differences are

observed rapidly when cells are grown on biomaterials, suggesting that early cell-material interactions might be important in this process. One way to quantify such early interactions is to identify the sum of all adhesive reinforcement interactions by measuring adhesion strength.

Adhesion is a dynamic process which undergoes a predictive series of events. Initially, protein adsorption occurs within seconds as the material comes into contact with a proteinaceous solution. Following this, as a cell approaches a surface, it has been suggested that glycosaminoglycans forming a 'fuzzy coat' around the cell (the glycocalyx) initiate interactions with the surface. As cells then reach a secondary energy minimum, cells can undergo specific interactions with the surface via integrin binding, forming adhesive reinforcement through recruitment of additional proteins to these attachment points, creating focal complexes and adhesions, or fibrillar adhesions (depending on the components of these adhesion plaques). During this process of reinforcement, the number of cells that attach to a surface plateaus prior to proliferation. Given these findings, we believe that the total sum of adhesive interactions at the attachment plateau affects downstream function of human MSC, and that the differences in cellular adhesion strength between biodegradable polymers of interest may be predictive for assessing whether polymers support specific cellular function. If our hypothesis holds true, then determining a global adhesion strength for hMSC on biodegradable polymers could be a novel tool for assessing biocompatibility of newly designed biomaterials.

**Results**

Physical and chemical properties of biomaterials

PLGA, PCL and alginate vary by molecular composition and weight and were therefore characterized to ultimately examine the effects of mechano-chemical properties on cellular interactions.

Surface hydrophobicity was quantified using the sessile drop method and the water contact angle was determined for each surface. The control, PDMS, showed the greatest degree of hydrophobicity ($110\pm3^{o}$) followed by the PLGA groups (containing either acid end groups or ester-capped ends) ($65\pm2^{o}$ to $95\pm3^{o}$) and PCL ($57\pm1^{o}$ to $65\pm2^{o}$). It has been reported that water contact area may change while contact angle is stable, and that contact area is static when contact angle is initially changing, however for a time period of one minute, these changes were not displayed for the polymers of interest [156]. As expected, those surfaces demonstrating decreased hydrophobicity displayed increased relative water contact area (from 2.2-3.2$mm^2$) as determined by linear regression ($R^2$=0.75) (Figure 2.1). Water contact angle could not be measured on alginate, because as a hydrogel, water is fully absorbed on the surface (making the water contact angle zero, and water contact area infinity). PCL and ePLGA groups were significantly different from one another for both water contact angle and contact area data ($p<0.05$) (Figure 2.1a-b). Surfaces were next visualized with environmental SEM at magnifications of 350x - 800x in order to confirm that the glass cast films to be used for consequent cell studies were indeed smooth. While slight inconsistencies were displayed on the surfaces of the polymers, scanning images in cross-section confirmed that the surfaces were smooth on the micron scale (Figure 2.2a). Approximate film thickness was also quantified using ESEM and ranged from 40-120µm (Figure 2.2b). Bulk elastic modulus was quantified in compression for all

surfaces studied and whereas crosslinked alginate was found to have a modulus of 20-40 dynes/cm$^2$, both PCL and PLGA displayed significantly greater moduli, at 200-400 and 200-2300 dynes/cm$^2$, respectively (Figure 2.2c). Total protein adsorption studies found that no significant difference existed between individual surfaces (for 2% serum protein at 2hrs incubation), however PCL and PLGA groups did show a significant increase in protein adsorption over alginate ($p<0.05$) (Figure 2.2d).

Cell attachment and adhesion on biomaterials

Conditionally-immortalized hMSC lines were created from primary cells derived from vertebral aspirates. Detachment experiments for two hMSC lines on all surfaces of interest involved plating cells and quantifying attached cell number from the order of minutes to hours for a maximum of 72hrs (Figure 2.3). Using Vogler's curve [38] as a reference, by plotting these values, the plateau, or $t_{max}$ region could be estimated. For both cells lines on all surfaces of interest (13 in total), the first few hours of attachment fell within this plateau region and for the remainder of adhesion experiments, the timepoint of one hour was chosen to represent this region of reinforced dynamic adhesion, which occurs prior to proliferation [38]. Using this data, a proliferative index was calculated based on attachment points occurring beyond the plateau region. Table 2.1 demonstrates these values, and it can be seen that a/mPLGA surfaces (containing acid-ended monomers) displayed a greater proliferative index than ePLGA (containing ester-capped monomers), PCL and the hydrogel, alginate, respectively. Cell morphology on the biomaterials was evaluated using confocal microscopy (Figure 2.4). A poor degree of spreading was displayed for cells on alginate with respect to the polyesters as would be expected on a highly negatively charged surface [157]. A proportion of cells on PLGA and PCL surfaces were able to spread, exhibiting a well-developed cytoskeleton. However, some cells exhibited an unspread phenotype and

this mix of spread and unspread cells was displayed consistently across both PLGA and PCL surfaces (Figure 2.4). Additionally, cells demonstrated a range of number of focal adhesions per cell as determined from paxillin antibody staining in confocal images (Table 2.2).

Adhesion strength on biomaterials

Adhesion strength was quantified via two complementary methods; using a custom-built fluid shear device [93] and a spinning disk device [94]. Using a relatively small sample size (n=3) with one cell line, measurements made with the fluid shear device demonstrate that alginate exhibited the weakest adhesion, as can be expected for a hydrogel, while PCL and the higher molecular weight PLGA demonstrated much higher adhesion strengths, however only PLGA was considered statistically significant from the other polymer groups (Figure 2.5a). Experiments with the spinning disk device with a much larger sample size, and data pooled from both cell lines (n=9-14) demonstrates a relatively complex relationship. Upon examination of the detachment forces of cells to the polyesters of interest (both varieties of PLGA and of PCL), statistical differences were exhibited within the ePLGA and PCL groups, but not in the a/mPLGA group. However, the a/m PLGA group was found to have significantly higher mean adhesion strength with respect to the other polymer groups ($p<0.05$) (Figure 2.5b). Due to both greater samples sizes and reliability of the spinning disk data, these results will be used for reference in all consequential studies.

In an attempt to understand what material characteristics may affect adhesion strength of hMSC to these surfaces, adhesion strength data was fit using a restricted cubic spline to both elastic modulus ($R^2$=0.65) and contact angle ($R^2$ = 0.68). Such a fit was used as data initially exhibited discrete relationships within polymer groups, and in this

way the groups could be fit individually and meshed together for a complete model. In fitting $\tau_{50}$ to both elastic modulus and contact angle, a positive relationship was found with each parameter, yielding optimums of approximately 20 000-30 000 kPa and 65-75$^{o}$, respectively (Figure 2.6). Because the properties of elastic modulus and contact angle are highly collinear ($R^2$=0.83), determining whether there is a main effect for either property on adhesion strength is not appropriate for ANCOVA analysis and becomes hard to predict, although the model $R^2$ value does suggest that contact angle may have a greater effect on adhesion strength than elastic modulus.

Differentiation of hMSC on biomaterials

Following the characterization of cell-polymer attachment on each of the surfaces, differentiation experiments were carried out on all surfaces, however PCL and ePLGA were determined to be most appropriate as alginate demonstrated very poor adhesion which negatively affected long-term cell viability. As well, a/mPLGA exhibited degradation during the course of the extended differentiation assays (data not shown) resulting in acidification of growth media.

Both cell lines demonstrate a distinct gene expression profile when induced with either dexamethasone or BMP6 on tissue culture polystyrene, and in particular exhibit a large induction in osteomodulin and collagen 1$\alpha$1 expression. Further, both treatments also display similar quantities of mineral formation (data not shown). Because BMP treatment did not enhance osteogenesis any greater than dexamethasone treatment, only dexamethasone was used to induce osteogenic differentiation throughout the remainder of this work (Figure 2.7).

Both hMSC lines showed an increase in alkaline phosphatase activity at day 15 and calcium phosphate deposition at day 21 (monitored by either Alizarin Red staining or CPC free-calcium assay) on PCL of mid and high molecular weights, rather than PCL of low molecular weight (Figures 2.8 and 2.9). The changes in osteogenic index (relative change in alkaline phosphatase activity per cell) appear to correlate with adhesion strength of PCL when the outlier of Line 2 on PCL high is removed ($p<0.05$) (Figure 2.10).

Differentiation on ePLGA of both hMSC lines showed an increase in alkaline phosphatase activity at day 15 and calcium phosphate deposition at day 21 or 34 (monitored by either Alizarin Red staining or CPC free-calcium assay) with respect to molecular weight (Figure 2.11). The changes in osteogenic index correlate well with adhesion strength of ePLGA (Figure 2.12).

Pooling the osteogenic index data of both cell lines on PCL and ePLGA demonstrates relatively poor correlation with adhesion strength (Figure 2.13) as well as with measured material properties of elastic modulus and contact angle (data not shown).

**Discussion**

The polymer groups used in this study are common to the field of bone tissue engineering but are not often characterized for both material properties and cellular function. In particular, we have determined the properties of contact angle, bulk elastic modulus and film thickness for the purpose of trying to determine what role they might play in cellular adhesion strength, and ultimately osteogenic differentiation.

Water contact angles and areas were inversely correlated and demonstrated an expected range with the most hydrophilic surface (alginate) showing the smallest contact angle (and largest contact area) while the most hydrophobic surface (PDMS used as a control) showed the largest contact angle (and smallest contact area) (Figure 2.1). It is known that both charge and hydrophobicity affect cellular attachment with cells preferring a median range of both attributes [41, 153, 158, 159].

Surface roughness is known to affect cell function of hMSC [160] as well. We attempted to remove this variable from our system as all films were cast on glass plates and retained a smooth morphology on the micron scale, as displayed by ESEM imaging (Figure 2.2a), as opposed to differences in roughness as would be expected by spin-coating [161]. Bulk elastic modulus (E) was determined for the polymers of interest and was found to range from the order of kPa to MPa (Figure 2.2c). In general, we saw an increase in E with increasing molecular weight as would be expected for the polyesters as both hydrophobic interactions as well as physical entanglements created through solvent evaporation contribute to this value [162]. It is known that cells can feel down through their substrates as much as 10μm [104] and all surfaces of interest demonstrated a relatively large film thickness of greater than 40μm (Figure 2.2b) avoiding any confounding effects of variable film thickness on cells. Additionally, while a three-fold change in thickness could decrease storage modulus of these films [161], and as elastic modulus does depend on storage modulus there may be a decline in stiffness for the thickest films, however, most films fell within a range of 50% of one another (Figure 2.2b). Also, an accurate determination of this effect would need to be studied empirically as most thin film modulus equations involve substrate effects [163], which do not apply in our cell assembly system. It should be noted, however, that in

the previous study, it was found that for nano-thin films, the substrate no longer dominates in mechanical properties for films greater than 0.1μm thick [163] which is applicable for cells grown on drop-coated coverslips in our system. Recent literature suggests that hMSC may preferentially differentiate down either of the neurogenic, myogenic or osteogenic pathways based on substrate stiffness [153], however the range of moduli used remained on the order of kPa, and it is unknown how surfaces in the MPa range, as in our system, may affect differentiation.

Biomaterial protein adsorption is a complex and well-studied phenomenon which can vary greatly in different systems [164, 165]. As the hMSC lines used in the study require serum to differentiate, all experiments were done in media with a minimal amount of serum (2%). Interestingly, surfaces adsorb the greatest amount of serum protein in a 0.1% serum solution and competition for the surface by the great variety of proteins found in serum varies as both total and relative protein concentrations change [166]. Functionality of proteins adsorbed to a surface can be attributed to conformation of the protein on that surface, which can be difficult to predict [167-169]. A simple adsorption and wash assay of whole 2% serum to the polymers of interest demonstrated very poor adsorption following several washes of the surfaces using a micro BCA assay as previously published [170]. The sensitivity of this assay was low and it showed that most of the polyester surfaces displayed greater serum protein adsorption than the hydrogel, alginate, as expected.

With an understanding of the materials of interest, we next examined attachment of hMSC to the surfaces. Following Vogler's curve approximation of cell attachment over time [38] (Figure 1.1) cells were cultured for 72hrs and harvested over several timepoints to formulate a similar curve for each cell line on the various polymer groups.

Despite the varied surfaces the cells were presented with, each line showed a similar timespan for reaching the plateau prior to proliferation (on the order of 1-3 hours (Figure 2.3). This is a time period of great dynamic adhesion as cells begin to reinforce integrin-ECM interactions through the formation of focal contacts and focal adhesions [38]. While studying several timepoints would be of great interest to this study, the timepoint of one hour was chosen for experimental standardization. In summarizing the attachment curves and identifying the linear proliferative region of the curve, it was found that the proliferative index of a/mPLGA was greater than for ePLGA, PCL or for alginate (Table 2.1), which seems to correlate well with cell numbers quantified through successive experiments (data not shown).

Confocal imaging demonstrated that cells developed a more elaborate cytoskeleton on ePLGA than on any of the other surfaces and that cells on alginate failed to spread at all (Figure 2.4), exhibiting mainly cytoplasmic expression of the focal adhesion protein, paxillin, as can be expected in rounded cells [171]. In general, degree of spreading appears to be associated with average number of focal adhesions per cell as hMSC on ePLGA had the greatest and alginate the least numbers of focal adhesions (Table 2.2). Interestingly, others have shown with atomic force microscopy that an increase in focal adhesion staining correlates with increased elastic modulus of an osteoblast [172] suggesting that the result of cells growing on stiffer substrates is to form more focal adhesions and become stiffer themselves. Approximating cell shape at this timepoint is difficult as the general spreading effect across a cell population is not homogenous as even hMSC on ePLGA showed an array of morphologies from completely rounded to fully spread. The importance of this observation is not known, however, despite cell shape being implicated in hMSC differentiation [103, 141].

Adhesion strength of cells grown for 1hr on polymer surfaces was shown to vary somewhat based on the experimental system used (Figure 2.5). Using a fluid shear system, a relatively small sample number was used for hMSC line 1 and demonstrated that the two highest molecular weight mPLGA polymers showed the greatest adhesion strength while alginate exhibited a very weak adhesion strength (although this relationship is not statistically significant due to small sample size). Using a spinning disk device and a larger sample size, significant differences in adhesion strength were found within both the PCL and ePLGA groups, and for mean a/mPLGA across the other groups, but mean PCL and ePLGA adhesion strengths were not significantly different from one another (Figure 2.5). Given the unenclosed nature of the spinning disk system, alginate could not be quantified in this study.

We were then interested in understanding whether the polymer material properties may be correlated with cellular adhesion strength, and the data was fit to a restricted cubic spline with elastic modulus or contact angle as the independent variable and adhesion strength ($\tau_{50}$) as the dependent variable. Both fits demonstrated similar correlation coefficients yielding a slightly better fit between contact angle and adhesion strength (Figure 2.6). Multiple linear regression yields an improved fit ($R^2$=0.58, $p<0.05$) over simple linear regression for either elastic modulus ($R^2$=0.2, $p<0.05$) or contact angle ($R^2$=0.43, $p<0.05$) alone, and ANCOVA analysis also suggests that contact angle may be a stronger predictor for adhesion strength over elastic modulus, but due to the collinear nature of elastic modulus and contact angle variables ($R^2$=0.83, $p<0.01$) it is difficult to draw a firm conclusion. Based on the work of others investigating the role of either property on cellular function [41, 153], it is not surprising that while there is a positive correlation for both material properties, an optimum exists for both. In particular, surfaces that are either overly hydrophobic or too stiff may inhibit cellular

function [173]. Film thickness and serum protein adsorption showed very weak correlation to adhesion strength (data not shown).

Differentiation studies carried out on PCL and ePLGA demonstrated that hMSC lines differentiated to varying degrees as exhibited by the osteogenic markers used (Figures 2.8-2.11). On PCL, both hMSC lines exhibited greater relative alkaline phosphatase activity and Alizarin Red staining on the highest molecular weight PCL with respect to the lowest molecular weight PCL, echoing the relationship between the adhesion strength of these materials (Figure 2.10). On ePLGA, a distinct relationship was seen between relative alkaline phosphatase activity and adhesion strength of cells to this surface (Figure 2.11), and a relationship was also seen in Alizarin Red staining, although all cells mineralized much sooner on ePLGA than on PCL, with hMSC line 2 showing accelerated mineralization relative to hMSC line 1 (Figure 2.11b). A similar relationship was seen in free calcium levels with hMSC line 1 and adhesion strength, although these values were not statistically significant. While these effects of adhesion strength on differentiation held true within each polymer group, this relationship did not hold when the data was pooled across groups (Figure 2.12), suggesting that other factors such as surface chemistry [160, 174-176] may be affecting differentiation independent of adhesion strength. Similarly, poor correlation was seen between osteogenic index and elastic modulus or with contact angle across groups ($R^2$=0.34 or $R^2$=0.26, respectively ($p>0.05$)) reinforcing the need for additional investigation of properties that may be contributing to differentiation status of hMSC.

In summary, the polymer groups commonly utilized in tissue engineering studies were characterized in this study, and exhibit a wide range of material properties including elastic modulus and contact angle. Dynamic cellular attachment was quantified and

immortalized hMSC were found to attach along a similar time scale but proliferate differently on these surfaces. Cellular adhesion strength was determined for cell lines on each of the polymers in the adhesive reinforcement region of the attachment curve and a moderate correlation of adhesion strength ($\tau_{50}$) with both elastic modulus (E) and degree of hydrophobicity (contact angle) was found. Differentiation studies of both hMSC lines on PCL and ePLGA established a significant relationship between osteogenic index and cellular adhesion strength, but not with the material properties that were characterized. Further exploration of how material properties may influence hMSC differentiation both dependent and independent of adhesion strength would contribute to improved design of biomaterial scaffolds for successful tissue-engineered constructs.

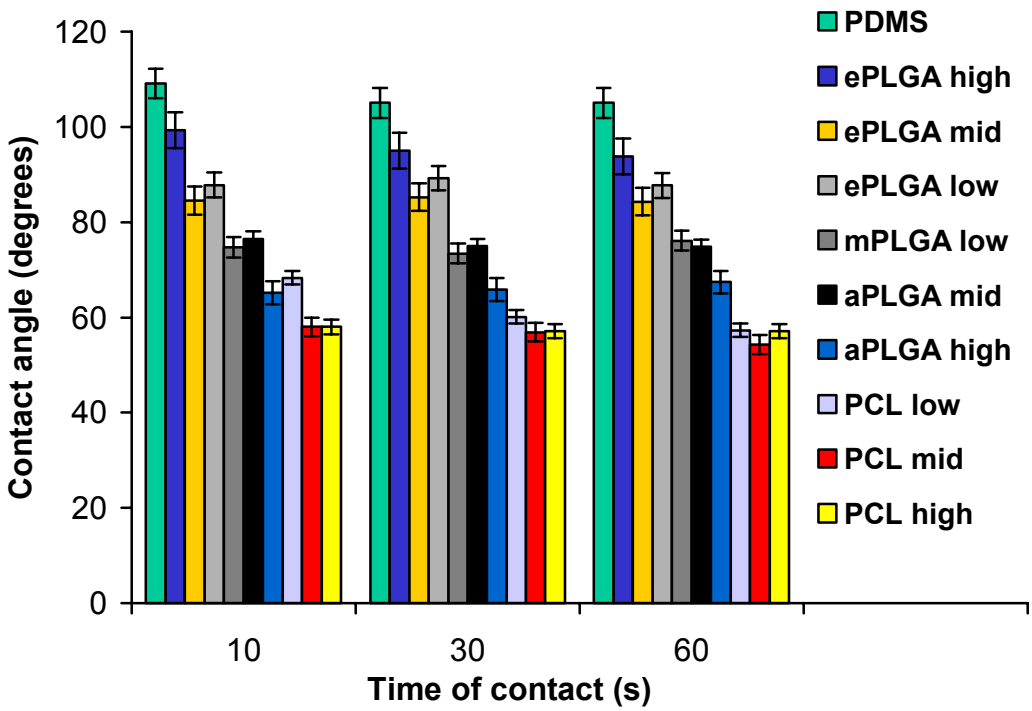


Figure 2.1a. Contact angles on polymer films. Sessile drop measurements were taken at 10, 30 and 60 seconds. PCL and ePLGA polymer group means are significantly different from one another; $p<0.05$.

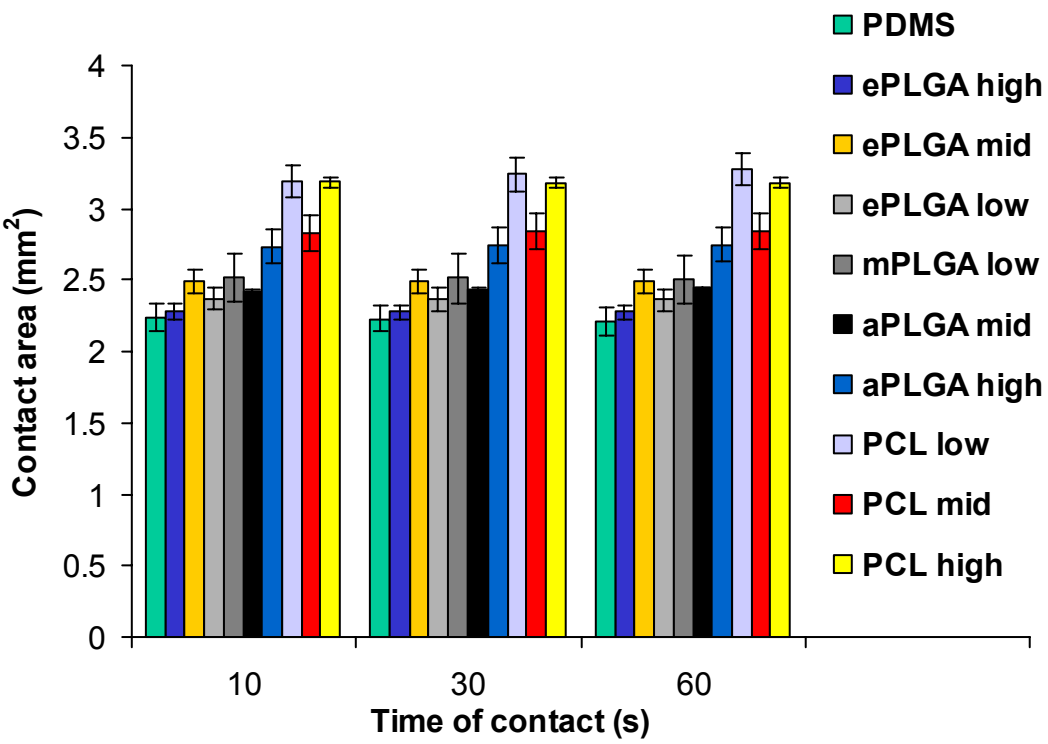


Figure 2.1b. Water contact area on polymer films. Image measurements were taken at 10, 30 and 60 seconds. PCL and ePLGA polymer group means are significantly different from one another; $p<0.05$.

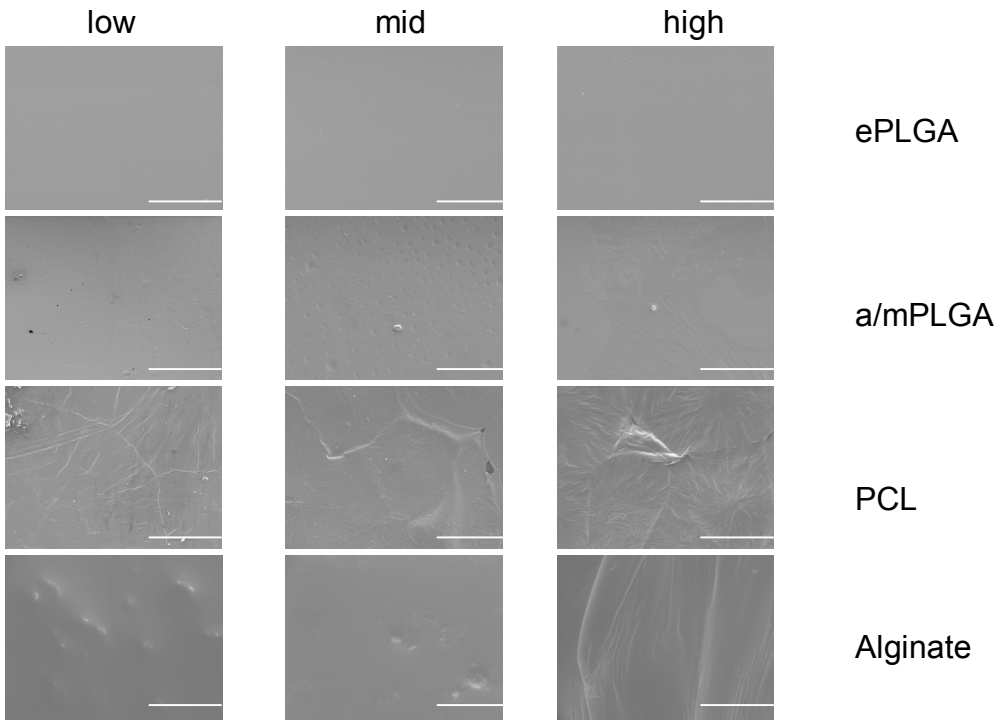


Figure 2.2a. Environmental SEM imaging of polymer films. All films exhibited a smooth appearance at the micron scale; 650x magnification, polyesters were imaged under high vacuum, and alginate was imaged under wet mode conditions, scale bars = 50μm.

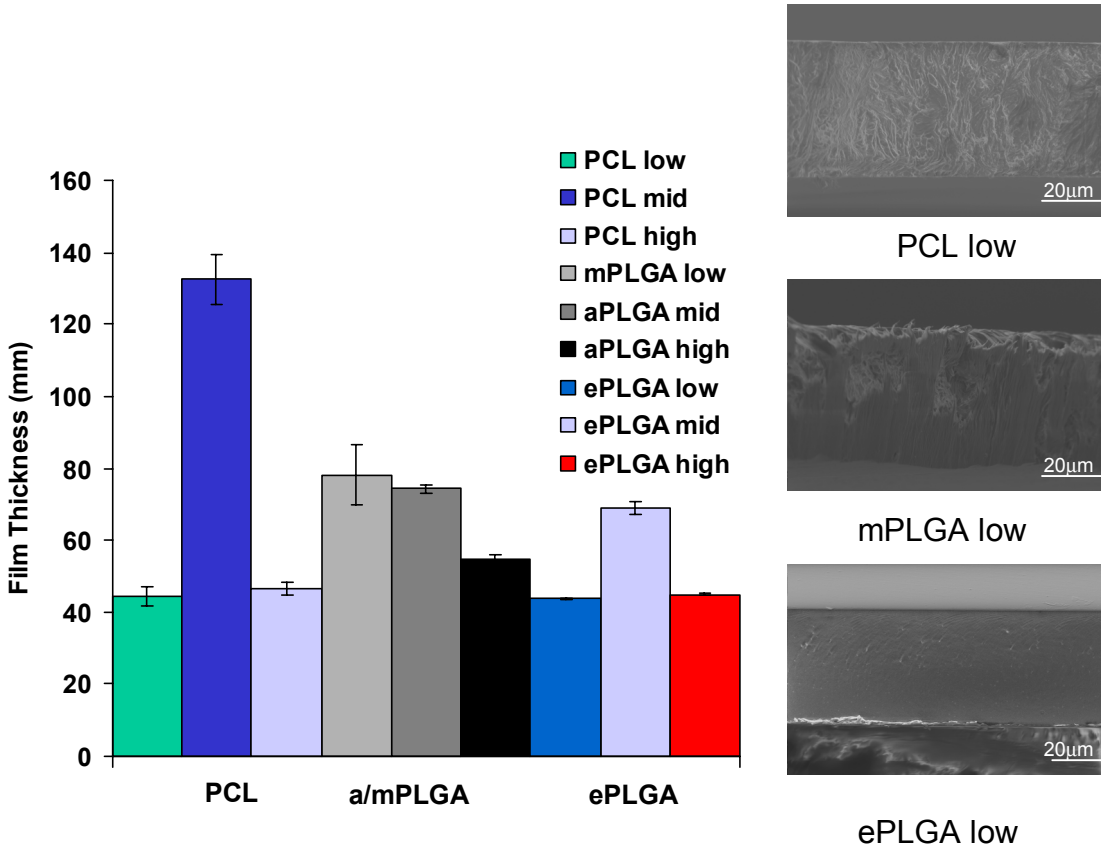


Figure 2.2b. Film thickness of cast polyesters measured by ESEM. Values plotted are means from 10 measurements +/- SE. Insets show representative images of cross-section ESEM images taken at 5.0kV, 1000-1200x under high vacuum. Means for polymer groups are not significantly different from one another.

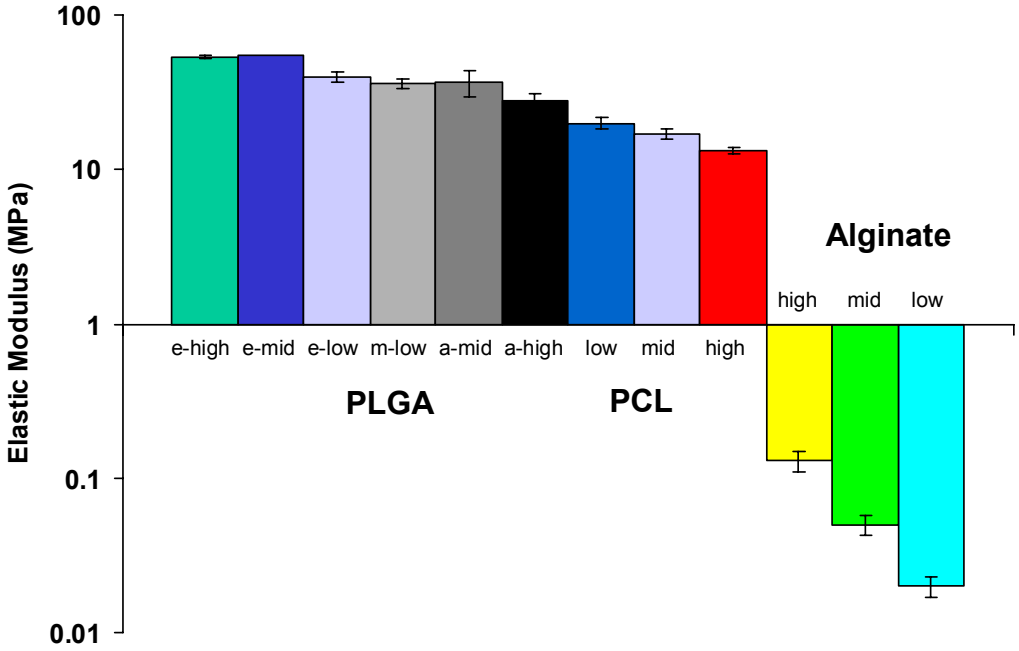


Figure 2.2c. Bulk elastic modulus measured in confined compression for polymer groups. Means of 8-12 samples are plotted +/- standard error. All polymer groups are significantly different from one another, $p<0.05$.

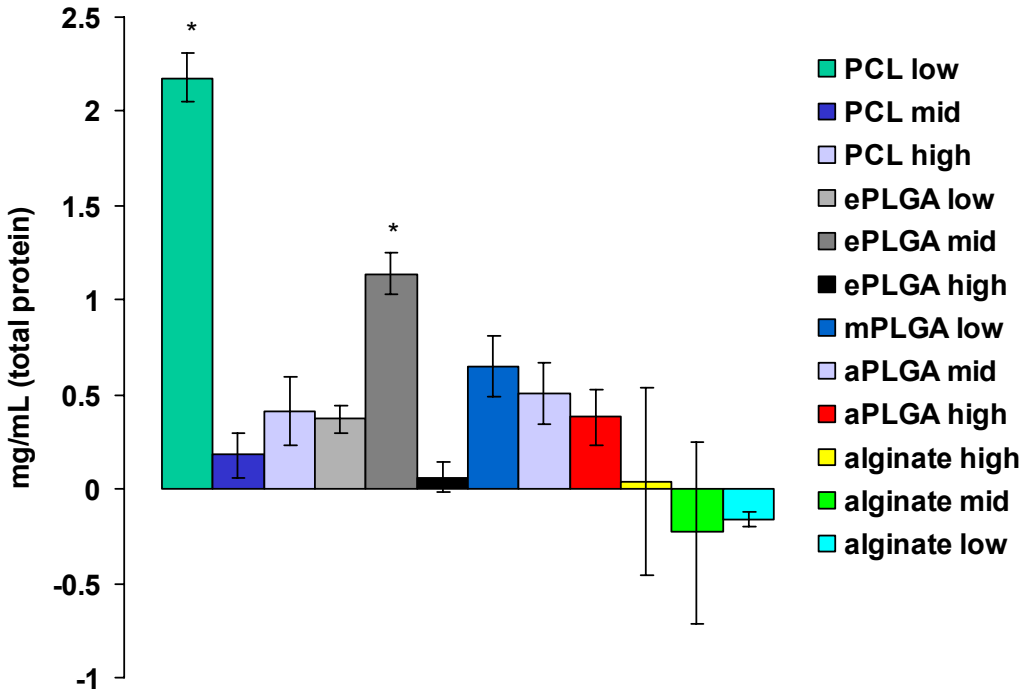


Figure 2.2d. Adsorption of 2% serum on polymer groups. Adsorbed serum was measured using an SDS wash assay. PCL low and ePLGA mid had significantly different protein adsorptions from one another, which were greater than for all other surfaces; *p<0.05, values plotted are means of 8 samples +/- standard error.

a.

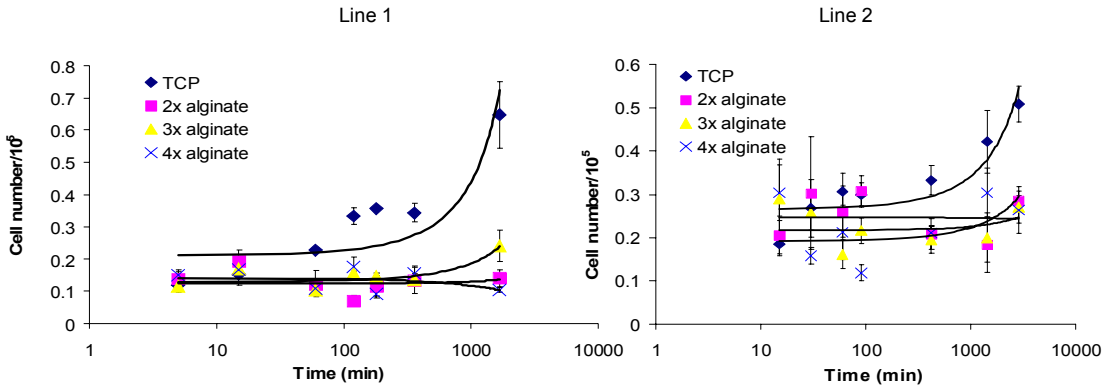


b.

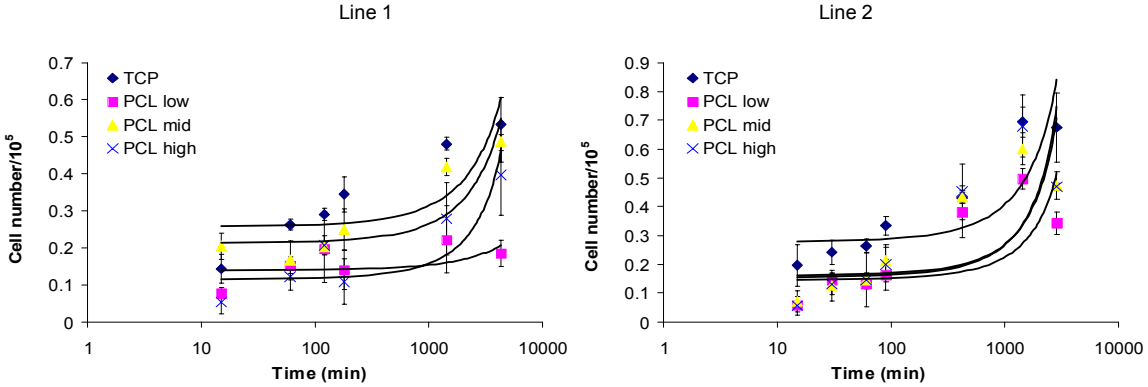


Figure 2.3a-b. Attachment of hMSC immortalized lines on alginate and PCL. Both hMSC lines were cultured for various lengths of time up to a period of 72hrs on (a) alginate and (b) polycaprolactone. Trendlines indicate fit to an exponential curve.

c.

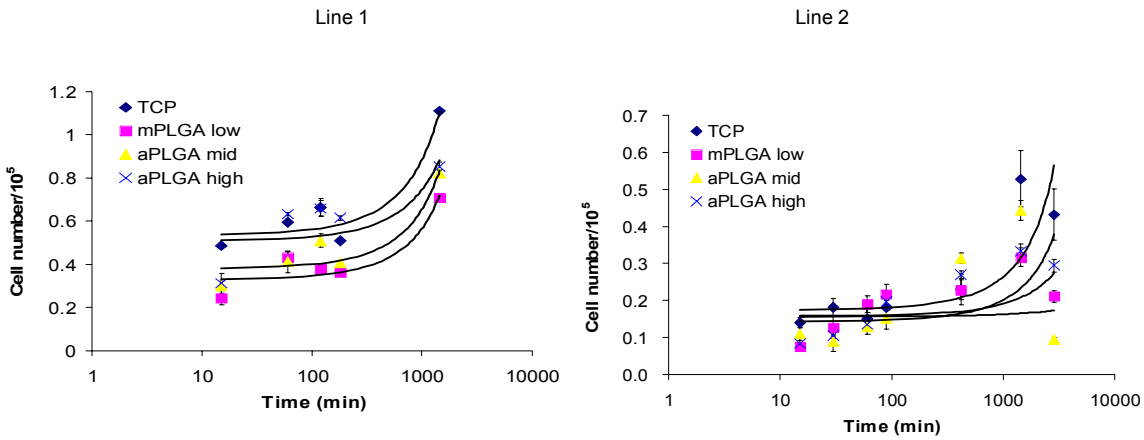


d.

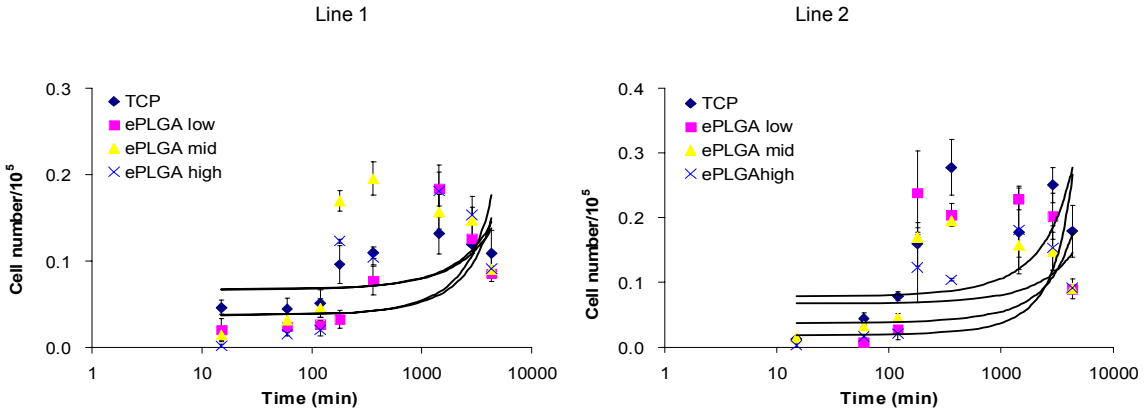


Figure 2.3c-d. Attachment of hMSC immortalized lines on a/m PLGA and ePLGA. Both hMSC lines were cultured for various lengths of time up to a period of 72hrs on (c) a/m PLGA and (d) ePLGA . Trendlines indicate fit to an exponential curve.

Table 2.1. Proliferative index of hMSC on all polymer groups.

| k/100 | 2x alginate | 3x alginate | 4x alginate | PCL low | PCL mid | PCL high | ePLGA low | ePLGA mid | ePLGA high | mPLGA low | aPLGA mid | aPLGA high |
|---|---|---|---|---|---|---|---|---|---|---|---|---|
| Line 1 | .02 | .04 | .01 | .04 | .08 | .05 | .1 | .05 | .07 | 4.3 | 2.6 | 2.1 |
| Line 2 | .03 | .04 | .03 | .07 | .1 | .05 | .07 | .04 | .04 | 3.2 | 1.6 | 1.9 |

Proliferative index is determined by slope of the exponential growth phase of hMSC on polymers in Figure 2.3.

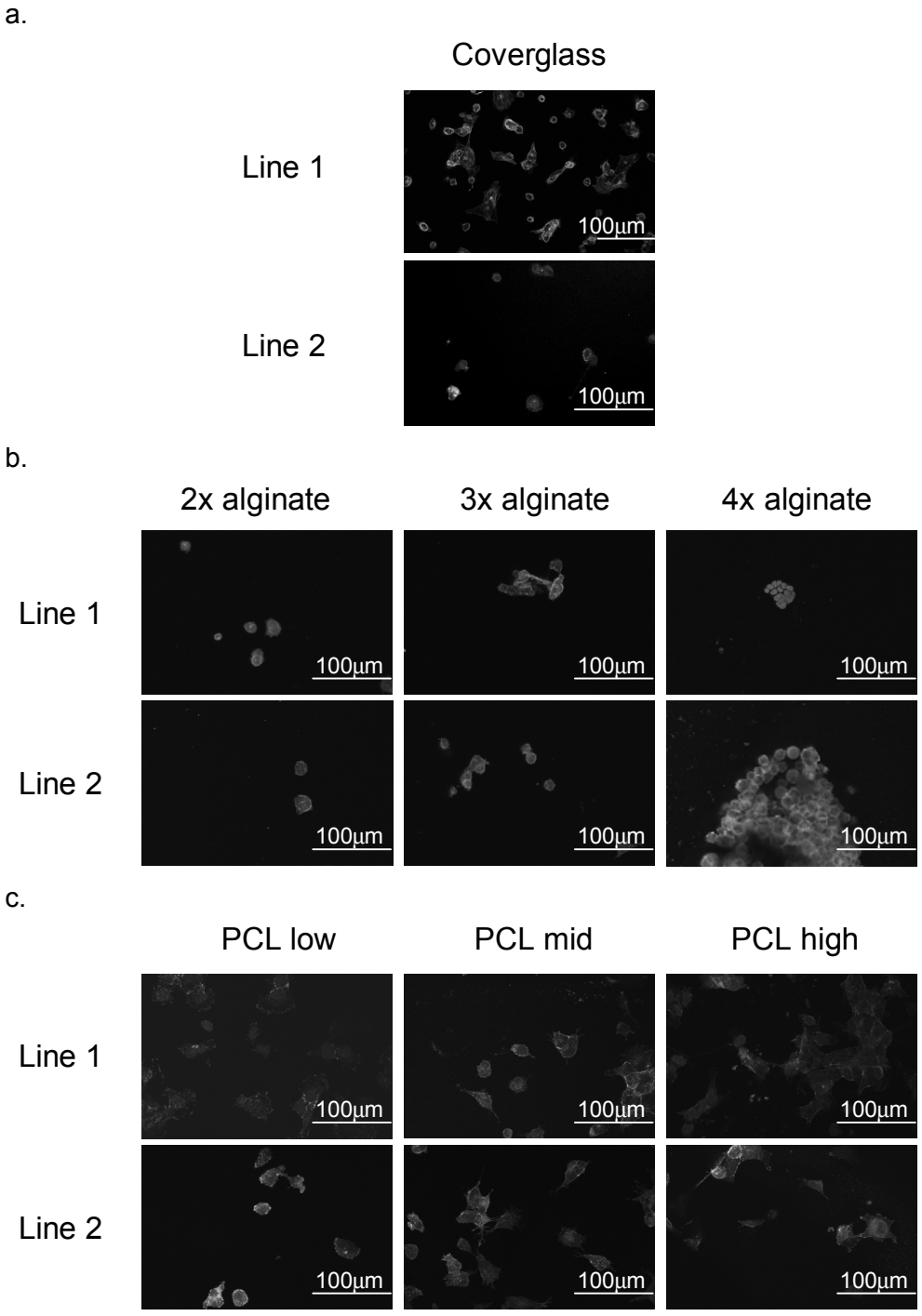


Figure 2.4a-c. Morphology of hMSC attached at one hour to coverglass, alginate and PCL. Surfaces shown above include coverglass (a) alginate (b) and PCL (c). Cells are stained for cytoskeleton (actin and paxillin) and nuclear (DAPI) proteins. Confocal images are projections of 0.8μm slices.

d.

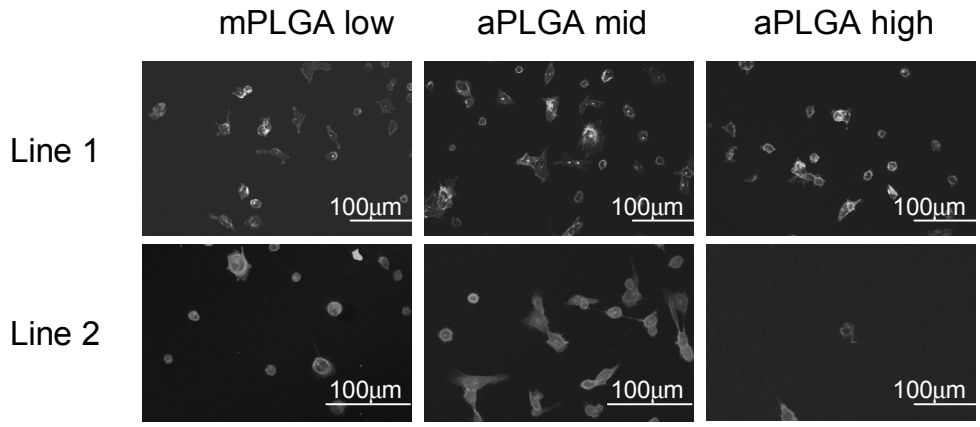


e.

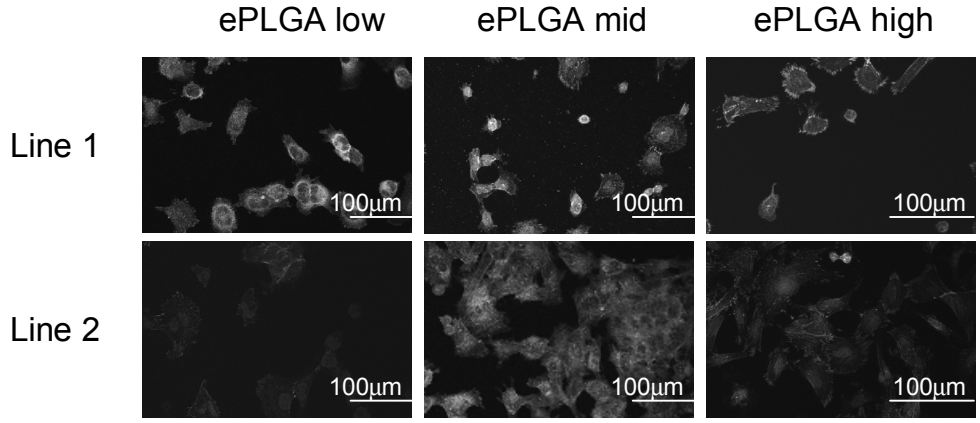


Figure 2.4d-e. Morphology of hMSC attached at one hour to PLGA. Surfaces shown above include a/m PLGA (d) and ePLGA (e). Cells are stained for cytoskeleton (actin and paxillin) and nuclear (DAPI) proteins. Confocal images are projections of 0.8μm slices.

Table 2.2. Relative numbers of focal adhesions of hMSC on all polymers.

| **Surface** | **Line 1** (mean = 37.6) | **Line 2** (mean = 38.5) |
|---|---|---|
| Coverglass | 29.4 | 33.9 |
| ePLGA low | 71.5 | 41.1 |
| ePLGA mid | 67.5 | 72.3 |
| ePLGA high | 93.1 | 96.5 |
| PCL low | 34.7 | 31.7 |
| PCL mid | 44.4 | 45.9 |
| PCL high | 41.4 | 57.0 |
| mPLGA low | 29.9 | 26.7 |
| aPLGA mid | 27.4 | 27.7 |
| aPLGA high | 17.7 | 38.0 |
| 2x alginate | 9.1 | 14.8 |
| 3x alginate | 12.5 | 8.1 |
| 4x alginate | 10.9 | 6.7 |

Focal adhesions per cell are based on the presence of paxillin from confocal microscopy. Mean focal adhesion numbers between hMSC lines 1 and 2 are not statistically significant ($p>0.05$).

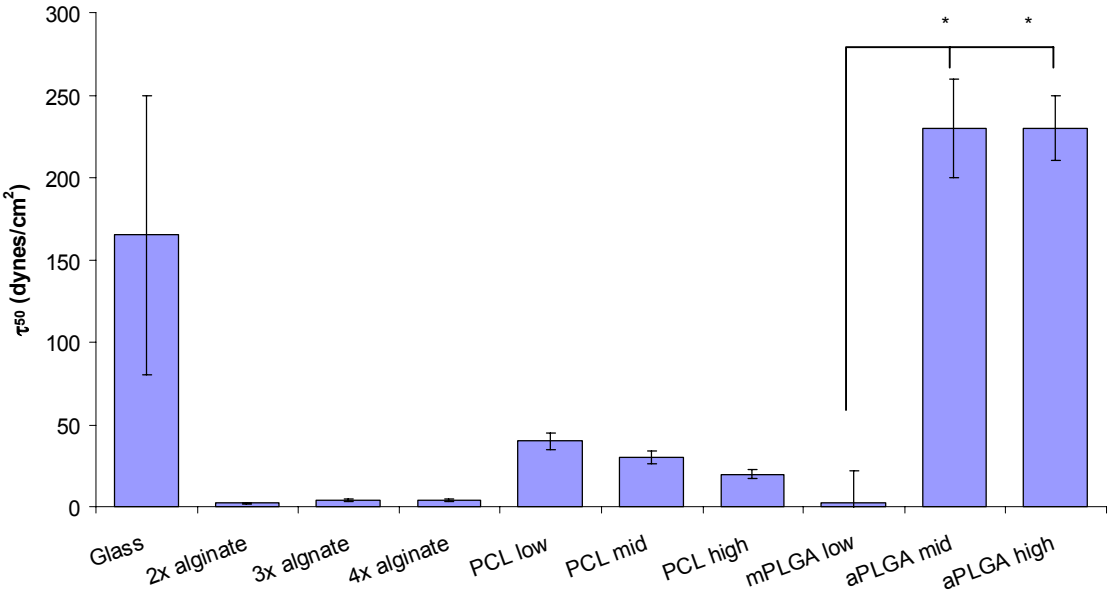


Figure 2.5a. Determination of $\tau_{50}$ using a fluid shear system. $\tau_{50}$ values (50% detachment strengths) of hMSC line 1 are plotted. There is no significant difference within alginate and PCL groups but statistically significant differences were noted in the a/mPLGA group; *p<0.01, n=3.

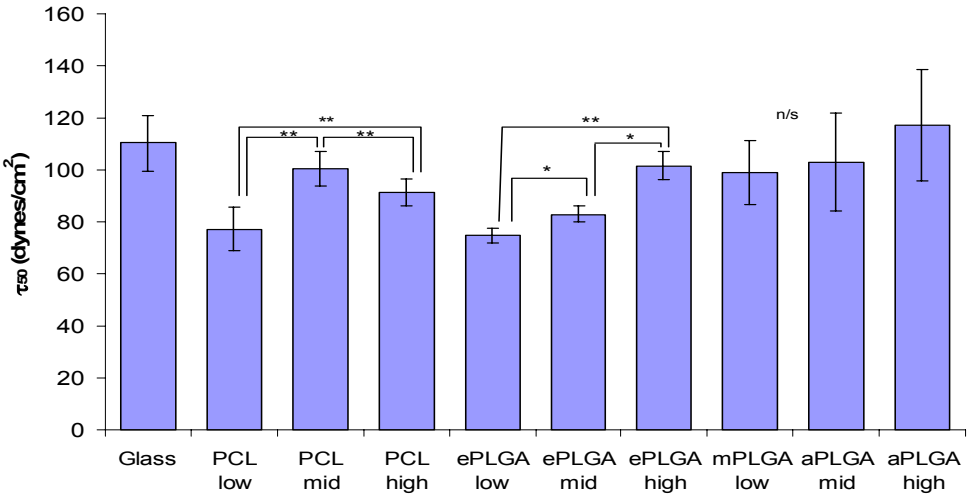


Figure 2.5b. Determination of $\tau_{50}$ using a spinning disk device. $\tau_{50}$ values (50% detachment strengths) of hMSC lines 1 and 2 are plotted. The a/mPLGA polymer group has significantly greater mean $\tau_{50}$ than the ePLGA and PCL groups (p*<0.05), however significance does not exist between mean $\tau_{50}$ of PCL and ePLGA; **p<0.01, n≥9.

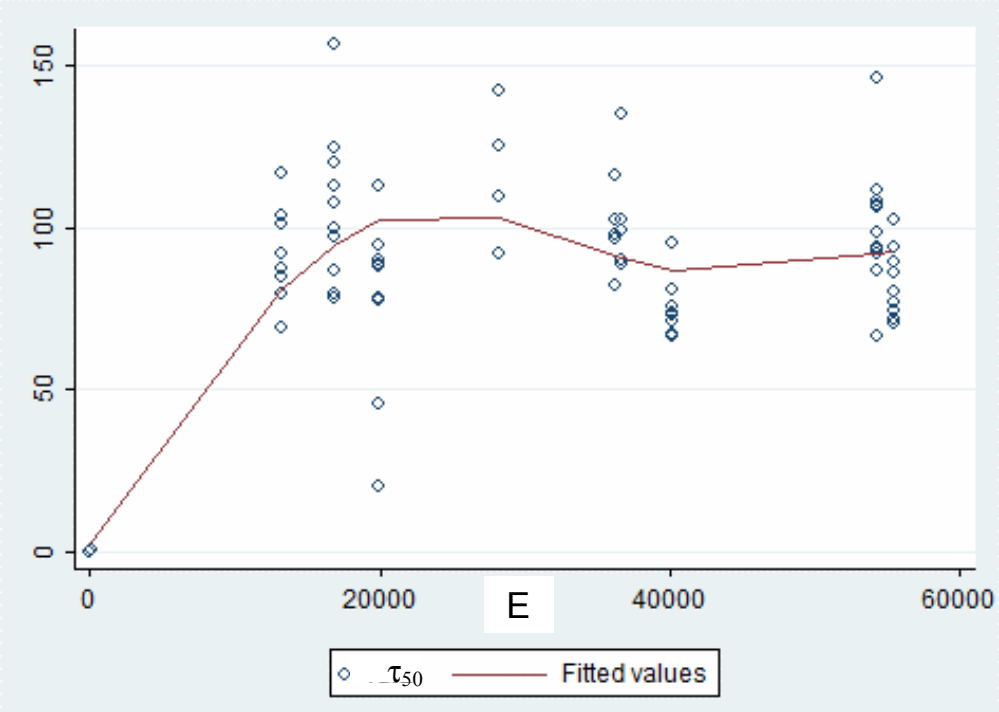


Figure 2.6a. Fit of $\tau_{50}$ with polymer elastic modulus (E) using a restricted cubic spline. Spinning disk data was fit with 4 knots ($R^2$=0.65). Units: $\tau_{50}$ (dynes/cm$^2$); E (kPa).

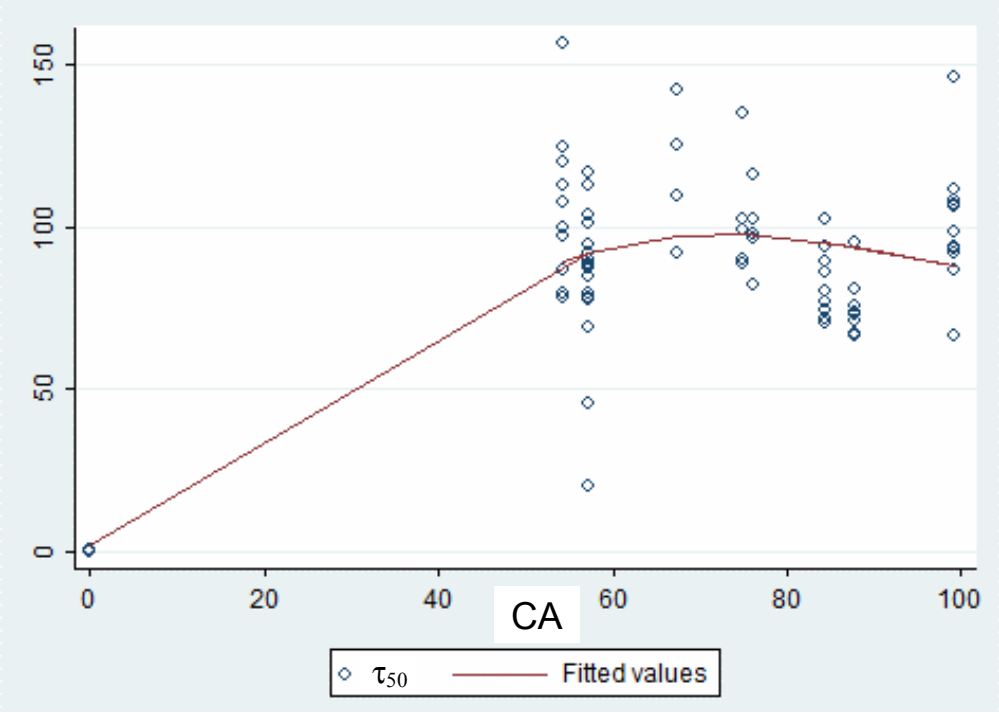


Figure 2.6b. Fit of $\tau_{50}$ with polymer contact angle (CA) using a restricted cubic spline. Spinning disk data was fit with 3 knots ($R^2$=0.68). Units: $\tau_{50}$ (dynes/cm$^2$); CA (degrees).

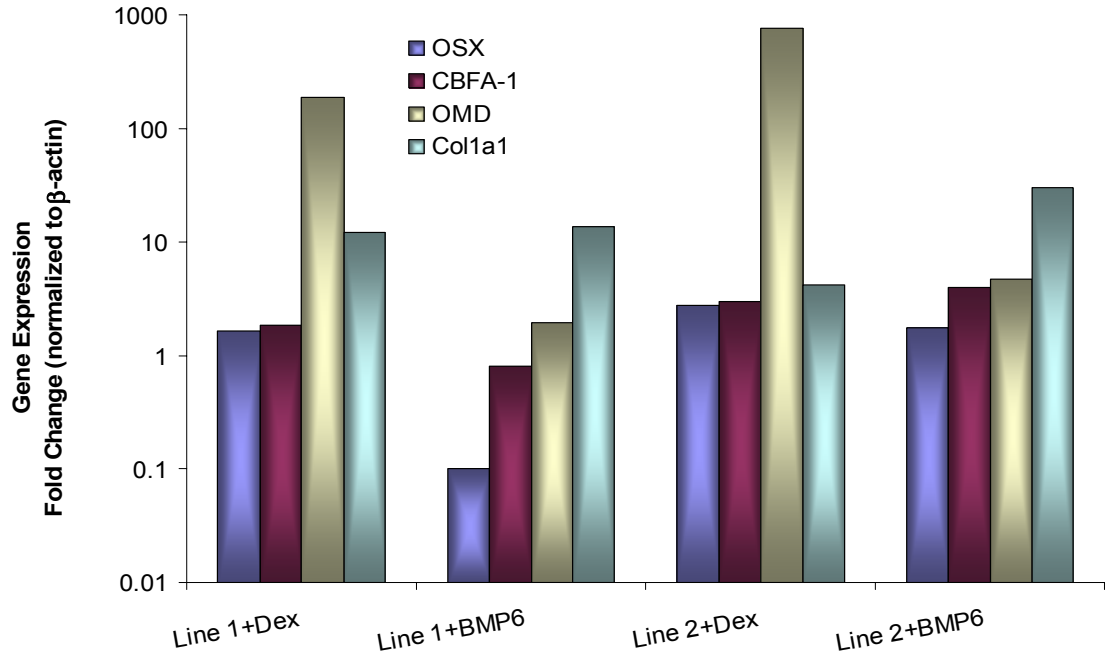


Figure 2.7. Typical osteogenic gene expression profile of hMSC lines 1 and 2. Cells were induced with either dexamethasone or BMP6 on TCP (data represents mRNA expression from 3 pooled samples relative to β–actin expression).

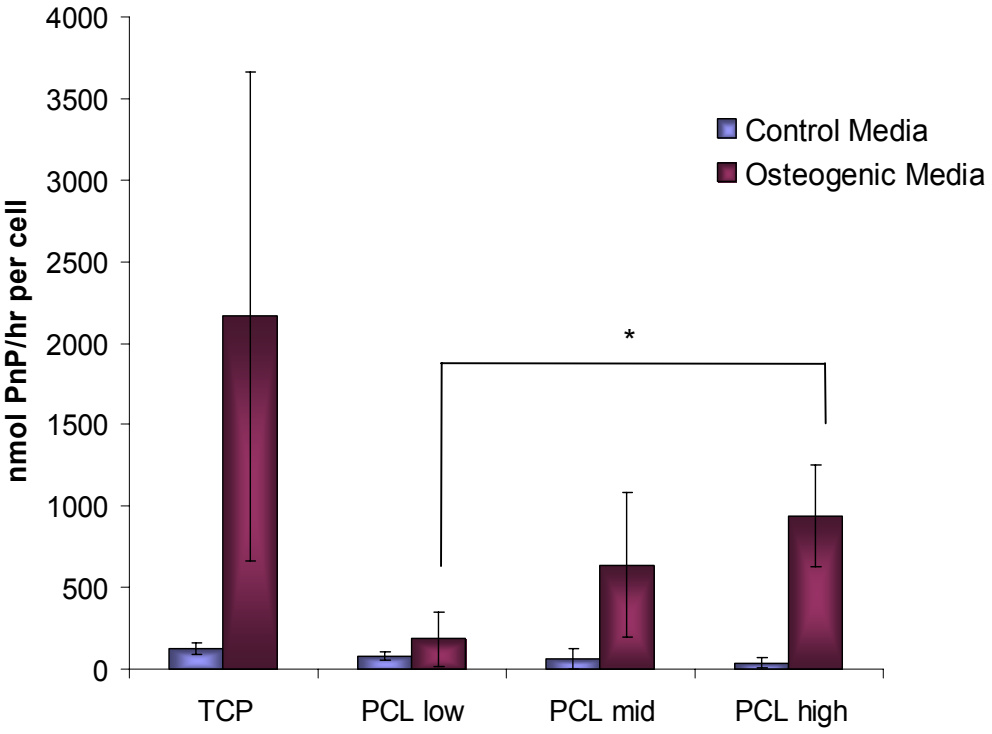


Figure 2.8a. Alkaline phosphatase activity of hMSC line 2 on PCL. Cells were harvested on day 15 and assayed for alkaline phosphatase activity using a colorimetric assay and normalized to cell number using the Cyquant assay; *p<0.05, n=3-4.

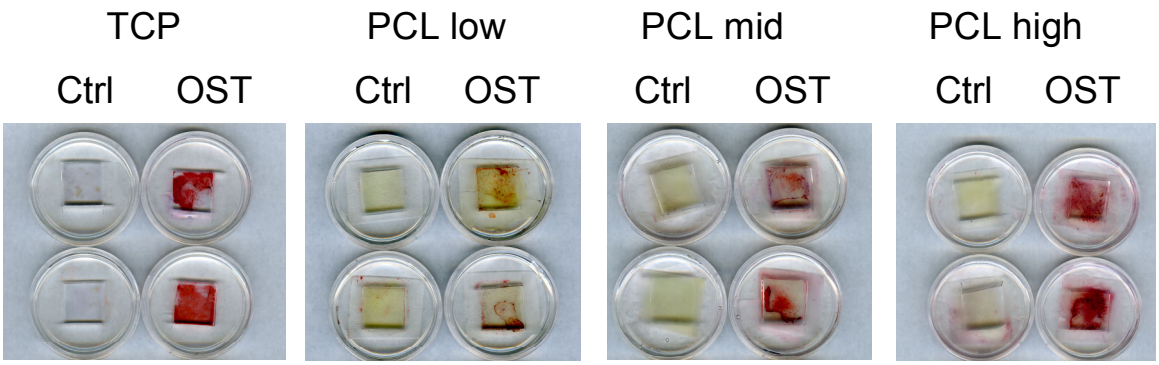


Figure 2.8b. Alizarin Red staining of hMSC line 2 on PCL. Cells were harvested on day 21 and stained for calcium phosphate with Alizarin Red; n=3.

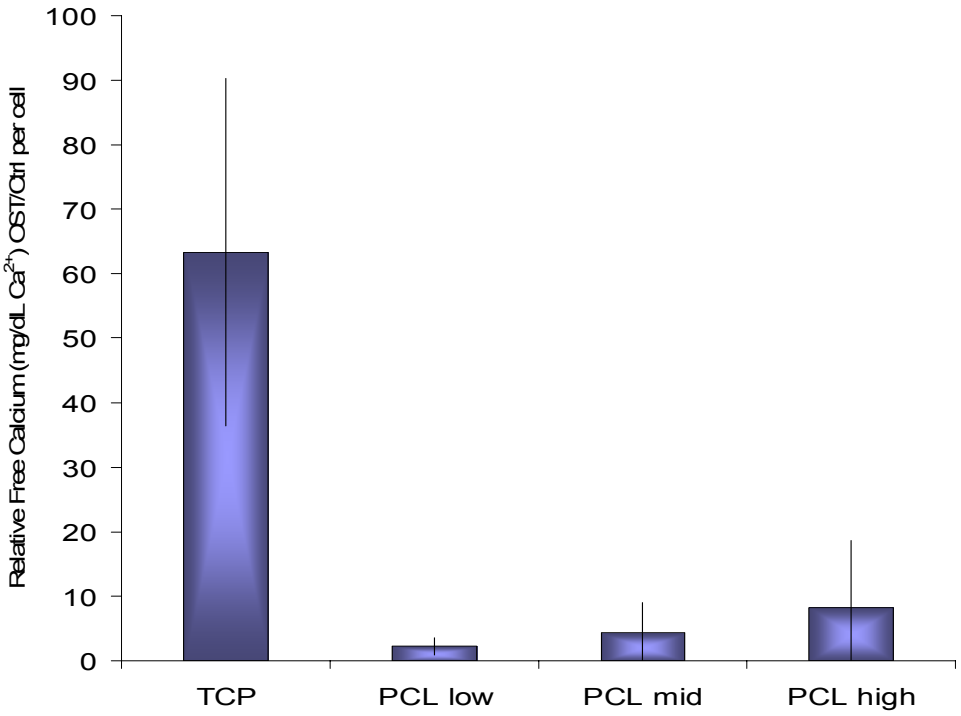


Figure 2.8c. Matrix-embedded calcium of hMSC line 2 on PCL. Cells were harvested on day 21. Mineral deposition was examined following liberation of calcium from the matrix overnight via CPC calcium assay as an alternative to Alizarin Red staining; n=3-4.

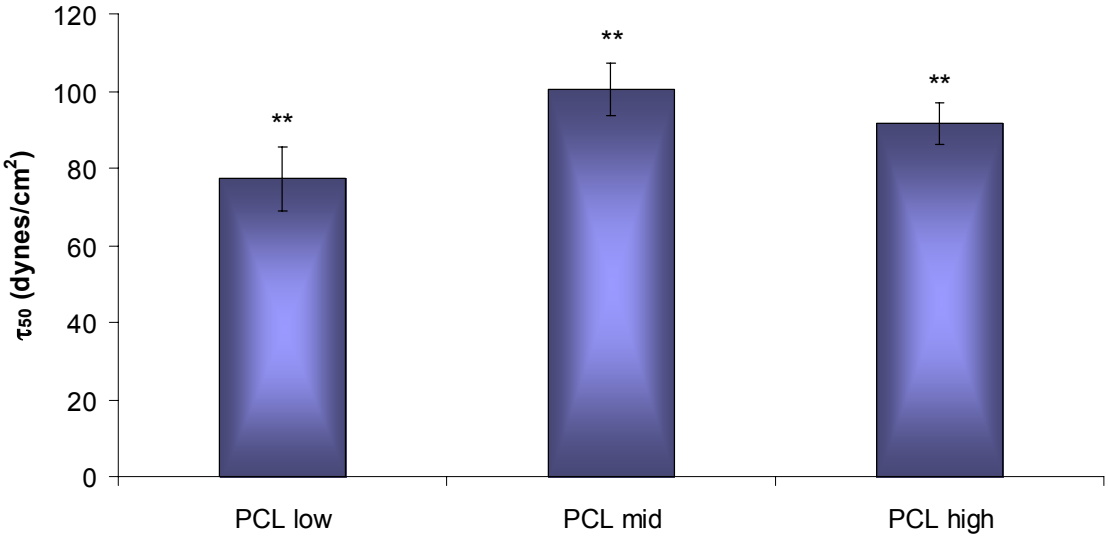


Figure 2.8d. Adhesion strength on PCL (I). $\tau_{50}$ for PCL is plotted for comparison with Figures 2.8a-c. All values are significantly different from one another; **p<0.01. Data originates from spinning disk data in Figure 2.5b.

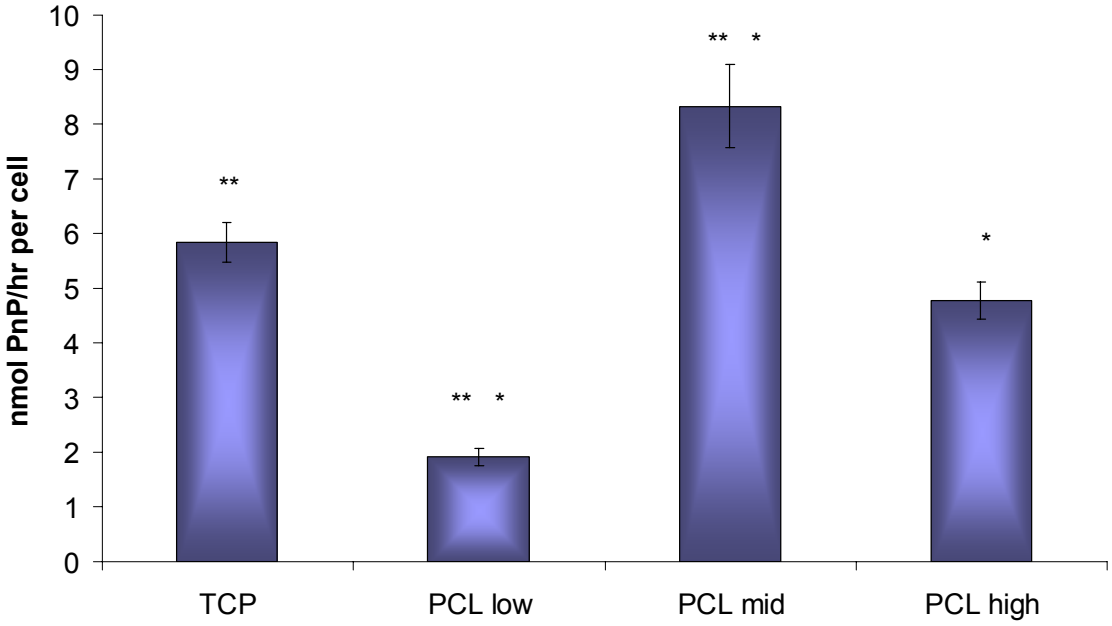


Figure 2.9a. Alkaline phosphatase activity of hMSC line 1 on PCL. Cells were harvested on day 15 and assayed for alkaline phosphatase activity using a colorimetric assay and normalized to cell number using the Cyquant assay. Values plotted express fold change in osteogenic versus control treatment. Matched symbols represent statistically significant differences at the following levels; *p<0.05, **p<0.01, n=3-4.

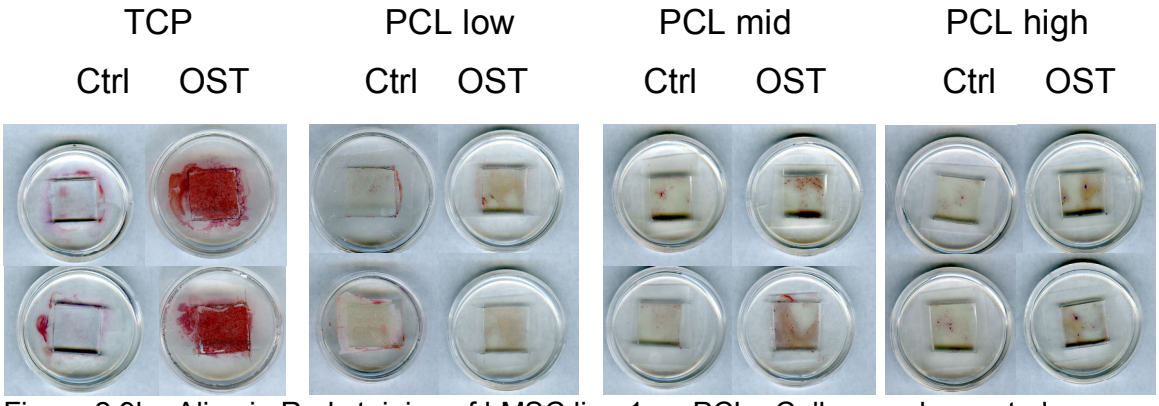


Figure 2.9b. Alizarin Red staining of hMSC line 1 on PCL. Cells were harvested on day 21 and stained for calcium phosphate with Alizarin Red; n=3-4.

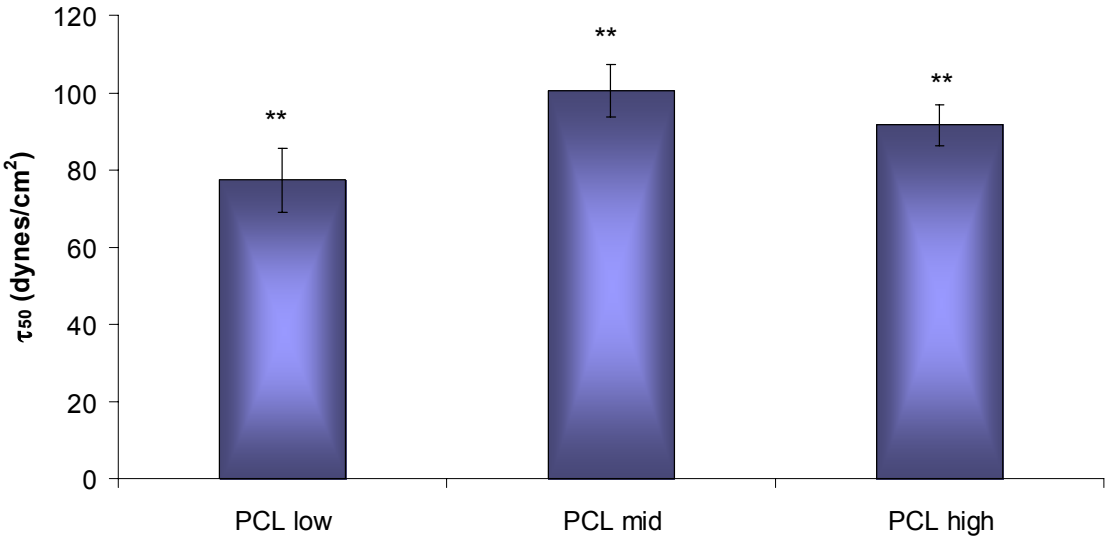


Figure 2.9c. Adhesion strength on PCL (II). $\tau_{50}$ for PCL is plotted for comparison with Figures 2.9a-b. All values are significantly different from one another; **p<0.01. Data originates from spinning disk data in Figure 2.5b.

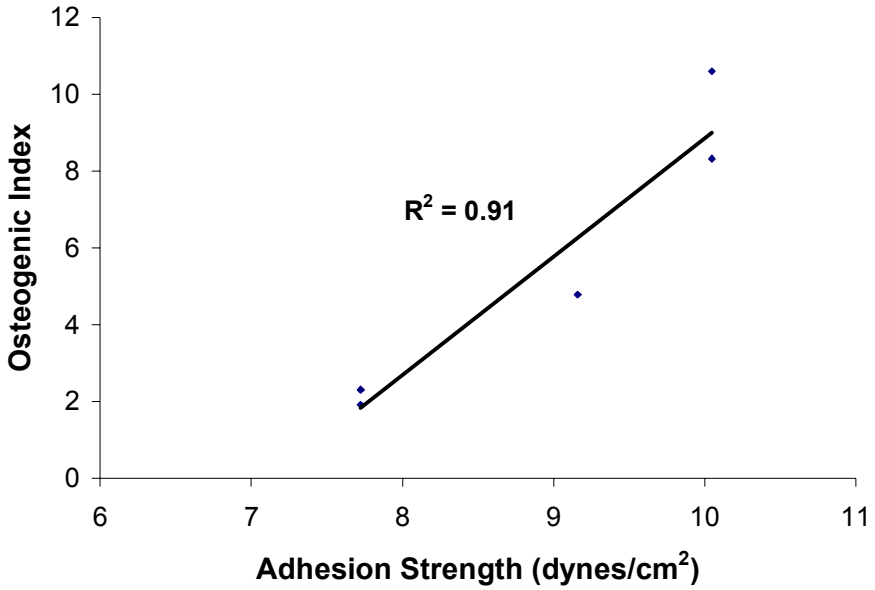


Figure 2.10. Relative osteogenic index correlation with adhesion strength on PCL. Normalized alkaline phosphatase activity for osteogenic relative to control treatment for hMSC lines 1 and 2 (from Figures 2.8a and 2.9a) is plotted against adhesion strength for PCL as determined by spinning disk. Trendline indicates a linear fit; $p<0.05$.

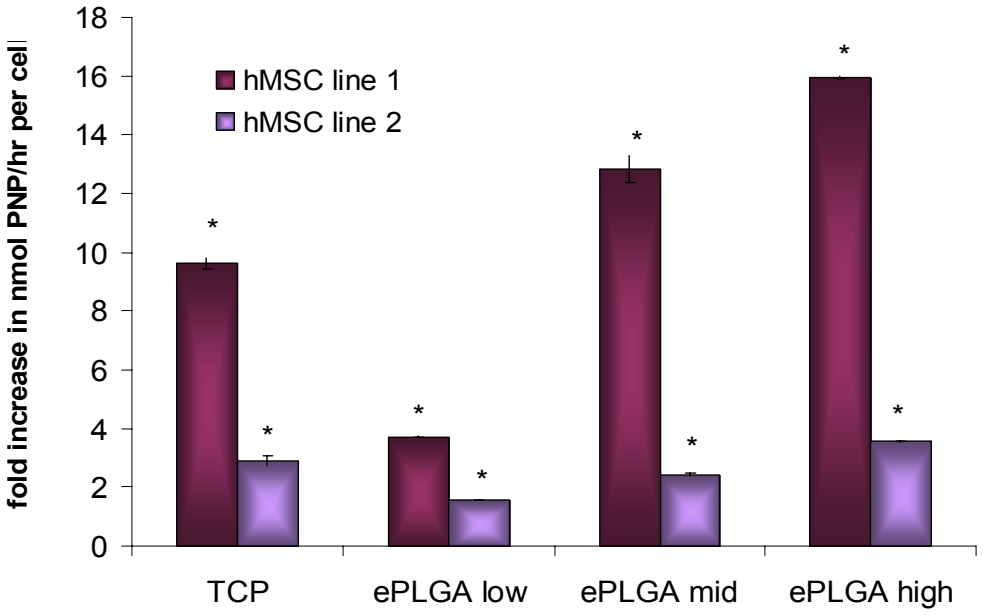


Figure 2.11a. Alkaline phosphatase activity of hMSC lines 1 and 2 on ePLGA. Cells were harvested on day 15 and assayed for alkaline phosphatase activity using a colorimetric assay and normalized to cell number using the Cyquant assay. All values are significantly different from one another; *p<0.05, n=3-4.

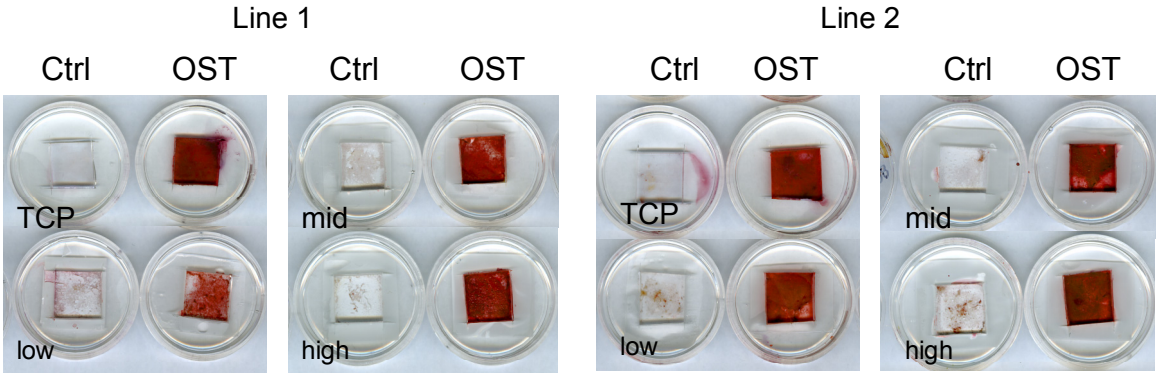


Figure 2.11b. Alizarin Red staining of hMSC lines 1 and 2 on ePLGA. Cells were harvested on day 34 and stained for calcium phosphate with Alizarin Red; n=3-4.

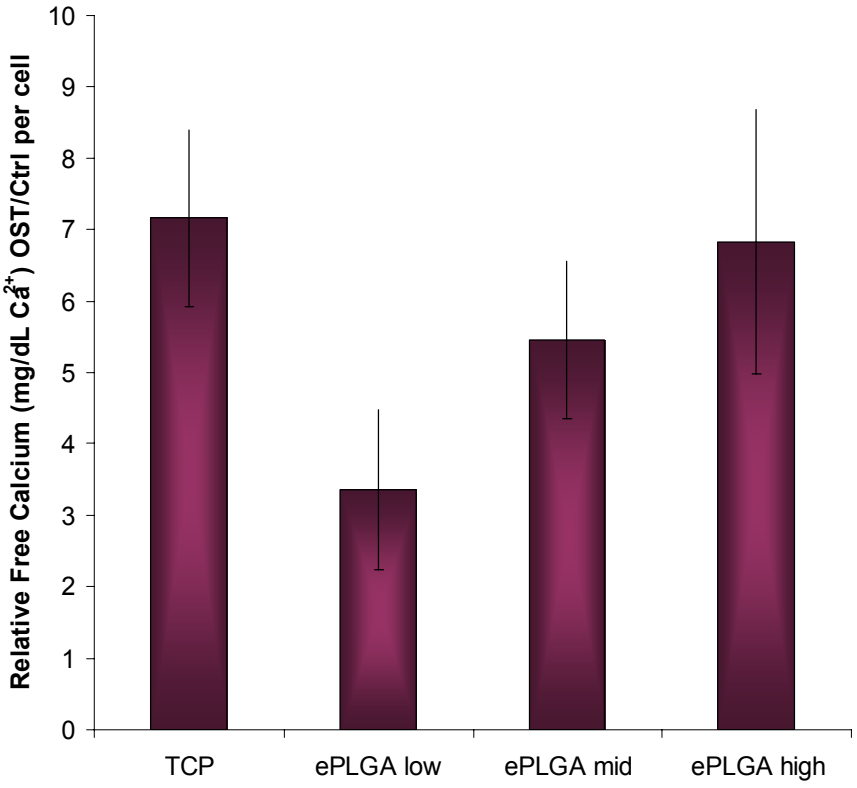


Figure 2.11c. Matrix-embedded calcium of hMSC lines 1 and 2 on ePLGA. Cells were harvested on day 21. Mineral deposition was examined following liberation of calcium from the matrix overnight via CPC calcium assay as an alternative to Alizarin Red staining; n=3-4.

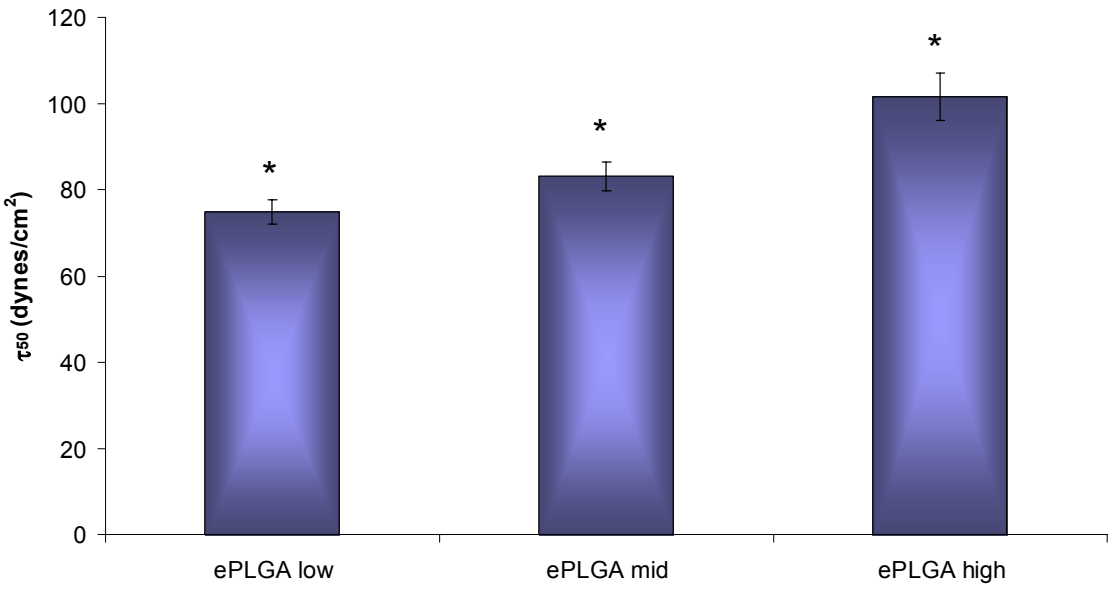


Figure 2.11d. Adhesion strength on ePLGA. $\tau_{50}$ for ePLGA is plotted for comparison with Figures 2.11a-c. All values are significantly different from one another; *p<0.05. Data originates from spinning disk data in Figure 2.5b.

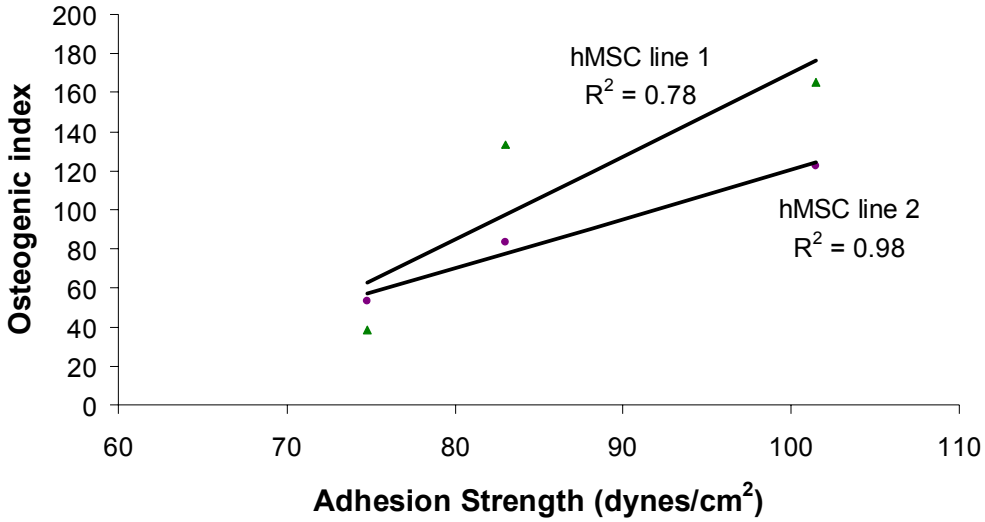


Figure 2.12. Relative osteogenic index correlation with adhesion strength on ePLGA. Normalized alkaline phosphatase activity for osteogenic relative to control treatment for hMSC lines 1 and 2 (from Figure 2.11a) is plotted against adhesion strength for ePLGA as determined from spinning disk data. Trendline indicates a linear fit; p<0.05 for hMSC line 2.

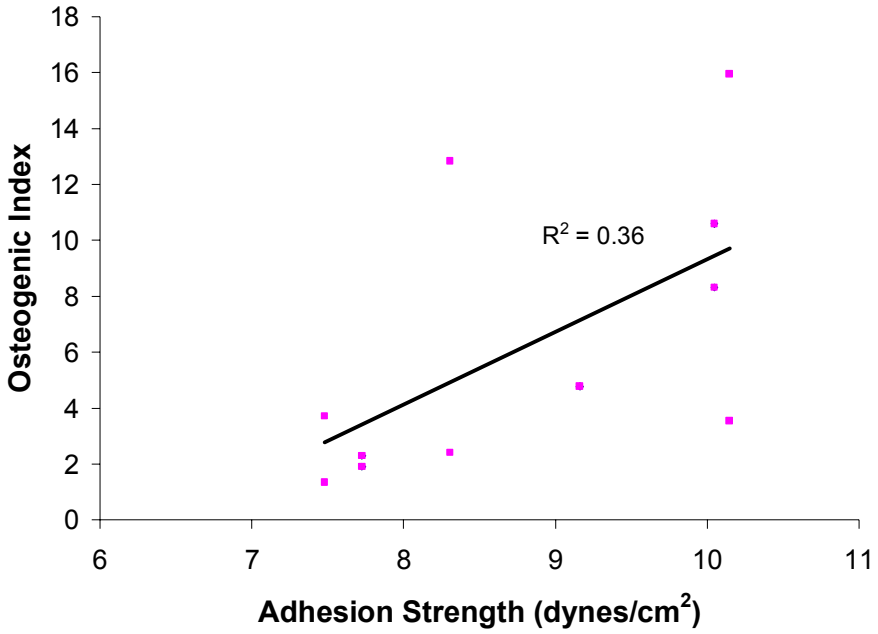


Figure 2.13. Relative osteogenic index correlation with adhesion strength on both PCL and ePLGA. Normalized alkaline phosphatase activity for osteogenic relative to control treatment for hMSC lines 1 and 2 (from Figures 2.8a, 2.9a and 2.11a) is plotted against adhesion strength for both PCL and ePLGA as determined by spinning disk data. Trendline indicates a linear fit; $p>0.05$.

# CHAPTER III

## hMSC ADHESION SIGNALING IN OSTEOGENIC DIFFERENTIATION ON BIODEGRADABLE POLYMERS

### Introduction

Cellular adhesion is a highly dynamic process that relies upon the specific signaling of effector molecules such as focal adhesion kinase and the small family GTPases. Focal adhesion kinase (FAK) is a 132kDa protein containing a focal adhesion targeting domain and numerous phosphorylation sites, including the tyrosine autophosphorylation site, Y397 which requires integrin-tethering to its substrate for activation [177]. RhoA, a member of the small family GTPases is required for focal adhesion formation and is important for stress fiber formation in the cytoskeleton and further is suppressed by FAK during focal adhesion turnover [110] [74]. Both FAK and RhoA have been shown to influence hMSC differentiation.

FAK promotes hMSC osteogenesis via ERK1/2 signaling and transient knockdown of total FAK using siRNA inhibits overall differentiation, although differentiation effects on a per cell basis were not reported [178]. FAK has been similarly found to be important for hMSC differentiation on laminin-5 [51].

RhoA mediates hMSC osteoblast and adipocyte differentiation in cells of different shapes through a Rho-kinase (ROCK) mechanism [103]. Recently, it was found that the neuronal protein Stathmin-like 2, which takes part in cytoskeletal regulation, is

increased during hMSC osteogenesis by dexamethasone treatment, is inhibited by treatment with the RhoA kinse inhibitor, Y27632 and is essentially unexpressed during adipogenesis [179]. This suggests that Stathmin-like 2 may be a part of the RhoA signaling pathway which modulates hMSC differentiation.

Little is known, however about the importance of either FAK or RhoA activity in mediating hMSC-biomaterial interactions. One group showed that PLGA and PCL selectively adsorbed collagen type I and vitronectin, respectively [144], and in a follow-up study showed that despite hMSC displaying different profiles of integrins in response to surfaces coated with either types of proteins, both interactions were dependent on FAK signaling, and ostegenesis was decreased when FAK was disrupted in hMSC grown on either protein [180]. Less still is understood about the role of RhoA in hMSC-biomaterial interactions although RhoA has been implicated in osteogenesis and BSP expression seen in murine MC3T3E1 cells grown on nanofibrous PLLA thin films. In particular, cells demonstrating improved osteogenesis markers on nanofibrous films exhibited decreased RhoGTPase activity with respect to smooth PLLA films [181].

In Chapter II, we demonstrated that when cells are grown on materials that show higher adhesion strength, there is an increase in osteogenic differentiation. Thus given that FAK and RhoA are critical adhesion signaling molecules found in multiple cell types, we sought to determine whether modulation of the activity of these proteins will impact hMSC-biomaterial adhesion interactions and osteogenic differentiation on ePLGA in particular. We hypothesize that disruption of FAK and Rho signaling will result in decreased osteogenesis on high adhesion strength ePLGA.

**Results**

Focal adhesion kinase studies on ePLGA

Immortalized hMSC were transduced with a pRLP2-based retroviral vector containing either eGFP, the FAK mutants DTER, Y397 or FRNK, or empty vector pRLP2 as a control. Successful transduction was displayed by observing high eGFP expression in the control (Figure 3.1a) and also by quantifying Y397 phosphorylation status by ELISA (Figure 3.1b). Observing hMSC transduced with either control or FAK mutant retroviruses on ePLGA surfaces or tissue culture plastic at approximately one hour of interaction, all mutants displayed a phenotype that differed from the control vector, pRLP2 (Figure 3.2). In particular DTER and FRNK mutants displayed very poor adherence while Y397 cells exhibited improved actin cytoskeleton formation, but aberrant cell morphology. On coverglass, low and mid ePLGA, Y397 cells demonstrated an elongated phenotype distinct from pRLP2, while on high ePLGA, spreading improved, as evidenced by increased staining for vinculin at the cell edges. These changes in morphology corresponded with normalized numbers of focal adhesions as Y397 cells had similar numbers of focal adhesions as pRLP2 cells, while both FRNK and DTER cells exhibited dramatically fewer focal adhesions than either Y397 or pRLP2 hMSC (Table 3.1).

Cell-fibronectin interactions can promote focal adhesion formation [69], and we next sought to determine whether quantities of adsorbed fibronectin varied across surface type, potentially explaining the changes seen in focal adhesion number within a single cell type. Radiolabeling studies with iodinated fibronectin on ePLGA demonstrated no significant difference in fibronectin adsorption, except at the maximal dose of 20μg/mL, where both ePLGA mid and high had greater adsorption than ePLGA low ($p<0.05$) (Figure 3.3).

Transduced cells were plated on ePLGA and TCP for a period of 15-27 days (Figure 3.4a). Alkaline phosphatase activity demonstrated that FAK mutants showed an increase in osteoblastic activity on a per cell basis with respect to control. In particular, both DTER and Y397 hMSC showed a large increase in alkaline phosphatase activity over the control vector. Further, within each cell type, those grown on ePLGA high showed the greatest degree of osteoblastic activity (although Y397 did not show a significant increase) ($p<0.05$) (Figure 3.4a).

At day 27, a similar relationship within cell type was seen for deposited mineral as evidenced by Alizarin Red staining (Figure 3.4b) and quantification of matrix-embedded calcium (Figure 3.4c). Alizarin Red staining in this experiment may be difficult to interpret as cell number varied substantially for the different cell types. In particular, DTER cells grew very poorly and stained mineral is difficult to see on a macroscopic scale. However, it does appear that for all cell types, ePLGA high demonstrated the greatest promotion of mineral formation (although not statistically significant with respect to the other ePLGA surfaces, Figure 3.4c). Expression of osteogenic transcript markers at 12 days of culture for pRLP2 and DTER cells on TCP or ePLGA showed similar but very high induction of osteomodulin with DTER hMSC showing increased expression of collagen 1$\alpha$1, and the transcription factors osterix and Cbfa1 over the pRLP2 control (Figure 3.4d).

RhoA studies on ePLGA

Immortalized hMSC were transduced with a retrovirus containing either constitutively expressed RhoA (RhoV14), dominant negative RhoA (RhoN19), empty vector (pRET) or transduction control vector (eGFP). Success of transduction was evidenced by

examining the pRET-eGFP virus cells using fluorescence microscopy (Figure 3.5a) and via analysis of RhoA activity using a commercially available ELISA (Figure 3.5b). Attachment of RhoV14, RhoN19 and pRET control cells to tissue culture plastic over a period of 7 days showed that RhoV14 and RhoN19 cells attached and proliferated sooner than control cells on all surfaces, with RhoV14 showing the greatest cell-substrate interaction (Figure 3.6). When plated on ePLGA, RhoN19 cells appeared to develop greater reinforcement of adhesion complexes on ePLGA mid and ePLGA high and relatively poor adhesion on coverglass and ePLGA low (Figure 3.7). However when we quantified numbers of focal adhesions per cell, RhoN19 cells displayed somewhat fewer focal adhesions than control pRET cells on ePGLA mid and ePLGA high and higher numbers on coverglass and ePLGA low (although the means of pRET and RhoN19 cells were not significantly different, $p>0.05$) (Table 3.2). This represents an averaging effect as there were a large number of unspread RhoN19 cells on these surfaces as well as those represented in Figure 3.6. RhoV14 cells consistently displayed far larger numbers of focal adhesions than either RhoN19 or pRET cells, which was independent of surface type (mean focal adhesions are significantly different, $p<0.05$) (Table 3.2).

When grown under standard conditions on tissue culture plastic, RhoV14 cells displayed elevated levels of alkaline phosphatase activity and RhoN19 cells showed decreased alkaline phosphatase activity with respect to control at day 9, but not at day 6 (Figure 3.8a). During the course of differentiation, RhoA activity is dynamic which in our system shows greatest activity in cells demonstrating a subconfluent phenotype early on, while cells undergoing osteogenic induction display greater RhoA activity towards the terminal end of the experiment (Figure 3.8b) as found previously by others [103]. Additionally, calcium phosphate mineral is increased in RhoV14 cells at days 21

and 29 while RhoN19 cells show slightly decreased levels with respect to pRET controls (Figure 3.8c-d). The pRET retroviral vector contains an IRES-Puro for selection of cells expressing the transgene. When cells were selected for 10 days in puromycin and were then grown in differentiation media for a period of 21 days, the increase of mineral deposition in RhoV14 and decrease in RhoN19 cells with respect to control becomes further evident (Figure 3.8e).

Differentiation studies of RhoV14, RhoN19 and pRET cells on ePLGA versus TCP surfaces show that both alkaline phosphatase activity and matrix-embedded calcium is greatest for RhoV14 on all surfaces, and on ePLGA high in particular, while RhoN19 cells display alkaline phosphatase and calcium levels that are similar to pRET control cells on ePLGA high at day 15 (Figure 3.9a) and day 35 (Figure 3.9b) respectively.

Rho-associated kinase (ROCK) is an effector molecule of RhoA signaling, leading to stress fiber formation via phosphorylation of myosin light-chain kinase and has been shown to be important in hMSC osteogenesis [103] [153]. Y27632 is a synthetic compound that inhibits ROCK activity and has been commonly used in other investigations of RhoA signaling in vitro [124, 182]. When immortalized hMSC were plated on ePLGA surfaces and treated with or without Y27632 on a daily basis, cell morphology was strongly affected (Figure 3.10a) as cells treated with Y27632 showed increased numbers of processes, but poor membrane spreading and increased numbers of focal adhesions (or adhesion plaques) per cell (Table 3.3), which is in agreement with others [183]. When grown under differentiation conditions in the presence of Y27632, it was found that both alkaline phosphatase activity and mineral formation was significantly decreased in particular on surfaces displaying the largest adhesion strength (ePLGA high) (Figures 3.10b-d).

## Discussion

Focal adhesion kinase studies on ePLGA

Following transduction of hMSC with FAK mutants or empty vector control it is curious that only the DTER mutant caused a substantial decrease in phosphorylated Y397 as measured by ELISA. However, as the values from the ELISA were normalized to total protein, this does not necessarily mean that there is not an overall relative decrease in phopho-FAK at Y397. In particular, previous investigators using the same constructs found that both FRNK- and Y397F-transduced endothelial cells had similar levels of phosphorylated Y397 to control virus with respect to total protein, but that total FRNK or FAK levels (respectively) were substantially increased, leading to an overall decrease in phoshpo-FAK at Y397 [67]. While not directly quantifiable, total FAK protein of these lysates (as measured by Western Blot) also reflect these trends as both Y397 and FRNK have greater total FAK protein, and DTER has less total FAK than pRLP2 control (Figure 3.1b). Further, given that all FAK mutants displayed differences in proliferation over extended culture (not shown) and in morphology (Figure 3.2), this suggests that these constructs are indeed affecting FAK signaling in these cells. The morphology of both FRNK and DTER cells appears quite similar, which is not surprising considering both constructs are deletion mutants of FAK functional groups. DTER is a carboxy-terminus truncation mutant of FAK and lacks a kinase domain, while FRNK is a dominant negative of FAK which has been previously shown to cause delayed or impaired cell spreading [184]. These changes in morphology were strongly linked to decreased mean vinculin staining in DTER and FRNK cells with respect to Y397 and pRLP2 cells ($p<0.05$) (Table 3.1). Others have shown that endothelial cells transfected with the same Y397 or FRNK constructs in adenovirus have an inverse relationship depending on whether the cells are permitted to spread or not, as in spread cells, Y397 cells showed slightly increased area of focal adhesions than FRNK [67]. In this same

study, it is also interesting to note that in traction force studies, Y397 and control cells displayed similar amplitudes and frequency distributions while FRNK displayed increased cytoskeletal tension. Additionally, differences in vinculin staining suggests, perhaps that Y397 and pRLP2 had greater adhesion strength than FRNK or DTER cells as it has been shown that adhesion strength increases exponentially with both bound integrin numbers and vinculin recruitment [185] but this would need to be measured directly.

Changes in focal adhesion number within cell types do not appear to be linked to relative protein adsorption of the ePLGA surfaces as radiolabeling studies with iodinated fibronectin on ePLGA demonstrated no significant difference in fibronectin adsorption, except at the maximal dose of 20μg/mL, where both ePLGA mid and high had greater adsorption than ePLGA low ($p<0.05$) (Figure 3.3). This dose, however, is supraphysiologic as it is estimated that only 2-3μg/mL of fibronectin is present in 10% serum, which would be further reduced in our system as it uses only 2% serum [204]. Potentially, however, other adsorbed proteins such as vitronectin or collagen could have differential adsorption in our system, as previously shown to be important in PCL- or PLGA-hMSC interactions, respectively [143, 144, 180].

The results of differentiation experiments of FAK mutants and control virus hMSC on ePLGA and TCP suggest that negative modulation of FAK signaling and function increases osteoblastic activity in our system as both alkaline phosphatase activity and mineral deposition were all increased for these cells with respect to control virus. This was seen in particular for cells grown on ePLGA high, a surface previously demonstrated to have a relatively high adhesion strength for untransduced cells

(Figures 3.4a and Figure 3.4c). While these results are contrary to our hypothesis, these relationships are only elucidated when the respective data is normalized to cell number. It is particularly noteworthy that the DTER and even FRNK constructs negatively impact proliferation (data not shown) as others have described [67]. It has been suggested that the processes of proliferation and differentiation in hMSC are linked, but they appear to be regulated by numerous signaling proteins, such as the Wnts [186]. With respect to the role of FAK, a recent study showed that siRNA knockdown of FAK suppresses hMSC differentiation [178]. Although a wild-type FAK control or constitutively-active FAK was not used in our system, it does appear that FAK signaling may actually impair hMSC osteogenesis on a variety of surface-types. While seemingly contrary to the reference above, FAK is known to have dual roles in cell proliferation and could also have a dual role in hMSC osteogenesis [67]. An additional adhesion molecule that could offer further insight into the role of FAK in our system is Rac1. A member of the small GTPase family, Rac1, which localizes to focal adhesions and is important for membrane ruffling and cell spreading has recently been found to be regulated by betaPIX, which is phosphorylated by FAK [187]. The role of Rac1 in hMSC differentiation, however remains to be fully explored [110].

The unique gene expression profile of the pRLP2 and DTER cells on ePLGA vs TCP suggests additional signaling mechanisms to explore. While changes in expression of Cbfa1 were not significant in our system, others have found similar profiles in primary hMSC [178]. Osteomodulin (OMD) is an 85kDa proteoglycan that has been found to directly bind hydroxyapatite found in bone [188]. Osteomodulin contains as many as 8 tyrosine sulphated residues located in the N-terminal extension and is isolated from bone in a disulfide-bonded complex with osteonectin. Both osteomodulin mRNA and protein are expressed in bone trabeculae and can support in vitro adhesion of

osteoblasts as well as fibronectin via αvβ3 integrin [189]. Osteomodulin is expressed very highly by cells induced by dexamethasone, ascorbic acid and beta-glycerol phosphate in our system. A further investigation of osteomodulin and integrin expression of all the FAK mutants on ePLGA might serve to elucidate the importance of this interaction. It is difficult to draw any conclusions at this time as to how osteomodulin expression may be regulated by adhesion, thereby promoting osteogenesis, however recently, it was found that dexamethasone induces expression of the LIM protein, Four and half lim 2 (FHL2) in murine and human MSC. FHL2 was found to physically interact with beta-catenin and promote nuclear localization of the complex to stimulate canonical Wnt signaling via TCF/LEF transcription, resulting in increased alkaline phosphatase and Runx2 expression [190]. The hMSC lines studied here do express FHL2 mRNA, however it is unclear at this time whether dexamethasone stimulates its expression (data not shown). Interestingly, FHL2 has been shown to interact with a variety of integrins in myoblast and ovarian cells as well as pp125FAK (FAK) and its role has been suggested as an adaptor/docking protein involved in integrin signaling for focal adhesion formation, and was recently found to be important for extracellular matrix assembly [191]. Importantly, it has been shown to interact with $\alpha$5 integrins in osteoblasts and is critical for osteogenesis [192]. Additional study of FHL2 expression in our system may help clarify the mechanism of altered focal adhesion formation and signaling we have shown here. In reference to the increase in type I collagen expression in DTER hMSC, it has been shown that de novo formation of type I collagen protein is important for osteogenesis of hMSC on PLGA [193], further supporting the result that disregulation of FAK signaling by DTER supports increased osteogenesis of hMSC on ePLGA.

Rho Studies on ePLGA

As expected, hMSC transduced with RhoV14 displayed increased RhoA activity and reinforcement of adhesion complexes, while RhoN19 hMSC had decreased RhoA activity and altered morphology. Although RhoN19 cells displayed consistently decreased osteogenic activity with respect to RhoV14 cells, it is somewhat surprising that in experiments on ePLGA, in a few instances RhoN19 hMSC had higher osteogenic activity relative to empty vector controls (Figure 3.9a-b). This may be due to the relatively weak decrease of RhoA activity due to high endogenous expression (Figure 3.5b and Figure 3.8b) which is thought to only occur on particularly stiff surfaces [127]. This could also suggest that modulation of RhoA activity either positively or negatively can increase osteogenic activity, however, this would warrant further investigation. Additionally, it should be re-iterated that as RhoA expression is dynamic, the effects seen at days 15 and even 35 may not be indicative of the continually changing activity levels of RhoA (Figure 3.8b). However, a similar relationship was found in the attachment and proliferation of Rho-modulated hMSC over a period of 7 days (Figure 3.6), suggesting that increasing RhoA activity positively impacts attachment, proliferation and differentiation, but that the dominant negative RhoN19 has a lessened effect with respect to increased activity (RhoV14). However, it is difficult to tell what relationship RhoN19 modulation of signaling may have relative to empty vector control (pRET). In particular, it should be noted that hMSC grown on ePLGA high consistently displayed decreased proliferation, but the greatest changes in osteogenic activity with respect to the other surfaces across all cell types, and specifically in RhoV14 hMSC (Figure 3.9a-b). This is further consistent with our findings in previous studies of FRNK and DTER expressing hMSC which also had inhibited cell growth, but showed increased osteogenesis.

Daily treatment with Rho-associated kinase (ROCK) inhibitor Y27632 lead to significant changes in hMSC cell morphology (Figure 3.10a) and increased vinculin staining (Table 3.3), but the greatest impact on osteogenic activity was witnessed on ePLGA high (Figures 3.10b-d), the surface demonstrating the greatest adhesion strength with unstransduced hMSC. As the effect of RhoA signaling on hMSC differentiation is transduced via phosphorylation of myosin-light chain kinase by ROCK, this is in agreement with earlier studies showing that increased RhoA and ROCK signaling positively affect hMSC differentiation and that blocking activity of this molecule negatively impacts this process [103]. The results of enhanced vinculin staining with Y27632 treatment are curious in light of results with Rho mutant hMSC described earlier, whereby increased focal adhesion number seems to correlate with enhanced differentiation. However, based on the data collected for ROCK inhibitor studies, adhesion plaque categories are difficult to determine. This may be important for understanding this effect, as Y27632 treatment has been shown to block progression of focal complexes into focal adhesions and stress fiber formation, despite increased expression of integrins particularly at the cell center [194-196]. In our system, Y27632 did appear to decrease stress fiber number, so it is possible that an effective decrease was seen in focal adhesions (which are associated with stress fibers) but there was an increase in focal complex number. This hypothesis, however, would need to be tested directly with additional analysis.

Finally, the consistent relationship of altered osteogenic activity being the most perturbed on the ePLGA surface exhibiting the greatest adhesion strength in unstransduced cells suggests that perhaps adhesion strength of hMSC expressing both Rho and FAK constructs is significantly altered on this surface and warrants further investigation. Additionally, if hMSC ostegenesis is dependent on cellular adhesion

strength, it appears that disregulating FAK and RhoA signaling may disrupt this dependence.

In considering the results obtained from these studies, we can begin to develop a picture of how for a material type, adhesion strength, focal adhesions and FAK, and Rho and ROCK signaling influence hMSC differentiation. Larger adhesion strengths appear to promote hMSC osteogenesis via RhoA-ROCK signaling and cells exhibiting this behavior are associated with a greater degree of focal adhesions aligned with stress fibers. The role of FAK signaling in this process is less clear, but appears to be important for this system as disregulation caused by truncation of the c-terminus leads to reduced focal adhesion number and an increase in osteogenesis on a per cell basis, despite in some cases, showing a global decrease in osteogenesis. To further clarify an interaction effect of Rho and FAK signaling, it would be important to quantify perturbations in these pathways within the same system. It has previously been shown that FAK transiently suppresses RhoA activity and that FAK-/- cells can lead to constitutive activation of RhoA and loss of focal adhesion turnover [110]. Further understanding of how FAK and RhoA signals integrate for downstream effects on hMSC differentiation could potentially clarify a role for adhesion signaling molecules in hMSC osteogenesis on a variety of substrates.

**FAK Studies**

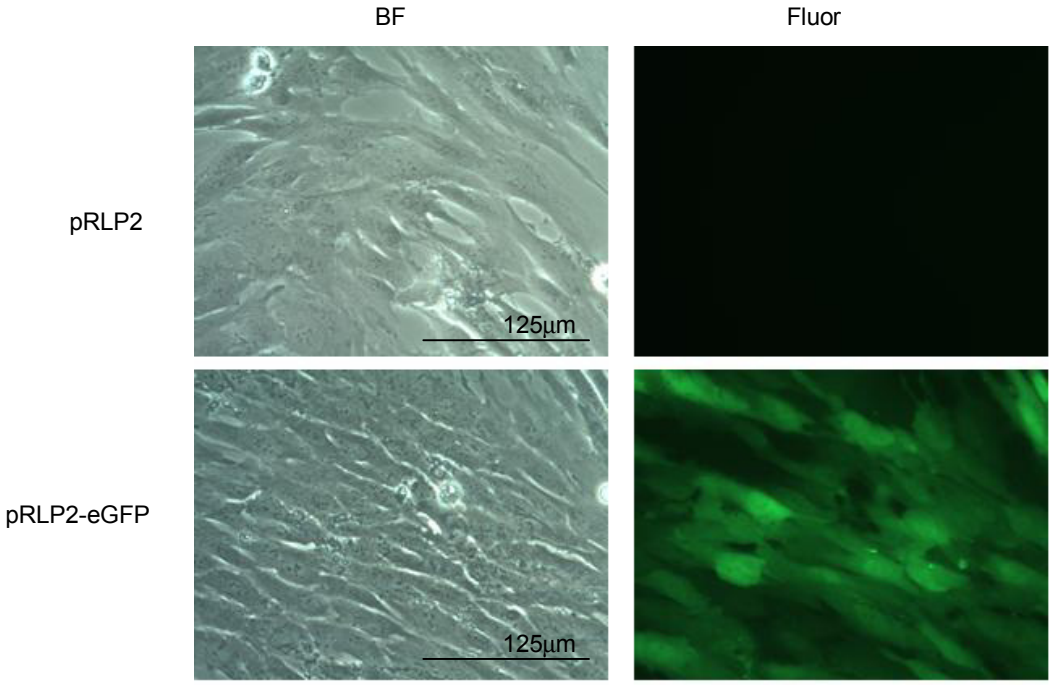


Figure 3.1a. Transduction efficiency of hMSC transduced with FAK mutant retroviruses. hMSC transduced with FAK mutant retroviruses demonstrated a high level of transduction efficiency, as evidenced by the pRLP2-eGFP image above. pRLP2 indicates empty retroviral vector. Other lines created include pRLP2-Y397, pRLP2-DTER and pRLP2-FRNK (not shown).

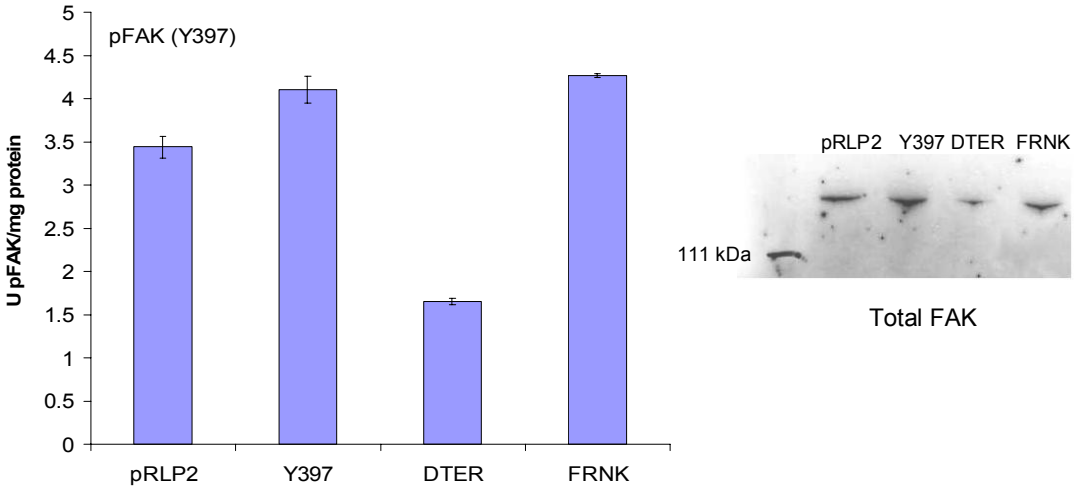


Figure 3.1b. hMSC phosphorylation of Y397 FAK following retroviral transduction with FAK mutant constructs. Following one week of culture under growth conditions, FAK mutant or control hMSC were lysed, and cell lysates were assayed for Y397 phosphorylation with an ELISA and normalized to total protein. Total FAK was assayed by Western Blot. Constructs used: pRLP2 (empty vector control), Y397 (phenylalanine substitution at Y397 phosphorylation site), DTER (truncation mutant) and FRNK (dominant negative).

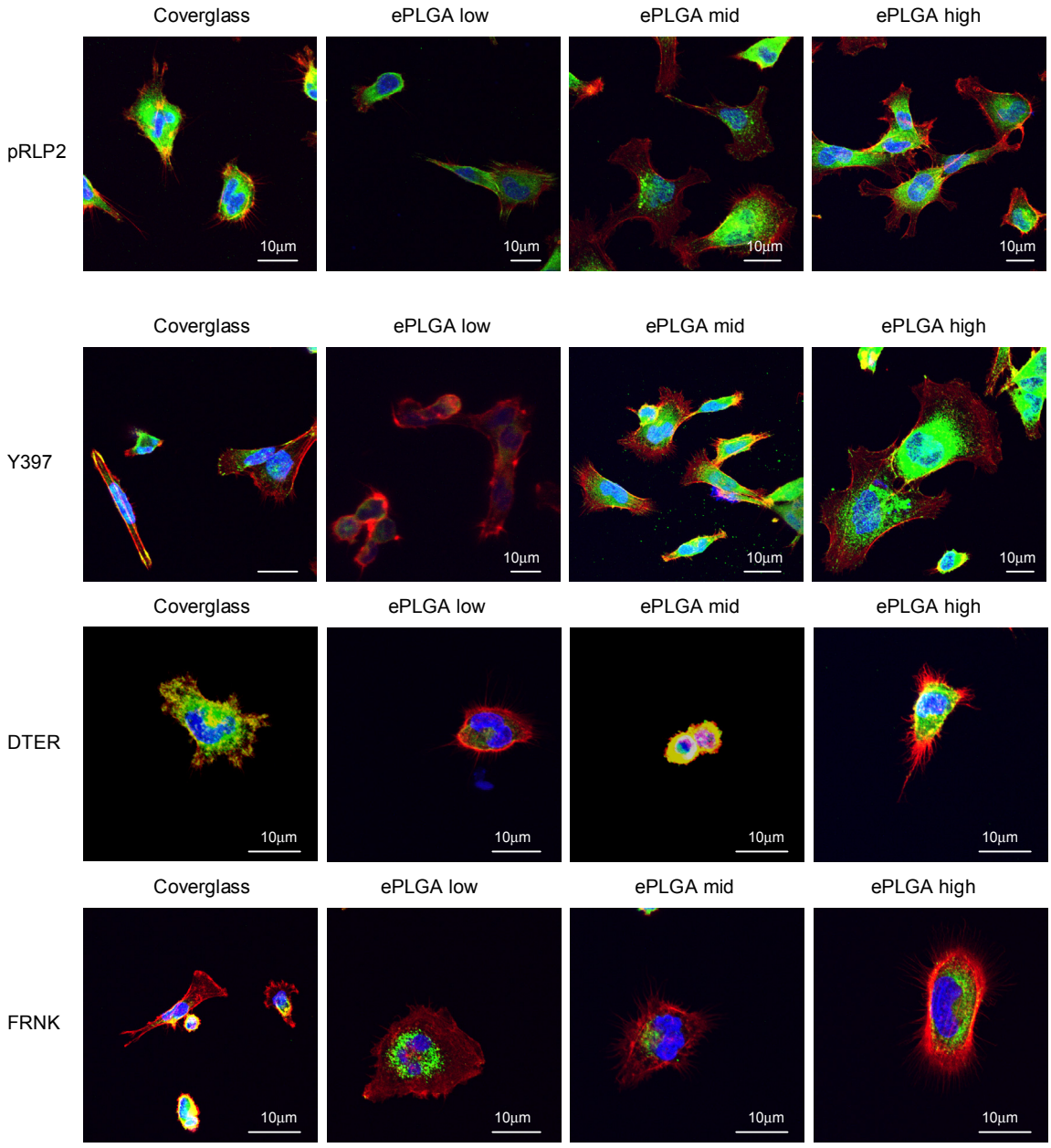


Figure 3.2. Morphology and vinculin distribution of FAK mutant hMSC on ePLGA. hMSC transduced with Y397, DTER, FRNK or empty vector (pRLP2) retrovirus were grown on polymer-coated coverslips for one hour, stained for actin (red), vinculin (green) and with DAPI (blue), and imaged at 40x magnification with zoom. Images are z-stack projections. Constructs used: pRLP2 (empty vector control), DTER (truncation mutant), Y397 (phenylalanine substitution at Y397 phosphorylation site), FRNK (dominant negative).

Table 3.1. Relative numbers of focal adhesions of FAK mutant hMSC on ePLGA.

| Surface | pRLP2 | Y397 | DTER | FRNK |
|---|---|---|---|---|
| Coverglass | 14.0 | 11.0 | 2.5 | 1.1 |
| ePLGA low | 29.3 | 25.5 | 1.9 | 3.3 |
| ePLGA mid | 39.5 | 26.8 | 5.7 | 5.0 |
| ePLGA high | 43.5 | 29.1 | 3.6 | 7.7 |

Focal adhesions per cell are based on presence of vinculin from confocal microscopy. Mean focal adhesion numbers are not statistically significant between pRLP2 and Y397, nor DTER and FRNK, however all other group comparisons are statistically significant; $p<0.05$. Constructs used: pRLP2 (empty vector control), DTER (truncation mutant), Y397 (phenylalanine substitution at Y397 phosphorylation site), FRNK (dominant negative).

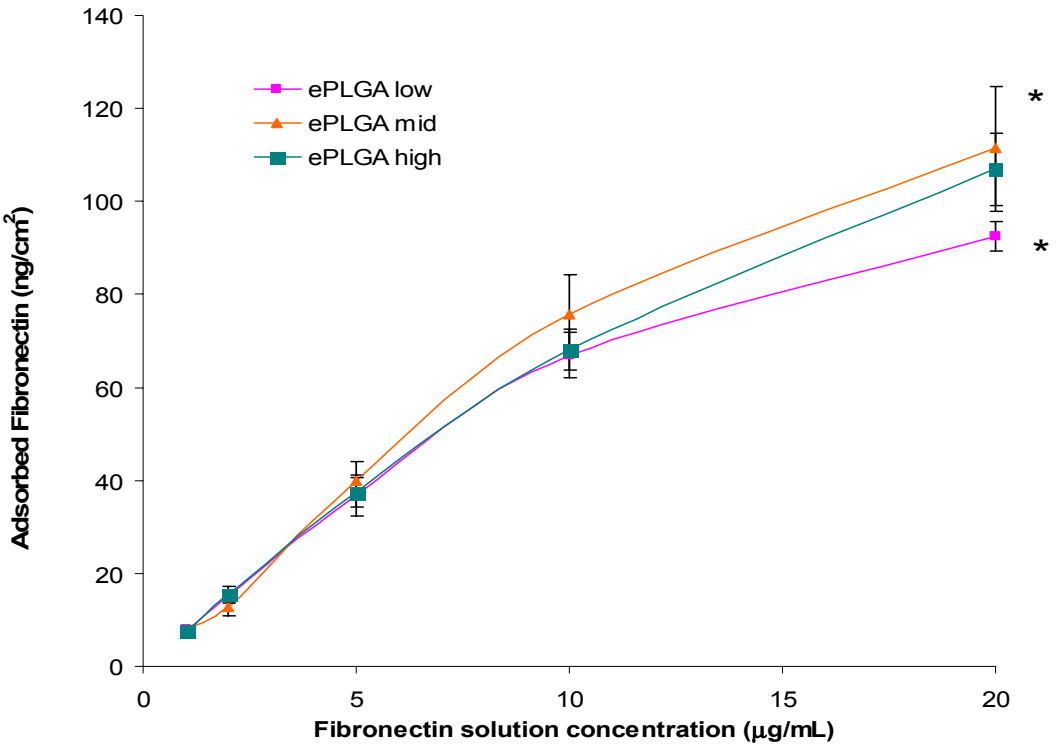


Figure 3.3. Adsorbed fibronectin on ePLGA surfaces. Iodinated fibronectin at 5 solution concentrations was brought into contact with ePLGA films for 1hr. Following multiple PBS rinses, radioactivity was measured in a gamma counter and absolute adsorbed fibronectin was calculated; $p<0.05$, experiment was repeated twice, n=6.

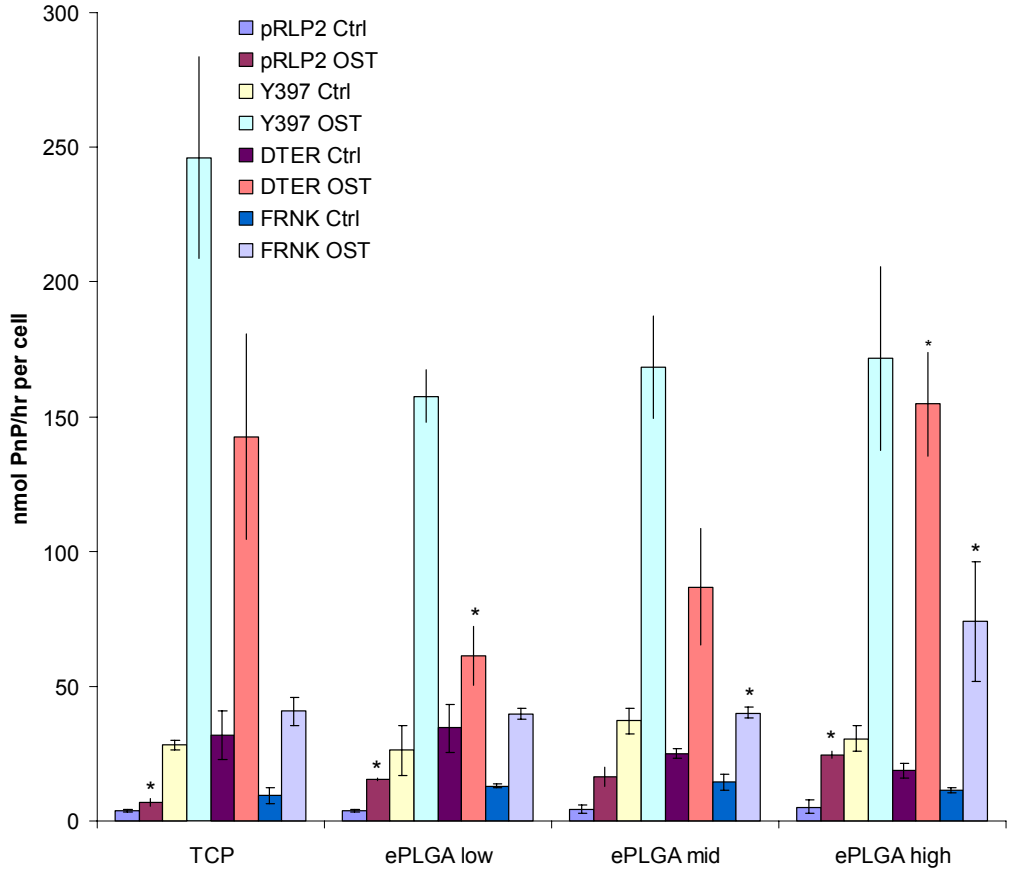


Figure 3.4a. Alkaline phosphatase activity of FAK mutant hMSC on ePLGA. pRLP2, pRLP2-Y397, pRLP2-DTER and pRLP2-FRNK hMSC were harvested on day 15 and assayed for alkaline phosphatase activity using a colorimetric assay and normalized to cell number using the Cyquant assay. Within each polymer group, all values for osteogenic treatments are significantly different from one another. Within a cell type, asterisks represent the values that are significantly different from one another; $p<0.05$, $n=3$.

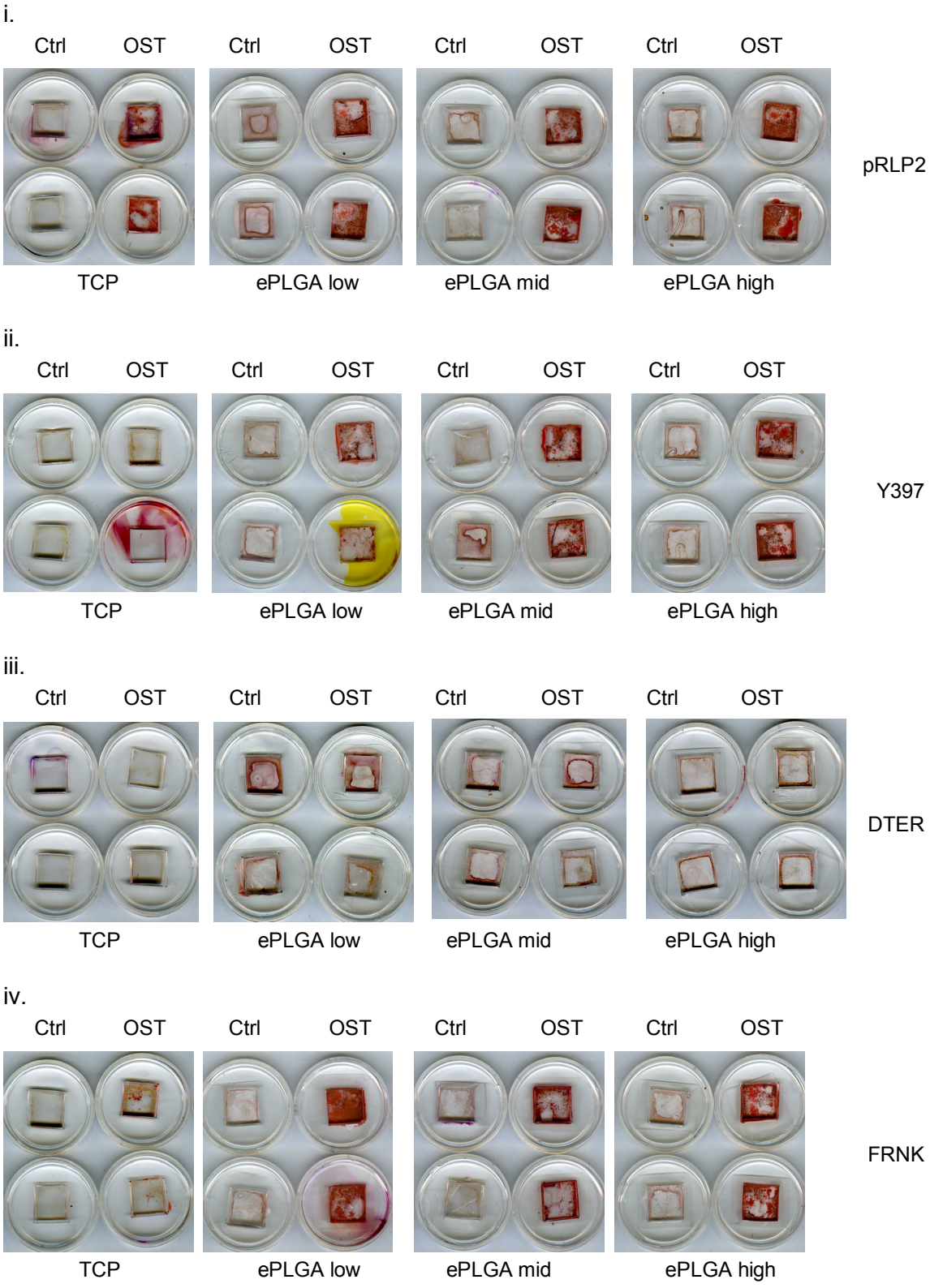


Figure 3.4b. Alizarin Red staining of FAK mutant hMSC on ePLGA. pRLP2 (i) and pRLP2-FAK mutant (ii-iv) hMSC were cultured on ePLGA for 27 days and then stained for calcium phosphate with Alizarin Red; n=3.

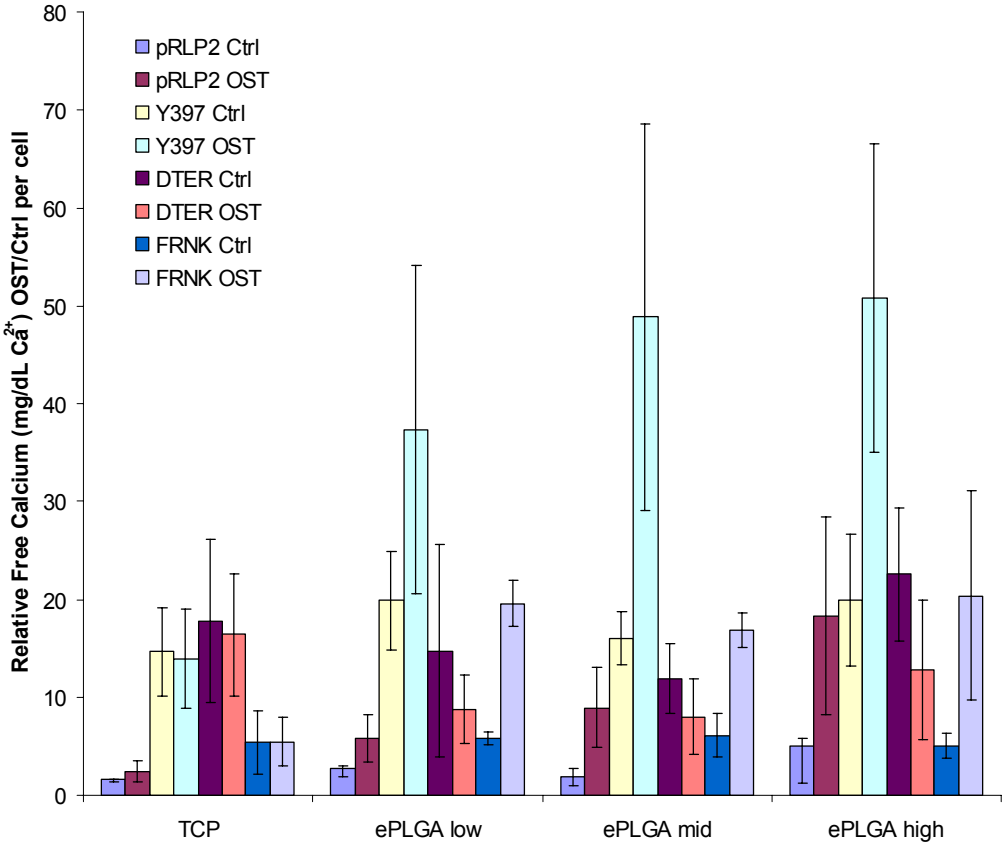


Figure 3.4c. Matrix-embedded calcium of pRLP2 and pRLP2-FAK mutant hMSC on ePLGA. Cells were harvested on day 27. Mineral deposition was examined following liberation of calcium from the matrix overnight via CPC calcium assay as an alternative to Alizarin Red staining; n=3. Values within cell types are not statistically significant; $p>0.05$.

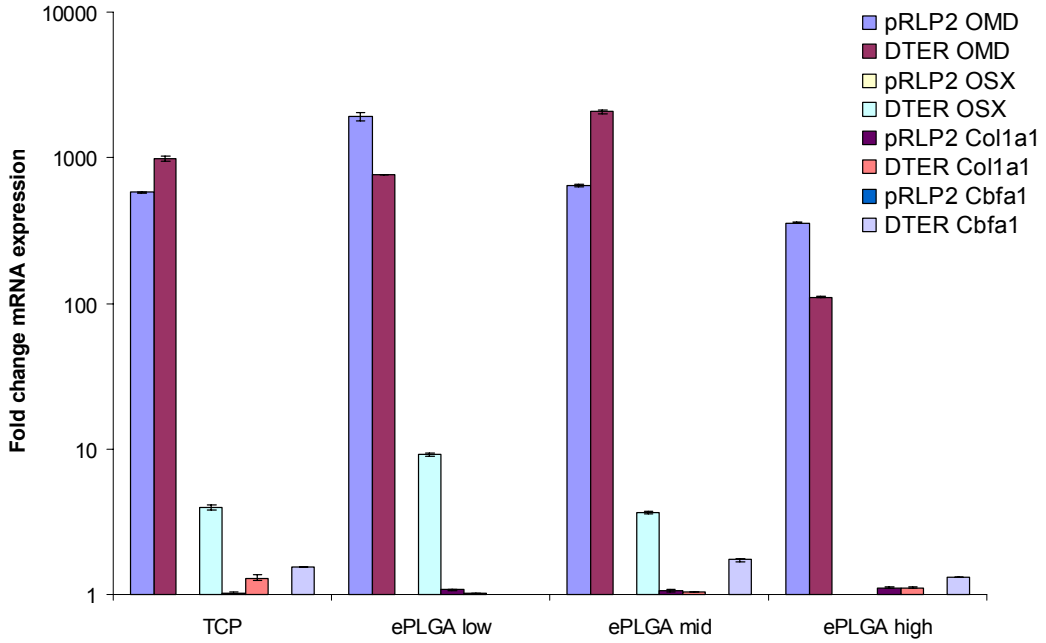


Figure 3.4d. Osteogenic gene expression changes in pRLP2 and DTER hMSC on ePLGA. pRLP2 and pRLP2-DTER hMSC were cultured for 12 days in osteogenic or control media. Gene expression was analyzed using the ΔΔCT method and fold change values represent osteogenic relative to control treatment, normalized to β-actin; data represents mRNA expression changes of 3 pooled samples.

**RhoA Studies**

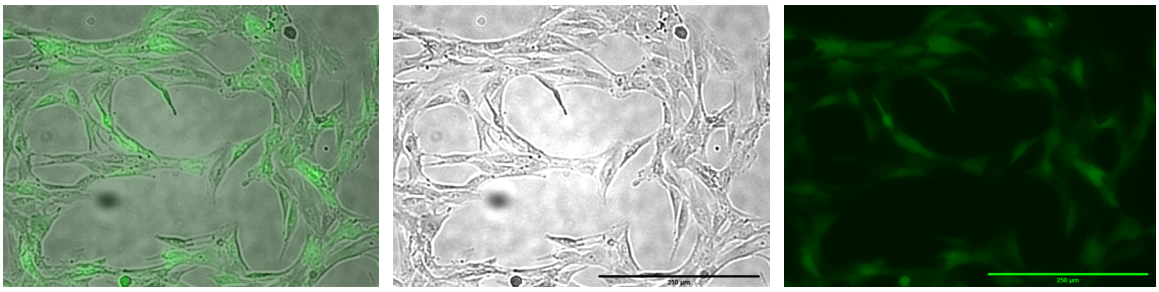

Figure 3.5a. Transduction efficiency of hMSC transduced with Rho constructs. hMSC were transduced with either dominant negative (pRET-RhoN19) or constitutively active Rho (pRET-RhoV14), empty vector (pRET) or an eGFP-transduction control. Here pRET-eGFP demonstrates a high level of transduction efficiency for this study as evidenced by transgene expression. A visible overlay is shown (left) of brightfield (middle) and fluorescence (right) images. Only pRET-eGFP is shown. Scale bar: 250μm.

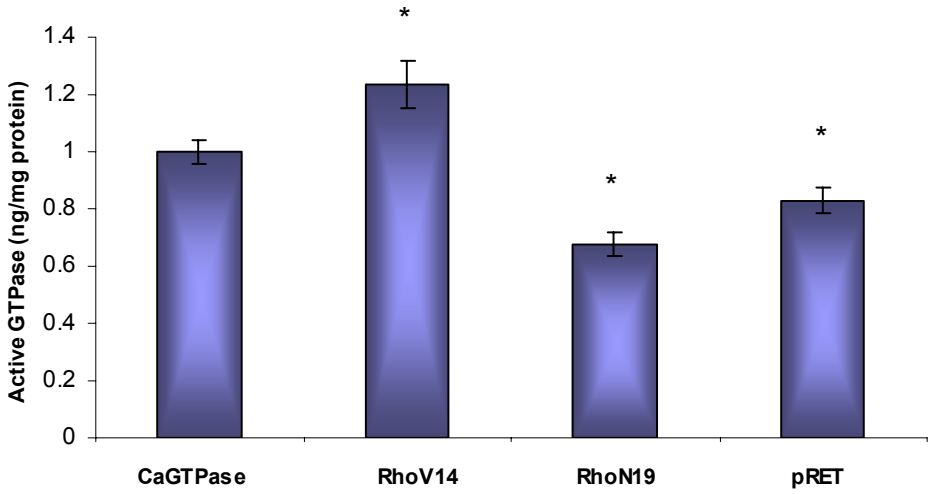


Figure 3.5b. RhoA activity of hMSC following retroviral transduction with Rho constructs. Following two weeks of culture under growth conditions, RhoV14, RhoN19 and pRET cell lysates were assayed for Rho-GTPase activity using a commercially available kit (GLISA) and normalized to total protein. Transduction of immortalized hMSC with RhoV14 retrovirus demonstrated increased RhoA activity, and RhoN19 showed decreased RhoA activity with respect to the pRET control. All hMSC GTPase activity is significantly different from one another; *$p<0.05$.

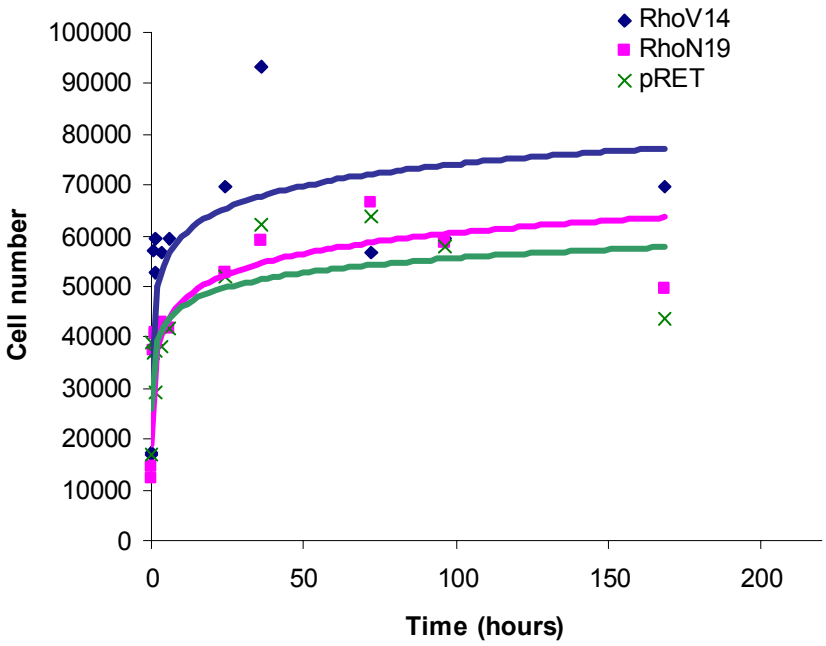


Figure 3.6. Attachment curves for RhoV14, RhoN19 and pRET hMSC on TCP. Cells were grown on TCP and harvested over a period of one week. Cell numbers were quantified using the Cyquant assay; n=6.

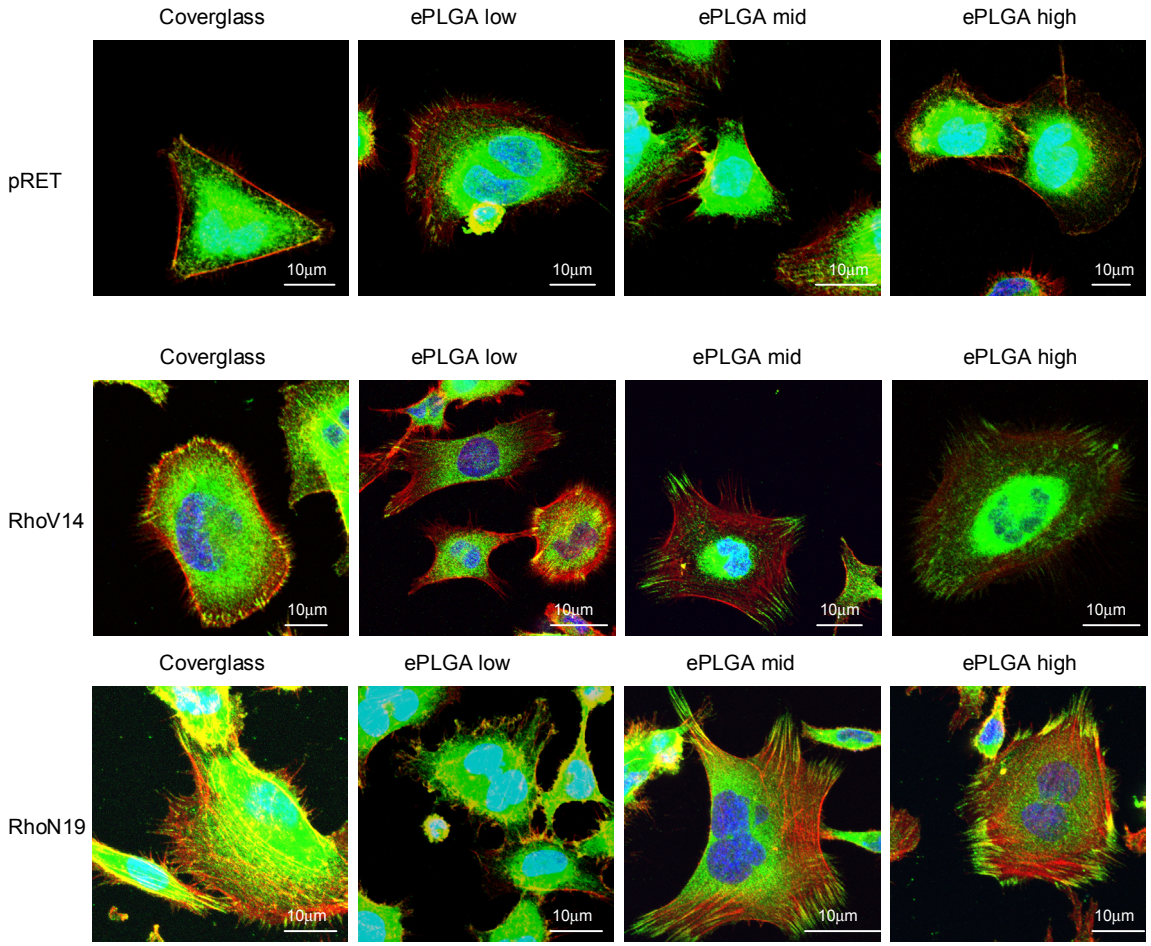


Figure 3.7. Morphology and vinculin distribution of Rho mutant hMSC on ePLGA. hMSC transduced with RhoV14, RhoN19, or empty vector (pRET) retroviruses were grown on polymer-coated coverslips for one hour, stained for actin (red), vinculin (green) and with DAPI (blue), and imaged at 40x magnification with zoom. Images are z-stack projections.

Table 3.2. Relative numbers of focal adhesions of Rho mutant hMSC on ePLGA.

| Surface | pRET | RhoV14 | RhoN19 |
|---|---|---|---|
| Coverglass | 14.2 | 64.9 | 42.4 |
| ePLGA low | 23.7 | 103.7 | 27.9 |
| ePLGA mid | 44.7 | 112.0 | 30.8 |
| ePLGA high | 40.9 | 122.8 | 29.6 |

Focal adhesion numbers per cell are based on presence of vinculin from confocal microscopy. Average focal adhesion numbers for RhoV14 are significantly different than both RhoN19 and pRET; $p<0.05$. RhoN19 and pRET means are not considered significantly different from one another; $p>0.05$.

i.

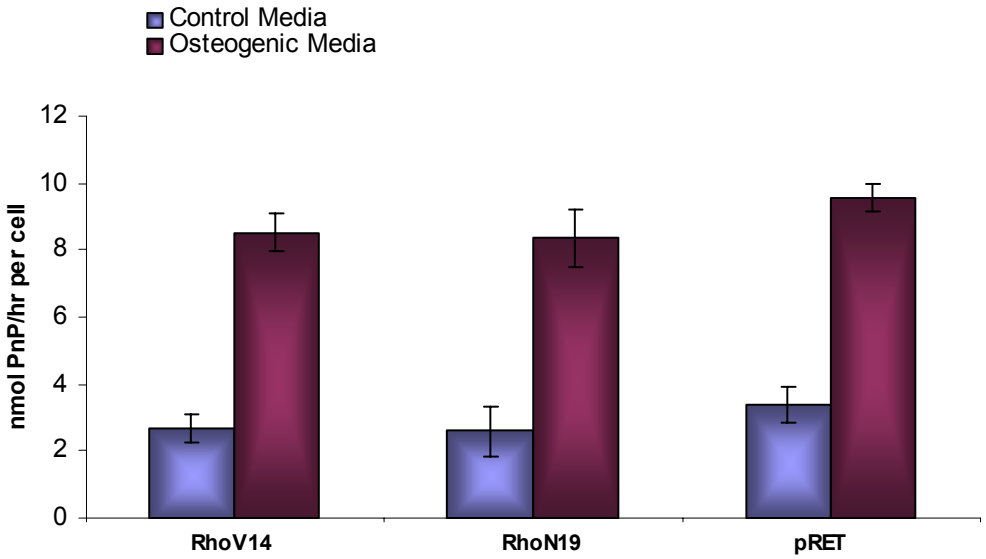


ii.

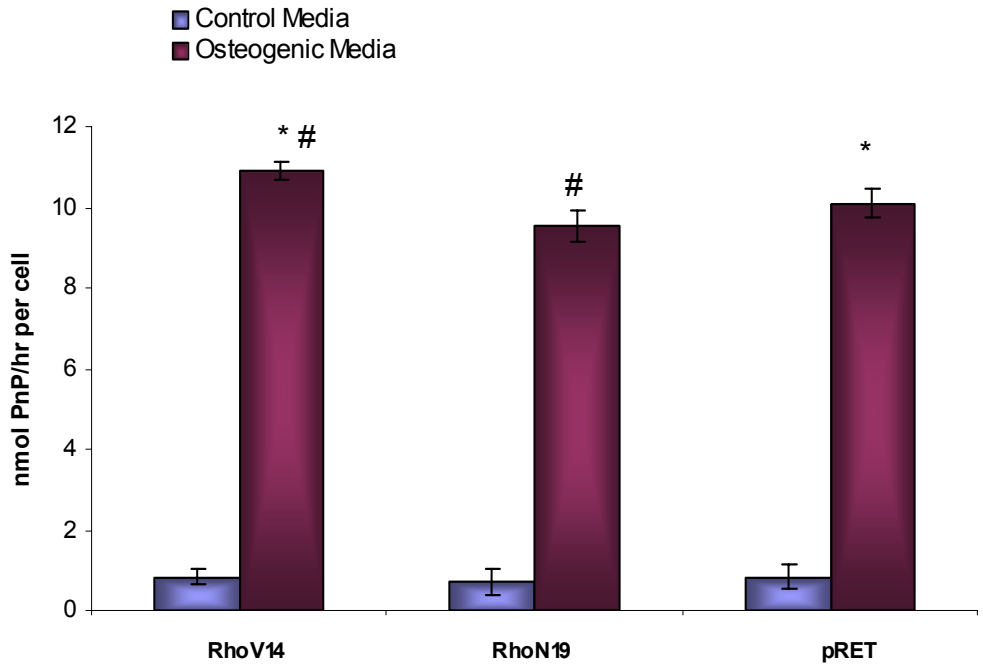


Figure 3.8a. Alkaline phosphatase activity of Rho mutant hMSC on TCP. RhoV14, RhoN19, and pRET hMSC were harvested on days 6 and 9 and assayed for alkaline phosphatase activity using a colorimetric assay and then normalized to cell number using the Cyquant assay. RhoV14 hMSC had greater alkaline phosphatase activity than either RhoN19 (#) or pRET controls (*); #, * $p<0.05$, n=3.

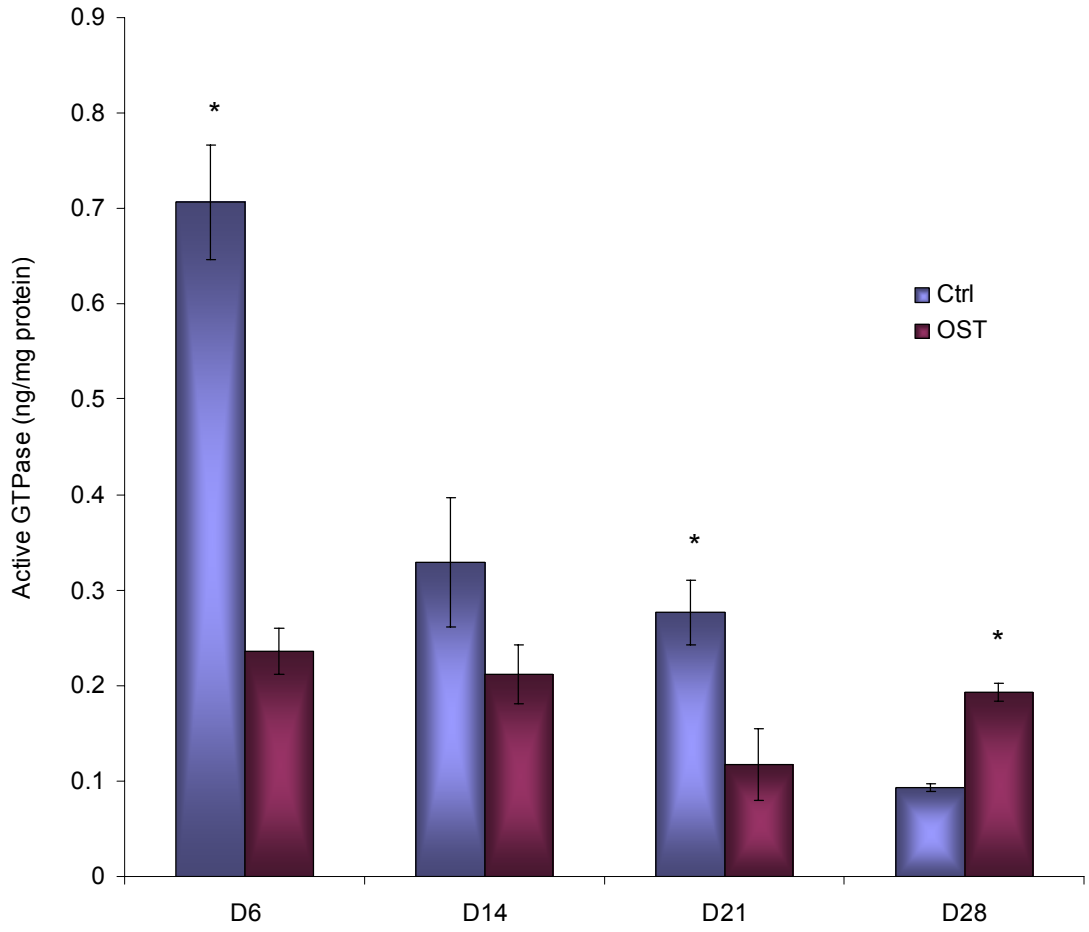


Figure 3.8b. Modulation of RhoA activity during osteogenesis. pRET hMSC were cultured on TCP for up to 28 days. Cell lysates were assayed for RhoGTPase activity using a commercially available kit (GLISA) and normalized to total protein. Values marked with an asterisk are significantly greater than the culture condition at the same timepoint; *$p<0.05$, $n=3$.

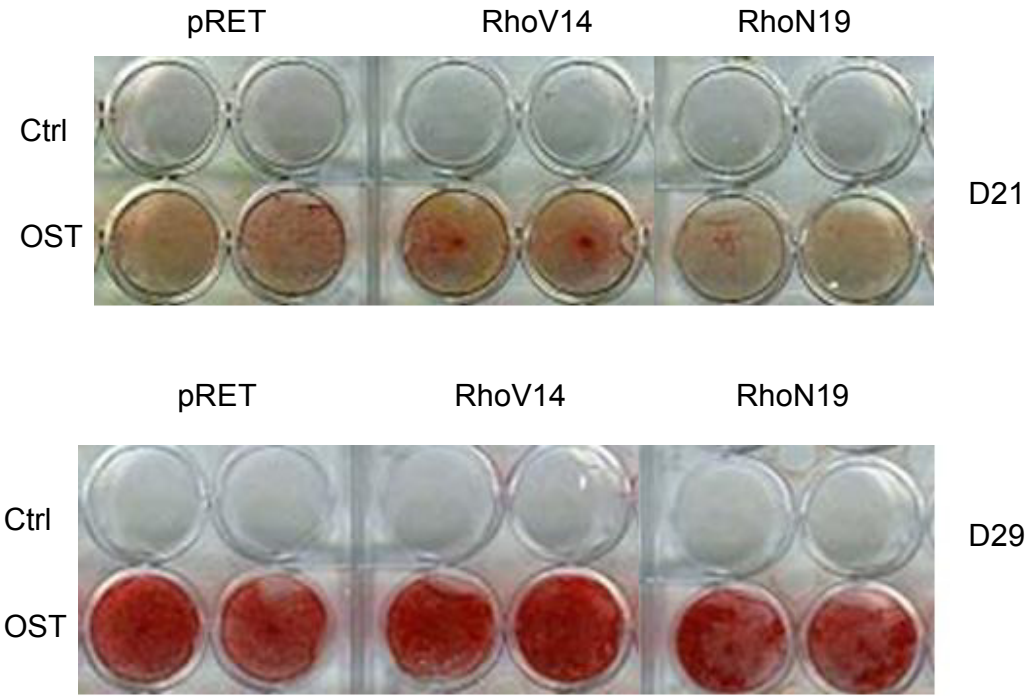


Figure 3.8c. Alizarin Red staining of Rho mutant hMSC on TCP. Calcium phosphate staining with Alizarin Red for pRET, pRET-RhoV14 and pRET-RhoN19 hMSC at 21 and 29 days. RhoV14 lead to increased mineral formation while RhoN19 produced decreased mineral formation with respect to pRET at both timepoints. Cell numbers were quantified and equivalent (data not shown); n=6.

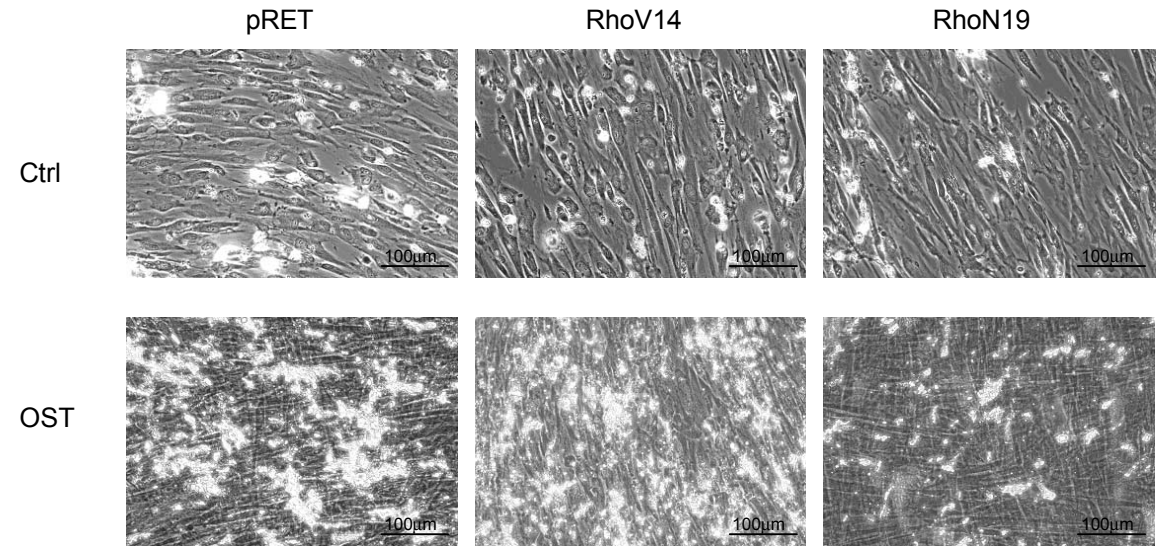


Figure 3.8d. Morphology and mineral deposition of Rho-transduced hMSC. Phase contrast images were taken at day 29 of culture.

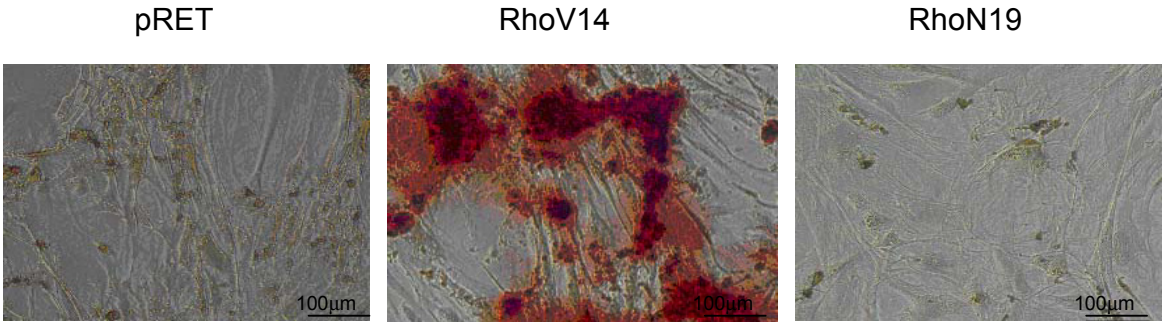


Figure 3.8e. Puromycin-selected Rho mutant hMSC Alizarin Red Staining. As the pRET retroviral vector contains the puromycin antibiotic resistance gene, hMSC transduced with pRET, RhoV14 and RhoN19 were selected and then cultured for 21 days under osteogenic (displayed) and control conditions (not shown). All cells demonstrated delayed mineralization at day 21, however upon magnification, RhoV14 appears to promote substantially more mineral formation, and RhoN19 less, than the pRET control; n=6.

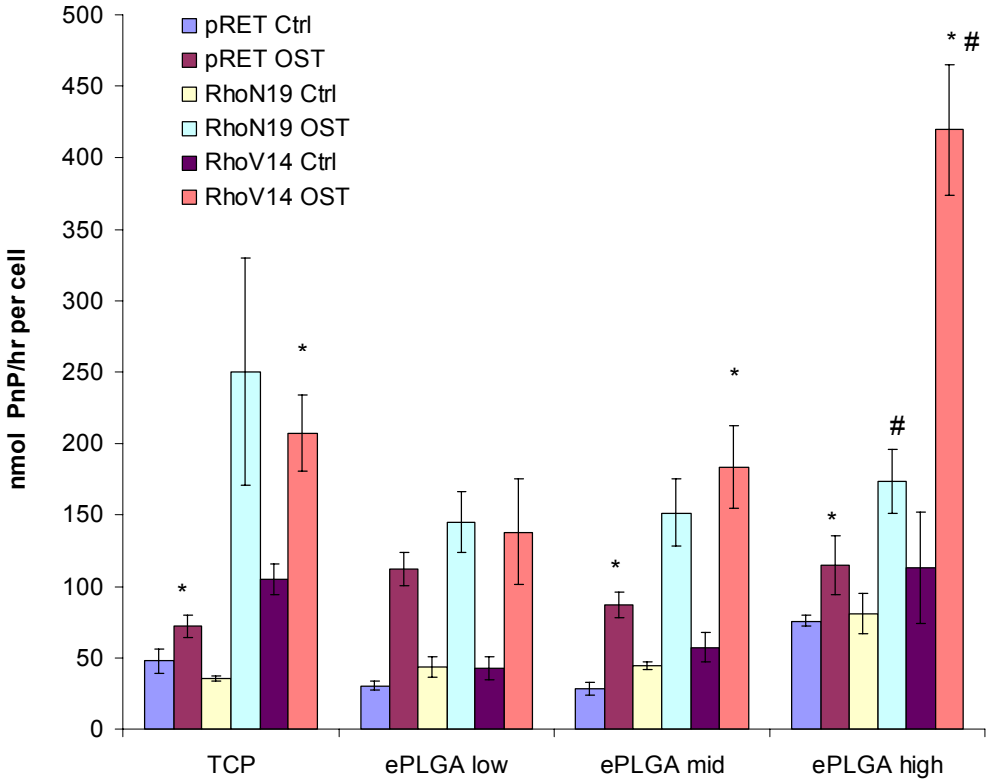


Figure 3.9a. Alkaline phosphatase activity of Rho mutant hMSC on ePLGA. hMSC transduced with empty vector (pRET), RhoN19 or RhoV14 demonstrate differing degrees of osteogenic activity on ePLGA at day 15 as measured by alkaline phosphatase activity using a colorimetric assay. These values were then normalized to cell number using the Cyquant assay. Values marked are significantly different from one another within a polymer group; *,#$p<0.05$, n=3.

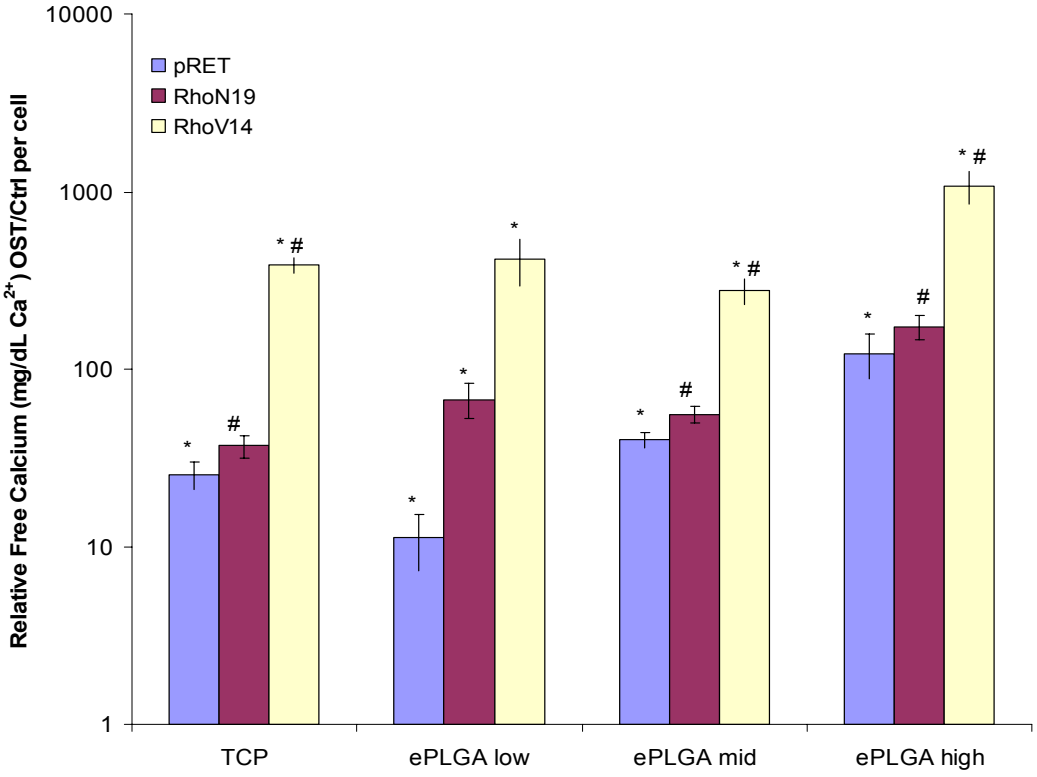


Figure 3.9b. Matrix-embedded calcium of Rho mutant hMSC on ePLGA. hMSC transduced with empty vector (pRET), RhoN19 or RhoV14 exhibit changes in matrix-associated calcium at 35 days of culture in osteogenic media. Mineral deposition was examined following liberation of calcium from the matrix overnight via CPC calcium assay as an alternative to Alizarin Red staining. For each cell type, ePLGA high supported the greatest significant increase in calcium levels. Values marked are significantly different from one another within a polymer group; #,*$p<0.05$, n=3.

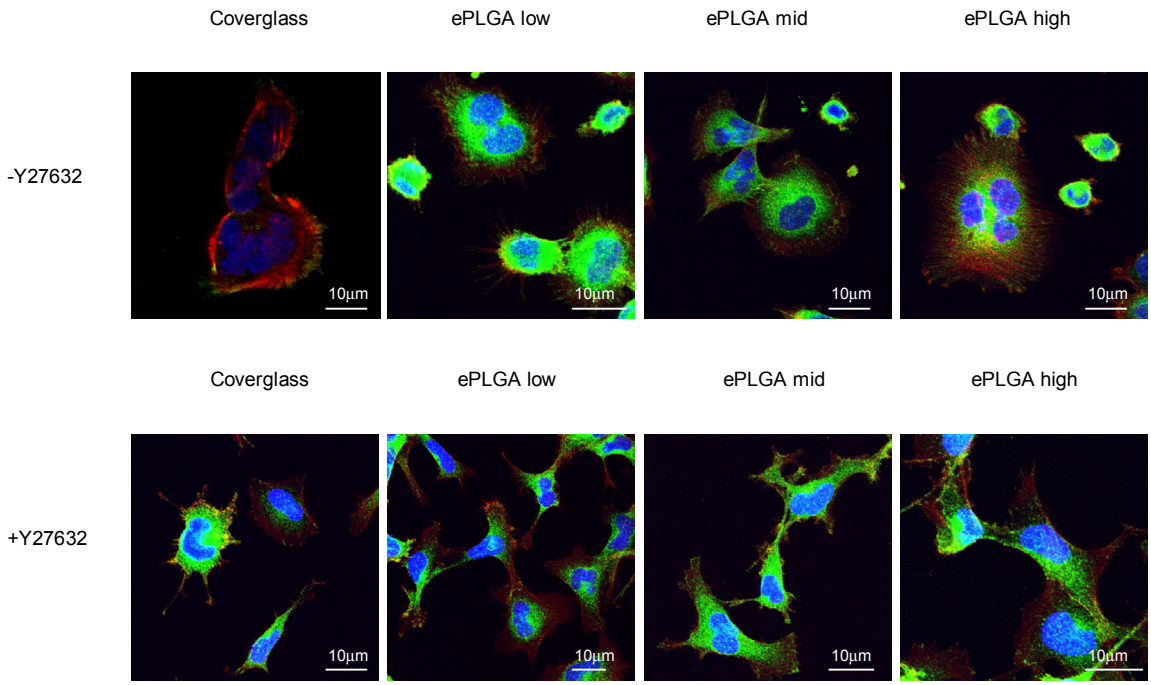


Figure 3.10a. Morphology and vinculin distribution of hMSC treated with or without the ROCK inhibitor Y27632 on ePLGA. Cells were grown on ePLGA coated coverslips for one hour and stained for actin (red), vinculin (green) and with DAPI (blue), and imaged at 40x magnification with zoom. Images are z-stack projections.

Table 3.3. Relative numbers of focal adhesions of hMSC with or without Y27632.

| **Surface** | **hMSC - Y27632** | **hMSC + Y27632** |
|---|---|---|
| Coverglass | 8.3 | 74.7 |
| ePLGA low | 35.0 | 107.1 |
| ePLGA mid | 40.5 | 102.1 |
| ePLGA high | 63.0 | 109.2 |

Focal adhesions per cell were based on presence of vinculin from confocal microscopy. Mean focal adhesion numbers with or without Y27632 treatment are considered significantly different from one another; $p<0.05$.

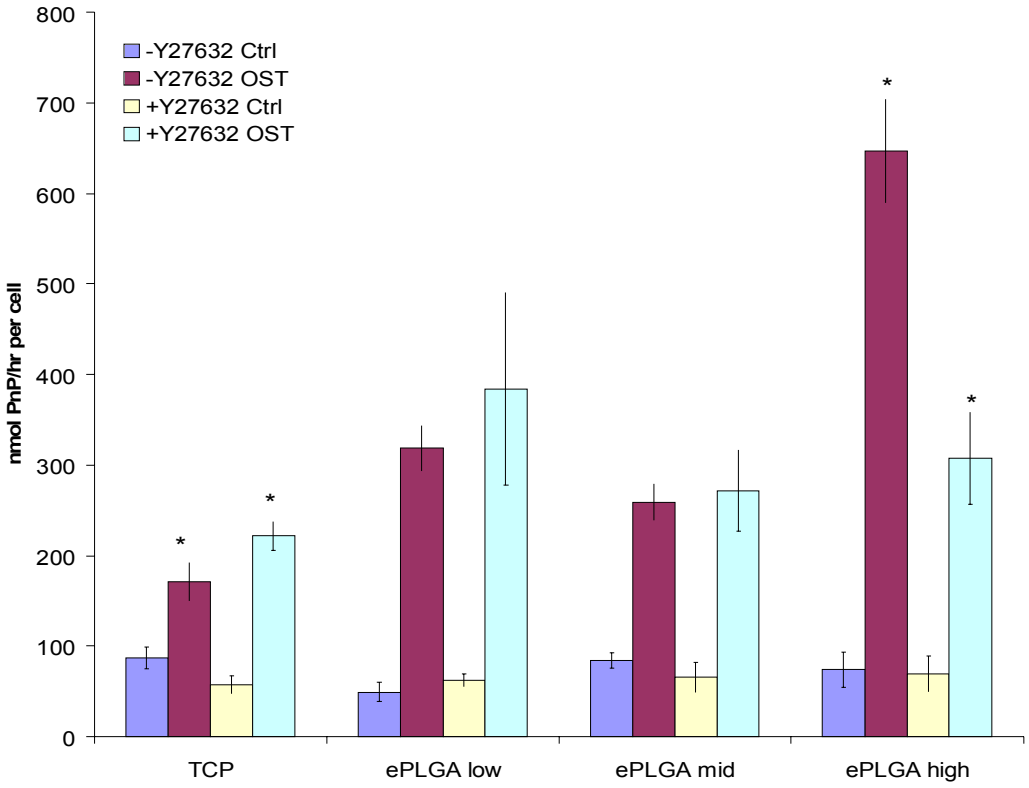


Figure 3.10b. Alkaline phosphatase activity of hMSC treated with or without the ROCK inhibitor Y27632 on ePLGA. Alkaline phosphatase activity was measured at day 15 using a colorimetric assay. These values were then normalized to cell number using the Cyquant assay. A 50% reduction in activity was seen on ePLGA high, the surface demonstrating the greatest adhesion strength. Marked values are significantly different from one another within a polymer group; *$p<0.05$, n=3, +/-SE.

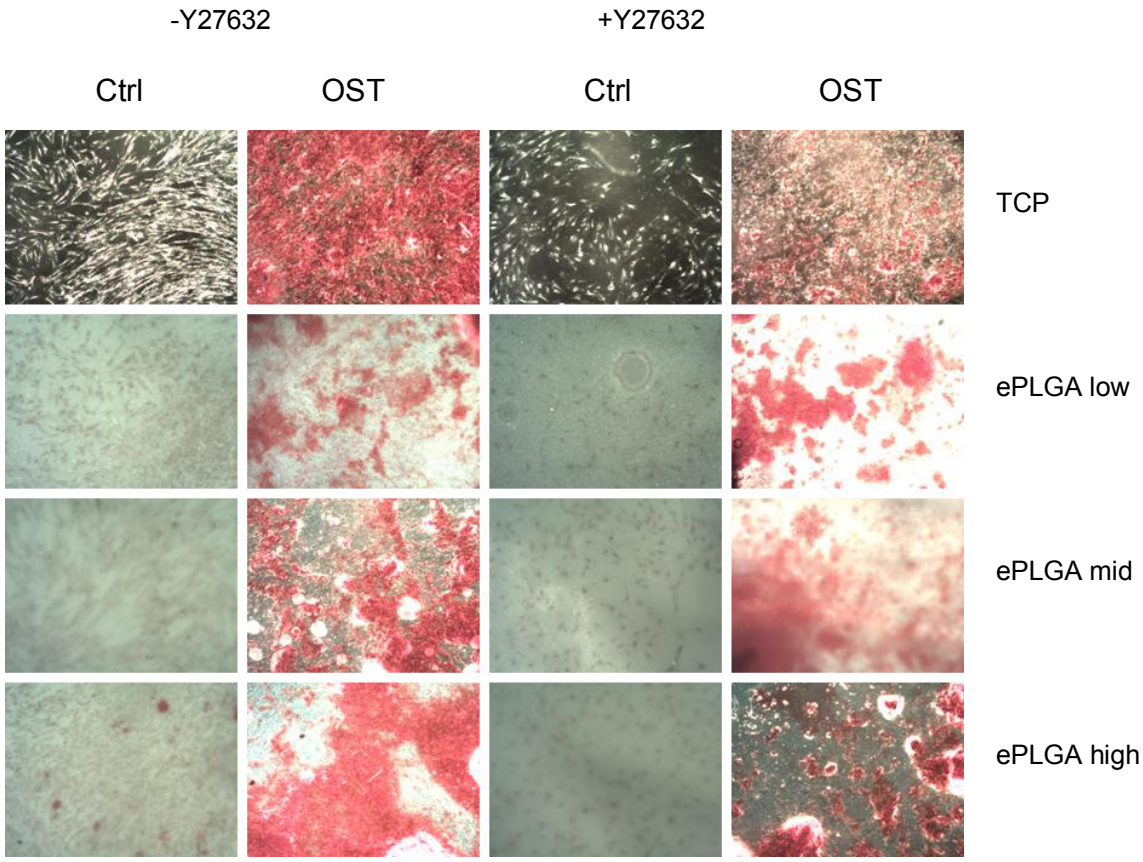


Figure 3.10c. Alizarin Red staining of hMSC treated with or without ROCK inhibitor Y27632 on ePLGA. Alizarin Red staining of calcium phosphate at day 23 showed visible reduction in hMSC on ePLGA high, the surface demonstrating the greatest adhesion strength; n=3.

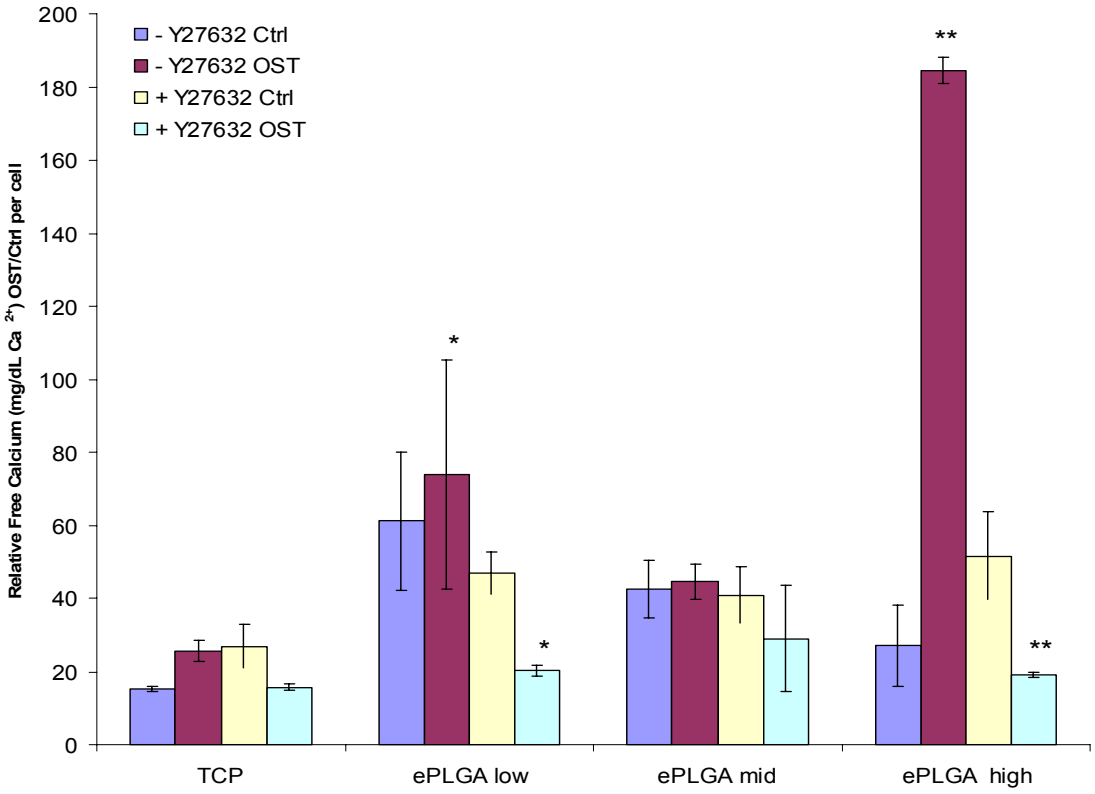


Figure 3.10d. Matrix-embedded calcium of hMSC treated with or without ROCK inhibitor Y27632 on ePLGA. Mineral deposition quantified via CPC assay and normalized to cell number is displayed for day 23 in culture. A 9-fold reduction in calcium was seen in cells grown on ePLGA high with Y27632 treatment, the surface demonstrating the greatest adhesion strength. Marked values are significantly different from one another within a polymer group; **p<0.01, *p<0.05, n=3, +/- SE.

# CHAPTER IV

# CONCLUSION

These studies examined how both material properties and adhesion strength contribute to osteogenic differentiation of hMSC on common biodegradable polymers in order to further understand how early adhesive events affect cell function. Tissue engineering studies often misrepresent the dynamic nature of adhesion when addressing the biocompatibility of a scaffold by taking a non-standardized approach towards the study of cell-material interactions. We have sought to unify all the contributing factors of adhesion into a single quantitative parameter, adhesion strength and have found that it appears to be a sufficient outcome measure for determining the relative osteogenic capacity of a polymer surface.

Initially, we characterized four polymer groups of interest (alginate, ePLGA, a/mPLGA and PCL) which demonstrated a range of both surface hydrophobicity (contact angle) and mechanical stiffness (E). By quantifying dynamic cell attachment, immortalized hMSC were found to have adhesion plateaus that extend over similar timeframes independent of polymer type, but cells proliferated differently on these surfaces. Additionally, both morphology and focal adhesion expression were shown to vary by polymer type. We then determined the adhesion strength ($\tau_{50}$) of two hMSC lines on the polymers in the adhesive reinforcement portion of the attachment curve. Using

both a fluid shear and spinning disk method, we found significant differences in $\tau_{50}$ among the polymer groups, with alginate demonstrating much less adhesion strength than the polyesters studied, while a/mPLGA had the greatest adhesion strength overall. Further, there is a positive correlation of adhesion strength with both elastic modulus and degree of hydrophobicity to an optimum.

When both hMSC lines were grown under osteogenic conditions on PCL and ePLGA, there was a demonstrated increase in alkaline phosphatase activity (osteogenic index) and mineral formation with increase in adhesion strength, particularly on those surfaces within the polymer group that demonstrated the greatest adhesion strength. The association of differentiation markers with adhesion strength was strong within polymer groups, but poor correlation was seen across polymer groups. Additionally, a poor correlation was also seen between osteogenic differentiation and the material properties that were characterized. This suggests that other polymer properties such as specific protein adsorption, surface roughness or chemistry may be important for differentiation.

In order to understand how these differences in adhesion strength might be mediating hMSC differentiation on ePLGA, the adhesion signaling molecules focal adhesion kinase, and RhoA GTPase, were investigated. hMSC were retrovirally transduced with mutant constructs of FAK (Y397, DTER or FRNK) and RhoA (RhoV14 or RhoN19) genes. Alternatively, hMSC were treated with the Rho-kinase inhibitor, Y27632. Both cells transduced with mutant RhoA or FAK constructs, or those treated with Y27632 displayed aberrant cell morphology and changes in focal adhesion numbers, but this was not related to quantity of fibronectin adsorption. Differentiation studies demonstrated that both constitutively active RhoA and mutants of FAK increase

normalized osteoblastic activity, while both dominant negative RhoA cells and hMSC treated with Y27632 exhibited a decrease in these markers. The most significant effects on osteogenesis resulting from these studies were seen on ePLGA demonstrating maximal $\tau_{50}$ in earlier studies, that is, the highest molecular weight ePLGA. This suggests that hMSC differentiation on polymers exhibiting high adhesion strength depends on FAK and RhoA as it appears that disregulating either FAK or RhoA signaling disrupts this dependence.

This is the first report examining the interplay of adhesion strength, focal adhesions and FAK, Rho and ROCK signaling and how they influence hMSC differentiation on biodegradable polymers. While larger adhesion strengths promote hMSC osteogenesis on numerous material types, this is specifically mediated via RhoA-ROCK signaling on ePLGA, supporting our initial hypothesis. Further this behavior appears to be associated with focal adhesions that correlate with stress fibers. FAK studies suggest a more complicated role for FAK signaling in this process, however it appears to be important for this system as disregulation in the focal adhesion targeting domain leads to reduced focal adhesion number and an increase in osteogenesis on a per cell basis, despite in some cases, showing a global decrease in osteogenesis. A model of our findings is presented in Figure 4.1.

The interdependence between FAK and RhoA signaling has been previously described and understanding this interaction in our system would further elucidate whether either molecule plays a greater role in the dependence of hMSC differentiation on adhesion strength to biodegradable polymers. The relative importance of these two signaling pathways remains to be seen for hMSC osteogenesis on biodegradable polymers and could be tested by quantifying perturbations in these pathways within the system

studied here. In particular, promotion of FAK signaling either via constitutively active FAK transduction of hMSC or fibronectin coating of polymers to promote focal adhesion formation would offer further insight. Similarly, additional information about the Rho-ROCK signaling axis in this system could be gained through promotion of ROCK signaling by transduction of hMSC with constitutively active ROCK.

The consistent nature of increased differentiation on surfaces exhibiting the greatest adhesion strength in untransduced cells, and the greatest disregulation of this process on these polymers in mutant RhoA and FAK hMSC was surprising to us. To directly link the studies discussed here, it will be important to quantify any changes in adhesion strength that may have been influenced by manipulation of either RhoA or FAK signaling pathways. Based on the varied morphologies of these cells, we hypothesize that there are significant differences in adhesion strength for these modified hMSC. Further identifying how adhesion strength may have been changed by forced expression of the RhoA and FAK mutant proteins would be instructive in elucidating whether there is a consistent relationship between adhesion strength and disregulation of differentiation in these latter studies. Another approach to understand this interaction could be to cause these adhesive surfaces to become less adhesive (through blocking of focal adhesion formation with integrin antibodies, or the use of deadhesive proteins such as thrombospondins) and study the effects on differentiation.

It may also be important to try to standardize experiments for cell number by pharmacologically inhibiting mitosis in these cells beyond normalizing output values to cell number, as there may be cooperative effects of having increased numbers of cells in an osteogenic population, beyond a linear increase. This is highly pertinent to studies involving manipulation of FAK, where cell proliferation is greatly impacted.

Additionally, it is still unclear as to whether there are subsets of material properties that dominate in contributing to adhesion strength, thereby supporting osteogenic differentiation of hMSC. Theoretically, a meta-analysis of studies such as ours would be one way to understand whether there are practical parameters for materials scientists to consider in promoting a functional biological outcome. A predictive design strategy could then lead to improved clinical applicability.

While polymer modification was not a part of our studies, our findings suggest new insights into biomaterial design. In particular, adhesion strength correlations suggest that both a median hydrophobicity and stiffness contribute to improved adhesion strength. And, within a particular polymer of interest, greater adhesion strength leads to improved osteogenic capacity. Some approaches to achieve these optimums could be to tailor the polymer backbone and end groups to make them optimally hydrophobic, or to manipulate polymer crosslinking or molecular weight in order to modify elastic modulus. However, it is important to reiterate that promotion of osteogenesis would only be anticipated to be correlated with these changes within one polymer type.

The surfaces used in these studies demonstrated stiffnesses in the MPa range, however additional studies identifying the effects of stiffnesses greater than (GPa, as in metals) and less than (Pa, as in hydrogels) those presented here might further elucidate the role for this material property in adhesion strength. It would however, be anticipated that while stiffness optimums might be seen in either range, a point would exist at which surfaces were either too stiff or soft to exhibit any further effect on adhesion strength.

To date, no other group has investigated the role of adhesion strength of hMSC on clinically relevant polymers for the purpose of identifying effects on differentiation. While direct extrapolation of the conclusions here to an in vivo model could be premature, preliminary evidence suggests that within polymer groups, greater adhesion strength could promote improved bone tissue regeneration. For tissue engineering, determining whether greater in vitro differentiation is predictive for improved tissue formation in vivo is fundamental for advancement in this discipline. Additional study into how adhesion strength might affect chondrogenesis, myogenesis or adipogenesis would also add to the tissue engineering arsenal. However, the additional complexities of 3-dimensional characteristics (such as pore size and consequent diffusion, biodegradation, physiological protein adsorption as well as other host responses, such as inflammation) will continue to make advances in this field a challenge. If, however, relative adhesion strength were to correlate to bone formation in vivo, measurement of this parameter in vitro could serve as a powerful tool for assessing osteoinductivity of novel biomaterials. A larger goal of the work here would be to see whether this interplay of adhesion strength, and Rho and FAK signaling seen on polymer films is predictive for bone and potentially other types of tissue regeneration in vivo.

It is hoped that the work presented here will contribute to connecting the gaps between the fields of biodegradable polymer design and stem cell biology. Further understanding of this kind should lead to a more inspired and purposed approach to orthopaedic and other tissue-specific material designs, as well as fundamental insight into the role early adhesive events have on long-term stem cell function.

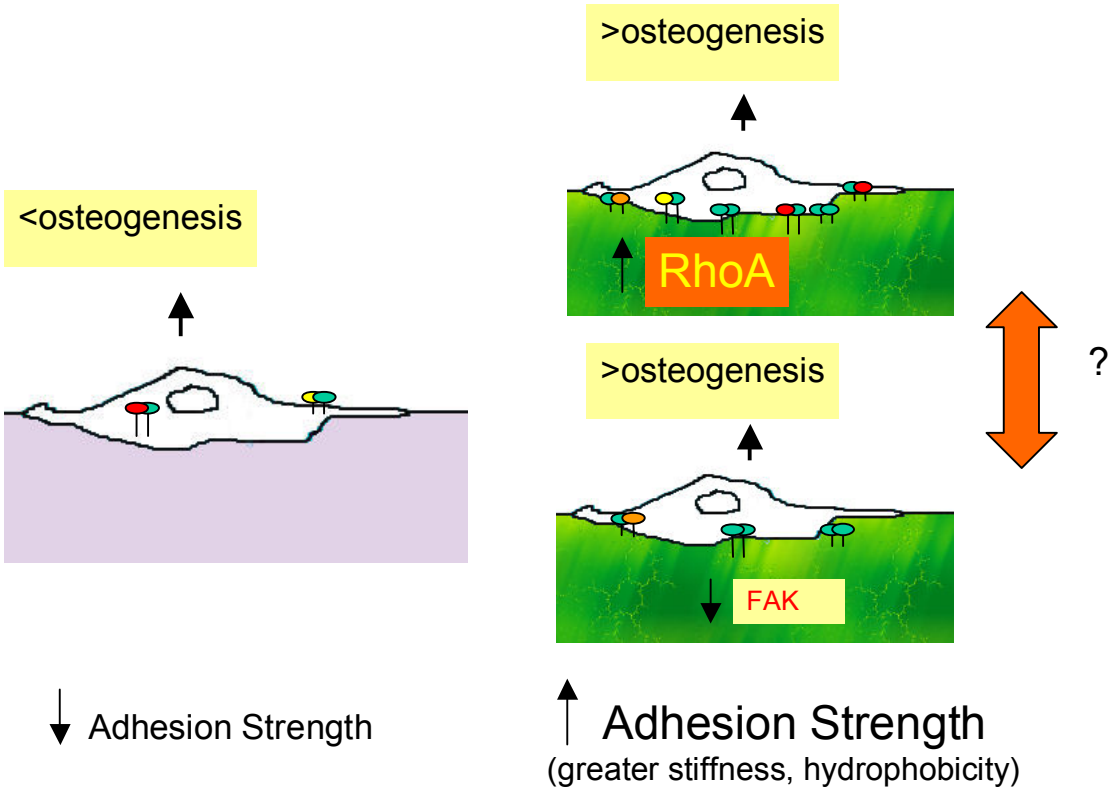


Figure 4.1. Model for adhesion strength, focal adhesions, FAK, and Rho/ROCK interactions affecting hMSC differentiation on biodegradable polymers. Substrates which demonstrate poor adhesion strength promote development of few focal adhesions and lead to decreased hMSC osteogenesis. Substrates such as those with greater stiffness or hydrophobicity, promote increased adhesion strength and exhibit increased hMSC osteogenic activity. This increase in osteogenesis is dependent on RhoA/ROCK and FAK signaling, whereby increased RhoA activity promotes focal adhesion formation and osteogenesis, while decreased FAK signaling also promotes osteogenesis, possibly through inhibition of proliferation. An understanding of the interplay between RhoA and FAK signaling would further clarify this model, as it is known that FAK transiently suppresses RhoA activity and that FAK-/- cells can lead to constitutive activation of RhoA and loss of focal adhesion turnover [110]. Further understanding of how FAK and RhoA signals integrate for downstream effects on hMSC differentiation would further clarify a role for adhesion signaling molecules in osteogenesis of hMSC on a variety of substrates.

# APPENDIX

## MATERIALS AND METHODS

### Cell culture

Human mesenchymal stem cells originated from whole marrow aspirates from vertebral bodies. Adherent cells were cultured in supplemented McCoy's 5A as previously described [197] with 20% defined FBS, and at passage 5, immortalized with a large T-antigen temperature permissive (32$^{o}$C) and tetracycline restrictive retrovirus (NIT construct kindly provided by Dr. Steven Suhr, University of Michigan). Cells were regularly cultured at the permissive temperature (32$^{o}$C), but upon plating were switched to the restrictive temperature (37$^{o}$C) in the presence of the tetracycline analogue, doxycycline [198]. For all experiments, cells were plated using 2% defined FBS. Control conditions were 2% defined FBS and 1μg/mL doxycycline in supplemented McCoy's 5A. Osteogenic conditions were 2% defined FBS, 1uM dexamethasone, 25μg/mL ascorbic acid, 5mM β-glycerol phosphate, 1% ITS supplement and 1μg/mL doxycycline (all reagents were from Sigma-Aldrich with the exception of ITS, which was from BD Biosciences). Media was changed every 3 days throughout experiments.

### Creation of retroviral constructs

The pRET-X-IRES plasmid typically used by our laboratory for hMSC transduction was used to construct recombinant retroviruses for RhoV14, RhoN19, DTER, FRNK and Y397. Rho and FAK plasmids were provided by Dr. Christopher Chen (University of Pennsylvania, Department of Bioengineering).

All plasmids were amplified using DH5α$^{TM}$ competent cells (Invitrogen) and consequent selected colonies were used for cloning into the pRET retroviral vector.
RhoV14, RhoN19 and DTER were cut out of the TF vector using BamHI-XhoI restriction enzymes and ligated to the pRET retroviral vector also cut with BamHI-XhoI. FRNK and Y397 were isolated from the pKH3 vector using BamHI-EcoRI and BamHI, respectively and ligated to linearized pRLP2 retroviral vector cut with the appropriate restriction enzymes. Clones containing correct sequences were quantified and used for subsequent production of retroviral supernatant as described below.

Generation of stable retroviral producer lines

Prior to retroviral transduction of hMSC, stable retroviral producer lines were first made. Phoenix E (ecotropic) cells were plated at $4x10^5$ cells/cm$^2$ in a 6-well plate and cultured for 24hrs upon which cells were given fresh media (high-glucose DMEM, 10% FBS, Pen-strep and L-glutamine). Five minutes prior to transfection, chloroquine dihydrochloride (Sigma, S764663) was added to phoenix cells. Approximately 2μg of supercoiled plasmid DNA was transfected into phoenix cells using the Promega Profection kit (E1200). The media was exchanged with fresh media at 8-10 hours following transfection. On the following day, media was changed again and the cells were shifted to 32$^o$C. PG-13 cells (GALV pseudotyped) were plated at $2.5x10^3$ cells/cm$^2$ in a 6-well plate and cultured overnight. The following day, retroviral supernatant was harvested from phoenix cells, 0.45μm filtered to remove cell debris and supplemented with a polycation (protamine sulfate (2.5μg/mL) or polybrene (1μg/mL)) in order to increase viral adsorption to the target cell membrane, before 2mL was added to the PG13 cells. This procedure was then repeated on the following two

days. The PG13 cells were then considered stable retroviral producer cell lines. The media was then changed from phoenix media to hMSC media for another 24hrs.

Retroviral transduction of hMSC

hMSC immortalized with NIT-Tag were plated at a density of $1x10^4$cells/$cm^2$ in a 6-well plate for 24hrs. Retroviral supernatant of PG13 cells grown in human culture medium (Assay McCoy's, 20% FBS) was harvested as described above or alternatively, filtered retroviral supernatant that was frozen at -80$^o$C was thawed to 37$^o$C and supplemented with either protamine sulfate or polybrene. Human culture media was replaced with 4mL of retroviral supernatant, plates were sealed with parafilm and centrifuged at 32$^o$C for 90 minutes at 1200g. Retroviral supernatant was then immediately replaced with fresh culture medium (Assay McCoy's, 20% FBS) following centrifugation, and this procedure was repeated on the following day.

Polymer film fabrication and assembly for cell culture

Poly-ε-caprolactone (with molecular weights of approximately 10 000, 42 500 and 80 000) (Sigma-Aldrich), poly(DL-lactide-co-glycolide) 50:50 (with molecular weights of approximately 27 000, 47 100 and 76 000 with acid end groups) and poly(DL-lactide-co-glycolide) 85:15 (with molecular weights of approximately 42 000, 66 100 and 95 000 with ester capped end groups) (both from Lakeshore Biomaterials) were dissolved in chloroform to 8% (weight-volume, so that films would have a theoretical film thickness of 100μm). They were then cast on glass plates coated with Sigmacote (Sigma-Aldrich) and vacuum-annealed at 80$^o$C for 12hr and then slowly cooled at a rate of 1$^o$C/min. Following a 24hr cooling period, films were peeled away from the plates.

Sodium alginate (Sigma-Aldrich) was crosslinked with calcium carbonate in the presence of D-(+)-Gluconic acid δ-lactone (GDL) (Sigma) as previously described [10]. Briefly, high-viscosity sodium alginate prepared from Macrocystis pyrifera (MP) (Sigma) was dissolved in deionized water to make a 2.5% solution and autoclaved. Calcium carbonate ($CaCO_3$) in combination with GDL was used as a source of calcium ions to initiate gelation. A $CaCO_3$ to GDL molar ratio of 0.5 was maintained to achieve neutral pH. A calcium ion to carboxyl molar ratio of 0.18 was designated as 1X. The crosslinking density was adjusted as a factor of this molar ratio; 2X had a molar ratio of 0.36 and so on. A $CaCO_3$ suspension was added to the sodium alginate solution, mixed and vortexed for one minute. A fresh aqueous GDL solution was then added to the new suspension and vortexed for 1 min to initiate gelation. Alginate was then cast within the wells of the cell assemblies by pipette. For PCL and PLGA, films were cut to size a 35mm well-cast PDMS 1.5cmx1.5cm-cut window and placed glass-side up within a 35mm plate. For PCL assemblies, in order to prevent leaks, Vaseline was placed around the edge of the PDMS windows. For control surfaces, wells contained only PDMS with or without Vaseline where appropriate (for PCL). All cell assemblies were then sterilized with ethylene gas (courtesy of Dr. Laura Smith, University of Michigan) with the exception of alginate assemblies, which were sterilized with UV disinfection for 20min prior to use.

Materials characterization

Contact angle and area measurements

Using the sessile drop method, 2μL of water was placed in duplicate on 10 samples of each of the materials of interest. Images were taken of the interface at 10, 30 and 60s with a standard digital camera and measured using ImageJ software (NIH).

Similarly, contact area of the water was captured at the same timepoints using either a 2x or 2.5x objective on an inverted microscope and quantified with either ImageJ (NIH) or AxioVision (Zeiss) software.

Film thickness measurement and imaging

Cross-sections and top-views of films were examined using Environmental SEM (FEI XL30) at 2-5kV using either high vacuum or wet mode where appropriate (Drexel University Centralized Research Facilities). Cross-sections were quantified over a range of the sample at 800-1000x magnification at 8-10 sample points.

Compression test

All polymers were cast into a custom-built mold housing creating cylindrical specimens that were $2cm^2$ in diameter, with a height to width ratio of 2:1. Polymers were either dissolved or crosslinked as described above. Following cooling/crosslinking for 24hrs, samples were tested on a mini Instron MTS machine at a rate of 5mm/min. Raw data was analyzed using a Matlab program (kindly provided by Jeff Meganck, University of Michigan) to identify the elastic region of the stress-strain curve in order to calculate compressive stiffness, E.

Total protein adsorption

A modified version of a previously published method was used to investigate whole serum protein adsorption on polymer films [170]. Cell assemblies were washed with 1X PBS, two times for 30 minutes. Eight assemblies per surface type were used. Each assembly received 0.75mL of 2% defined FBS in 1X PBS and was incubated at 37°C for 2 hrs. The serum solution was them removed from assemblies. Assemblies were

washed four times in 1X PBS, and a sample of each wash was saved for the assay. Blank anchors were then transferred to new 35mm plates. Adsorbed protein was removed by exposing assemblies to 0.75mL of 2% SDS in 1X PBS for 1hr at room temperature. Protein solutions were then assayed with a Micro BCA$^{TM}$ Assay as per manufacturer's instructions in triplicate (Pierce, Rockford, IL) and absorbance was read at 562nm in a plate reader and compared to a BSA standard curve in a 96 well plate.

Cell detachment assay

Prior to cell seeding, surfaces were exposed to two washes of 1x PBS for 30min. Cells were made into a homogenous solution first using cell lysis buffer and then trypsinization. Cells were plated in 2% defined FBS at $2x10^4$ cells/cm$^2$ on polymer film and control cell assemblies. Multiple timepoints were taken in order to establish an adhesion and proliferation curve as described by Vogler [38] for cells on each polymer. Three wells were harvested at timepoints ranging from 5min to 72hours. At each timepoint, wells were gently rinsed with PBS and frozen at -80$^o$C. The Cyquant® proliferation assay (Invitrogen) was performed on assemblies to quantify nucleic acid content at the conclusion of the experiment, as per manufacturer's instructions.

Adhesion strength assays

Shear loading assay

The bulk adhesive strength of cells bound to substrates at $t_{max}$ (Figure 1.1) was examined using fluid shear. Cells underwent a wall shear stress of 0-25 Pa using oscillatory fluid flow for 30 cycles. The shear required for 50% detachment of cells on each polymer ($\tau_{50}$) was determined using least squares analysis. The fluid shear

system has been characterized [93] and used for loading MSC, adipocytes and osteoblasts in the Orthopaedic Research Laboratories (University of Michigan).

Preparation of Culture Slides for Fluid Shear Device

In order to increase adhesion between glass slides and polymer films, glass slides were acid-etched and silanized [199][200] using γ-aminopropyltriethoxysilane followed by incubation in 0.25% gluteraldehyde. Cast silicone chambers with an adhesive sealant were then pressed onto the silanized slides creating a seal to allow casting of polymer films as previously described. Twenty four hours later, following sterilization, cells were seeded on the slides at $2x10^4$ cells/$cm^2$ and left to adhere for $t_{max}$ (1 hour). Slides were then inserted into the parallel plate flow chambers. Teflon lines connect the chambers to media-filled syringes attached to a motor controlled by custom-written computer programs generating oscillatory fluid flow at the required shear. Untouched samples in chambers served as relative controls. At the conclusion of the loading regimen, slides were rinsed in PBS, frozen at -80°C and later cell number was quantified by Cyquant assay (Invitrogen).

Spinning disk assay

Cells were plated on drop-coated polymer coverslips at a density of $2x10^4$ cells/$cm^2$ for $t_{max}$ (1 hour) prior to the assay. The device used has been previously characterized [201] and consists of a fluid-filled cylinder, the center of which contains the disk holder and sample. Briefly, cell-seeded coverslips were placed in the chamber which was then filled with adhesion buffer and each was spun for 5min at a rate such that the maximum shear induced at the edge of the coverslip was approximately 250 dynes/$cm^2$ (approximately 2500 rpm). After spinning, cells were fixed in 3.7% formaldehyde,

permeabilized in 1% Triton-X 100 and stained with DAPI. Cells were quantified using an upright microscope (Nikon Diaphot, Nikon, Japan) with an automated stage and imaging analysis software (Image-1, Universal Imaging, West Chester PA) which takes 61 fluorescent images of each coverslip automatically at specific radial distances representing demarcated shear values. A detachment curve for each experiment was then plotted and fit to a sigmoidal curve (as the number of cells decreases non-linearly with applied force). The 50% detachment strength was determined using least squares analysis/linear regression in SigmaPlot. For each experiment, 6-12 samples per cell type or surface were spun. Only experiments demonstrating a linear $R^2$ value of greater than or equal to 0.65 were reported.

Differentiation studies

Cells were plated at a density of $2x10^4$ cells/$cm^2$ on each surface at the restrictive temperature (37$^oC$) with 1μg/mL doxycycline and 2% defined serum. Cells were then induced with control (as above) or osteogenic media 48hrs post-plating. Osteogenic induction media consisted of 1μM dexamethasone, 2% defined FBS, 5mM β-glycerolphosphate, 33mg/mL ascorbic acid-2-phosphate (Sigma-Aldrich) and 1% ITS supplement (BD Biosciences) and media was changed every 3 days. For ROCK inhibitor experiments, Y27632 (Calbiochem) was used at a dose of 10μM and added daily. Cells were harvested on day 15 for alkaline phosphatase activity as well as the Cyquant assay for normalization to cell number. On days 21 through 35, cells were harvested for Alizarin Red staining, free-calcium measurements and the Cyquant assay.

Alkaline phosphatase activity assay

Cells plated for differentiation studies in cell assemblies as above were harvested at day 15 via media aspiration and one rinse in PBS. To quantify alkaline phosphatase activity, a pNPP based assay kit (Sigma, St. Louis, MO) was used. Alkaline reaction buffer (200μL) was added to each assembly followed by 200μL of 2x pNPP substrate solution and plates were then incubated for 10 minutes at 37$^{o}$C. pNP production was measured immediately using a Varioskan Flash microplate reader (Thermo Scientific) at 405nm and compared to a standard curve.

Calcium Assay

Calcium was liberated from deposited mineral via addition of 0.6M HCl into cell assemblies overnight with gentle agitation. To quantify released calcium, the Calcium (CPC) LiquiColor® Test using cresolphthalein complexone methodology was used (StanBio, Boerne, TX). Briefly, base and color reagents were mixed in equal proportions and were allowed to settle at room temperature for 10 min. Calcium lysate (300μL) was added to a 96 well plate in triplicate to which 60μL of the working reagent was added, tapped to mix and incubated at room temperature for 5-15min. The plate was then read on a Varioskan Flash microplate reader (Thermo Scientific) at 550nm and quantities were compared relative to a supplied standard.

Alizarin Red staining

The proportion of hMSC seeded on the polymers that differentiate to the osteoblastic lineage was determined via the cytochemical stain 1% Alizarin Red (for $Ca_2PO_4$). On the day of harvest (days 21-35), media was aspirated and assemblies were gently rinsed twice with PBS. Cells were then fixed in 50% ethanol for 3 minutes, followed by

staining in Alizarin Red solution for 5 minutes. Plates were then rinsed three times with distilled water to remove excess stain.

Quantitative RT-PCR

Cells were plated in either 6-well tissue culture plastic wells, or in cell assemblies adapted to 60mm plates. At harvest, total RNA was isolated using the Qiagen RNeasy kit. RNA was dissolved in DEPC dd$H_20$ and stored at -80$^0$C. Primers were designed for the following genes using Primer3 software (Whitehead Institute, Cambridge, MA); cbfa1, osterix, type I collagen and osteomodulin. These markers were normalized to the housekeeping gene β-actin. cDNAs were synthesized using the High Capacity RNA-to-cDNA Kit (Applied Biosystems) and then PCR was performed using SybrGreen Master Mix (Applied Biosystems) both according to manufacturer's protocols. All PCR samples were prepared in duplicate wells of a 96-well plate and PCR reactions were run on a 7500 Fast Real Time-PCR Machine (Applied Biosystems). To ensure primer specificity, melt curves were performed after 40 cycles of PCR. Fold changes in gene expression were calculated using the ΔΔCT method [202][203], comparing control samples to osteogenic-treated samples and normalizing to β-actin. Experiments were run in triplicate.

FAK Y397 activity

Phosphorylation of FAK Y397 was quantified using the PhosphoDetect$^{TM}$ FAK (pTyr$^{397}$) Elisa kit (Calbiochem). hMSC (pRLP2, Y397, DTER and FRNK) were grown in T75 flasks for 7 days under standard growth conditions. Cells were then lysed in cell lysis buffer (Cytoskeleton) and snap-frozen in liquid nitrogen and stored at -80$^0$C until use.

The protocol for the Elisa was as per manufacturer's instructions and samples were run in triplicate.

Western Blotting

Lysates from FAK mutant hMSC described in the FAK Y397 activity assay above were quantified using the Protein Red assay (Cytoskeleton), and equal quantities of protein were loaded onto NuPage gels (Invitrogen). Protein was transferred to Immobilon (Millipore) and probed using a primary antibody against FAK (BC3, Millipore) and a secondary Goat anti-Rabbit antibody (IgG, Pierce). Protein was detected using a chemiluminescent reagent (SuperSignal, Pierce).

RhoGTPase activity assay

The Cytoskeleton G-LISA$^{TM}$ RhoA Activity Assay Biochem Kit$^{TM}$ specifically quantifies the amount of GTP-bound RhoA within a cell lysate. Briefly, the cell lysate is incubated with an affinity plate containing the RDB domain, which binds the RhoA effector domain in the sample. RhoA is then specifically detected by incubation with first a specific primary antibody followed by a secondary antibody conjugated to horseradish peroxidase. The signal is then developed with a substrate and the colorimetric reaction product is read on a microplate reader at 490nm. Pilot RhoA activity assays conducted for control immortalized hMSC (pRET) lysates indicated an optimal GTPase concentration of approximately 0.5ng/mL lysate. hMSC providing this concentration were harvested and snap frozen in accordance with the protocol. Quantification of the RhoA activity levels for RhoV14 and RhoN19 immortalized hMSC relative to control cells (pRET) demonstrated the success of the introduced transgenes in increasing and decreasing the levels of active RhoA GTPase, respectively.

Immunofluorescence and imaging

In order to investigate both cell morphology and focal adhesions, cells were grown at $2x10^4$cells/$cm^2$ on drop-coated polymer coverslips in 35mm plates for one hour, rinsed twice with PBS and then fixed and permeabilized in 3.7% paraformaldehyde with Triton X-100 at $37^0$C for 30 minutes. Cells were then rinsed twice after removing the fixative solution and 500μL of blocking buffer (1% bovine serum albumin in PBS) was added. Coverslips were incubated in blocking buffer for 30 minutes at $37^0$C. Blocking buffer was then removed and diluted primary antibody (1:200 for either paxillin (Zymed) or vinculin (Chemicon)) was added and coverslips were incubated for 1 hour at room temperature in the dark. Primary antibodies were then removed and coverslips were washed three times in PBS. Diluted secondary antibody (1:200, goat anti-mouse, FITC conjugated, Chemicon) with Alexa Fluor 594 conjugated phalloidin (Invitrogen) was then added to coverslips for 45 minutes at room temperature in the dark. DAPI to 300nM was then added to the coverslips and they were incubated an additional 15 minutes. Coverslips were then washed three times in PBS and the solution was removed. Coverslips were allowed to air dry for a few minutes and were then mounted upright in ProLong Gold anti-fade mounting solution (Invitrogen), and then coverslipped again. Slides were stored at $4^0$C in the dark until imaged. All coverslips were imaged on an upright Olympus Fluoview FV1000 confocal microscope. Images were taken at 40x magnification under oil immersion with or without zoom. Due to the changing planes of focus caused by polymer irregularities, z-stack projections were made for each sample with 6-10 slices at 0.8μm each.

Focal adhesion quantification

Focal adhesion numbers were quantified from confocal images taken of hMSC lines on polymer-coated coverslips stained for either paxillin or vinculin (described above). Z-stack projections were analyzed using ImageJ (NIH) by first thresholding 40x images within saturation and pixels were counted via analysis of particles. Particles greater in size than 3μm were removed from the count as focal adhesions have been shown to be less than that size [58]. Numbers were normalized to total cell number in the image based on DAPI staining and reported. On average, 30-60 cells were analyzed per hMSC line or polymer type.

Quantification of Adsorbed Fibronectin

For radiolabeled adsorption experiments, fibronectin was iodinated using a 125I-labeled Bolton–Hunter reagent (DuPoint NEN, Boston, MA). The organic solvent in the reaction vessel was evaporated with nitrogen gas and 10mg of fibronectin in coupling buffer (0.1M sodium borate, pH 8.5) was added. After 15min of conjugation at 0$^{o}$C, the reaction was stopped with the addition of stop buffer (0.2M glycine, 0.1M sodium borate, pH 8.5). The radiolabeled fibronectin was purified by collecting the appropriate fractions from a 1mL size exclusion chromatography column (BioRad BioGel P10DG Desalting Column, Hercules, CA) that had been previously blocked overnight with hemoglobin. Various ratios of labeled to unlabeled fibronectin were used to prepare the final solution concentrations of 1, 2, 5, 10 and 20 μg/mL in PBS. Coverslips (15mm) cast with ePLGA (made as previously described) were oriented upright and incubated with 100μL of radiolabeled solution for 1 hr. Then coverslips were rinsed 5 times in PBS and samples were analyzed using a gamma counter

(Perkin Elmer Life Sciences, Boston, MA). Each condition was done with 6 replicates and the experiment was repeated twice.

### Statistics

All conditions in experiments were done at minimum in triplicate. For comparing two means, the student's t-test was used. For comparing mean groups (across polymer type or cell type), ANOVA/ANCOVA was used to test for significance followed by a post-hoc Tukey's test. Adhesion strength data was fit to material characterization data using a restricted cubic spline in STATA or multiple linear regression using SimStat v2.5.5. Statistical approaches were determined in discussion with The University of Michigan Center for Statistical Consultation and Research. On graphs, values are plotted as plus or minus standard error. A p-value of 0.05 was considered significant.

## REFERENCES


1 MedTech Insight. (2004) Trends and Opportunities in U.S. Orthopedic Markets for Implant, Reconstruction, and Trauma Products, A310

2 Liu, X. and Ma, P.X. (2004) Polymeric scaffolds for bone tissue engineering. *Ann Biomed Eng* 32, 477-486

3 Ma, P.X. (2003) Tissue Engineering. In *Encyclopedia of Polymer Science and Technology*

4 Kohn, J. and Langer, R. (1996) Bioresorbable and Bioerodible Materials. In *Biomaterials Science: An Introduction to Materials in Medicine* (Ratner, B.D. *et al*, eds.), pp. 64-69, Academic Press

5 Leitner, J.M. *et al*. (2008) The pharmacokinetics and pharmacodynamics of a new sustained-release leuprolide acetate depot compared to market references. *Int. J. Clin. Pharmacol. Ther.* 46, 407-414

6 Woodward, S.C. *et al*. (1985) The intracellular degradation of poly(epsilon-caprolactone). *J Biomed Mater Res* 19, 437-444

7 Pitt, C.G. *et al*. (1981) Aliphatic Polyesters .2. the Degradation of Poly(dl-Lactide), Poly(epsilon-Caprolactone), and their Copolymers Invivo. *Biomaterials* 2, 215-220

8 Barber, F.A. and Click, J.N. (1992) The effect of inflammatory synovial fluid on the breaking strength of new "long lasting" absorbable sutures. *Arthroscopy* 8, 437-441

9 Schuckert, K.H. *et al*. (2008) Mandibular Defect Reconstruction Using Three-Dimensional Polycaprolactone Scaffold in Combination with Platelet-Rich Plasma and Recombinant Human Bone Morphogenetic Protein-2: De Novo Synthesis of Bone in a Single Case. *Tissue Eng. Part A, Epub*

10 Kuo, C.K. and Ma, P.X. (2001) Ionically crosslinked alginate hydrogels as scaffolds for tissue engineering: part 1. Structure, gelation rate and mechanical properties. *Biomaterials* 22, 511-521

11 Smidsrod, O. and Skjak-Braek, G. (1990) Alginate as immobilization matrix for cells. *Trends Biotechnol* 8, 71-78

12 Bell, A. and Hart, J. (2007) Evaluation of two absorbent silver dressings in a porcine partial-thickness excisional wound model. *J. Wound Care* 16, 445-8, 450-3

13 van Schilfgaarde, R. and de Vos, P. (1999) Factors influencing the properties and performance of microcapsules for immunoprotection of pancreatic islets. *J. Mol. Med.* 77, 199-205

14 Whitford, G.M. *et al*. (1980) Subcutaneously implanted alginate as a continuous-release source of fluoride. *J. Dent. Res.* 59, 186-191

15 Ouyang, H.W. *et al*. (2002) Characterization of anterior cruciate ligament cells and bone marrow stromal cells on various biodegradable polymeric films. *Materials Science & Engineering C-Biomimetic and Supramolecular Systems* 20, 63-69

16 Lim, J.Y. *et al*. (2004) Systematic variation in osteoblast adhesion and phenotype with substratum surface characteristics. *J Biomed Mater Res A* 68, 504-512

17 Lawson, M.A. *et al*. (2004) Adhesion and growth of bone marrow stromal cells on modified alginate hydrogels. *Tissue Eng.* 10, 1480-1491

18 Lee, J.W. *et al*. (2004) Importance of integrin beta1-mediated cell adhesion on biodegradable polymers under serum depletion in mesenchymal stem cells and chondrocytes. *Biomaterials* 25, 1901-1909

19 Kotobuki, N. *et al*. (2005) Observation of osteogenic differentiation cascade of living mesenchymal stem cells on transparent hydroxyapatite ceramics. *Biomaterials* 26, 779-785

20 Kieswetter, K. *et al*. (1996) Surface roughness modulates the local production of growth factors and cytokines by osteoblast-like MG-63 cells. *J. Biomed. Mater. Res.* 32, 55-63

21 Keselowsky, B.G. *et al*. (2005) Integrin binding specificity regulates biomaterial surface chemistry effects on cell differentiation. *Proc. Natl. Acad. Sci. U. S. A.* 102, 5953-5957

22 Shin, H. *et al*. (2005) Osteogenic differentiation of rat bone marrow stromal cells cultured on Arg-Gly-Asp modified hydrogels without dexamethasone and beta-glycerol phosphate. *Biomaterials* 26, 3645-3654

23 Lee, K.Y. *et al*. (2004) Nanoscale adhesion ligand organization regulates osteoblast proliferation and differentiation. *Nano Letters* 4, 1501-1506

24 Shin, H. *et al*. (2004) Modulation of differentiation and mineralization of marrow stromal cells cultured on biomimetic hydrogels modified with Arg-Gly-Asp containing peptides. *J. Biomed. Mater. Res. A.* 69, 535-543

25 Tosatti, S. *et al*. (2004) RGD-containing peptide GCRGYGRGDSPG reduces enhancement of osteoblast differentiation by poly(L-lysine)-graft-poly(ethylene glycol)-coated titanium surfaces. *J. Biomed. Mater. Res. A.* 68, 458-472

26 Chen, J. *et al*. (2003) Human bone marrow stromal cell and ligament fibroblast responses on RGD-modified silk fibers. *J. Biomed. Mater. Res. A.* 67, 559-570

27 Cutler, S.M. and Garcia, A.J. (2003) Engineering cell adhesive surfaces that direct integrin alpha5beta1 binding using a recombinant fragment of fibronectin. *Biomaterials* 24, 1759-1770

28 Hersel, U. *et al*. (2003) RGD modified polymers: biomaterials for stimulated cell adhesion and beyond. *Biomaterials* 24, 4385-4415

29 Huang, H. *et al*. (2003) Enhanced osteoblast functions on RGD immobilized surface. *J. Oral Implantol.* 29, 73-79

30 Koo, L.Y. *et al*. (2002) Co-regulation of cell adhesion by nanoscale RGD organization and mechanical stimulus. *J. Cell. Sci.* 115, 1423-1433

31 Schliephake, H. *et al*. (2002) Effect of RGD peptide coating of titanium implants on periimplant bone formation in the alveolar crest. An experimental pilot study in dogs. *Clin. Oral Implants Res.* 13, 312-319

32 Kantlehner, M. *et al*. (2000) Surface coating with cyclic RGD peptides stimulates osteoblast adhesion and proliferation as well as bone formation. *Chembiochem* 1, 107-114

33 LeBaron, R.G. and Athanasiou, K.A. (2000) Extracellular matrix cell adhesion peptides: functional applications in orthopedic materials. *Tissue Eng.* 6, 85-103

34 Hosseinkhani, H. *et al*. (2006) Osteogenic differentiation of mesenchymal stem cells in self-assembled peptide-amphiphile nanofibers. *Biomaterials* 27, 4079-4086

35 Vasita, R. *et al*. (2008) Improved biomaterials for tissue engineering applications: surface modification of polymers. *Curr. Top. Med. Chem.* 8, 341-353

36 Hsiong, S.X. *et al*. (2008) Cyclic Arginine-Glycine-Aspartate Peptides Enhance Three-Dimensional Stem Cell Osteogenic Differentiation. *Tissue Eng. Part A, Epub*

37 Hsiong, S.X. *et al*. (2008) Differentiation stage alters matrix control of stem cells. *J. Biomed. Mater. Res. A.* 85, 145-156

38 Vogler, E.A. (1988) Thermodynamics of short-term cell adhesion in vitro. *Biophys J* 53, 759-769

39 Anselme, K. (2000) Osteoblast adhesion on biomaterials. *Biomaterials* 21, 667-681

40 Wilson, C.J. *et al*. (2005) Mediation of biomaterial-cell interactions by adsorbed proteins: a review. *Tissue Eng.* 11, 1-18

41 Arima, Y. and Iwata, H. (2007) Effect of wettability and surface functional groups on protein adsorption and cell adhesion using well-defined mixed self-assembled monolayers. *Biomaterials* 28, 3074-3082

42 Renner, L. *et al*. (2005) Fibronectin displacement at polymer surfaces. *Langmuir* 21, 4571-4577

43 Wang, H. *et al*. (2006) Modulating cell adhesion and spreading by control of FnIII7-10 orientation on charged self-assembled monolayers (SAMs) of alkanethiolates. *J. Biomed. Mater. Res. A*. 77, 672-678

44 Zaidel-Bar, R. *et al*. (2004) Hierarchical assembly of cell-matrix adhesion complexes. *Biochem Soc Trans* 32, 416-420

45 Reilly, G.C. *et al*. (2003) Fluid flow induced PGE2 release by bone cells is reduced by glycocalyx degradation whereas calcium signals are not. *Biorheology* 40, 591-603

46 Sampathkumar, S.G. *et al*. (2006) Metabolic installation of thiols into sialic acid modulates adhesion and stem cell biology. *Nat. Chem. Biol.* 2, 149-152

47 Vitte, J. *et al*. (2004) Is there a predictable relationship between surface physical-chemical properties and cell behaviour at the interface? *Eur. Cell. Mater.* 7, 52-63; discussion 63

48 Hynes, R.O. (2003) Structural biology. Changing partners. *Science* 300, 755-756

49 Larjava, H. *et al*. (2008) Kindlins: essential regulators of integrin signalling and cell-matrix adhesion. *EMBO Rep.,* Epub

50 Gronthos, S. *et al*. (1997) Integrin expression and function on human osteoblast-like cells. *J. Bone Miner. Res.* 12, 1189-1197

51 Salasznyk, R.M. *et al*. (2007) Activation of FAK is necessary for the osteogenic differentiation of human mesenchymal stem cells on laminin-5. *J. Cell. Biochem.* 100, 499-514

52 Salasznyk, R.M. *et al*. (2004) Adhesion to Vitronectin and Collagen I Promotes Osteogenic Differentiation of Human Mesenchymal Stem Cells. *J. Biomed. Biotechnol.* 2004, 24-34

53 Cool, S.M. and Nurcombe, V. (2005) Substrate induction of osteogenesis from marrow-derived mesenchymal precursors. *Stem Cells Dev.* 14, 632-642

54 Kumarasuriyar, A. *et al*. (2008) Glycosaminoglycan composition changes with MG-63 osteosarcoma osteogenesis in vitro and induces human mesenchymal stem cell aggregation. *J. Cell. Physiol.* 218, 501-511

55 Luo, W. *et al*. (2008) Disruption of cell-matrix interactions by heparin enhances mesenchymal progenitor adipocyte differentiation. *Exp. Cell Res.* 314, 3382-3391

56 Berrier, A.L. and Yamada, K.M. (2007) Cell-matrix adhesion. *J. Cell. Physiol.* 213, 565-573

57 Kreis, T.E. *et al*. (1982) Mobility of microinjected rhodamine actin within living chicken gizzard cells determined by fluorescence photobleaching recovery. *Cell* 29, 835-845

58 Franz, C.M. and Muller, D.J. (2005) Analyzing focal adhesion structure by atomic force microscopy. *J. Cell. Sci.* 118, 5315-5323

59 Zaidel-Bar, R. *et al*. (2007) A paxillin tyrosine phosphorylation switch regulates the assembly and form of cell-matrix adhesions. *J. Cell. Sci.* 120, 137-148

60 Zaidel-Bar, R. *et al*. (2007) Functional atlas of the integrin adhesome. *Nat. Cell Biol.* 9, 858-867

61 Guan, J.L. (1997) Role of focal adhesion kinase in integrin signaling. *Int. J. Biochem. Cell Biol.* 29, 1085-1096

62 Schaller, M.D. *et al*. (1994) Autophosphorylation of the focal adhesion kinase, pp125FAK, directs SH2-dependent binding of pp60src. *Mol. Cell. Biol.* 14, 1680-1688

63 Scheswohl, D.M. *et al*. (2008) Multiple paxillin binding sites regulate FAK function. *J. Mol. Signal.* 3, 1

64 Tafolla, E. *et al*. (2005) JNK1 and JNK2 oppositely regulate p53 in signaling linked to apoptosis triggered by an altered fibronectin matrix: JNK links FAK and p53. *J Biol Chem* 280, 19992-19999

65 Parsons, J.T. (2003) Focal adhesion kinase: the first ten years. *J Cell Sci* 116, 1409-1416

66 Hamadi, A. *et al*. (2005) Regulation of focal adhesion dynamics and disassembly by phosphorylation of FAK at tyrosine 397. *J. Cell. Sci.* 118, 4415-4425

67 Pirone, D.M. *et al*. (2006) An inhibitory role for FAK in regulating proliferation: a link between limited adhesion and RhoA-ROCK signaling. *J. Cell Biol.* 174, 277-288

68 Thomas, J.W. *et al*. (1999) The role of focal adhesion kinase binding in the regulation of tyrosine phosphorylation of paxillin. *J. Biol. Chem.* 274, 36684-36692

69 Wang, R. *et al*. (2005) Fibronectin's central cell-binding domain supports focal adhesion formation and Rho signal transduction. *J. Biol. Chem.* 280, 28803-28810

70 Ridley, A.J. and Hall, A. (1992) The small GTP-binding protein rho regulates the assembly of focal adhesions and actin stress fibers in response to growth factors. *Cell* 70, 389-399

71 Riveline, D. *et al*. (2001) Focal contacts as mechanosensors: externally applied local mechanical force induces growth of focal contacts by an mDia1-dependent and ROCK-independent mechanism. *J Cell Biol* 153, 1175-1186

72 Chrzanowska-Wodnicka, M. and Burridge, K. (1996) Rho-stimulated contractility drives the formation of stress fibers and focal adhesions. *J. Cell Biol.* 133, 1403-1415

73 Zigmond, S.H. (1996) Signal transduction and actin filament organization. *Curr Opin Cell Biol* 8, 66-73

74 Hotchin, N.A. and Hall, A. (1995) The assembly of integrin adhesion complexes requires both extracellular matrix and intracellular rho/rac GTPases. *J. Cell Biol.* 131, 1857-1865

75 Ji, L. *et al*. (2008) Fluctuations of intracellular forces during cell protrusion. *Nat. Cell Biol.* 10, 1393-1400

76 Gee, E.P. *et al*. (2008) Fibronectin Unfolding Revisited: Modeling Cell Traction-Mediated Unfolding of the Tenth Type-III Repeat. *PLoS ONE* 3, e2373

77 Van der Velde-Zimmermann, D. *et al*. (1997) Fibronectin distribution in human bone marrow stroma: matrix assembly and tumor cell adhesion via alpha5 beta1 integrin. *Exp Cell Res* 230, 111-120

78 Hughes, D.E. *et al*. (1993) Integrin expression in human bone. *J. Bone Miner. Res.* 8, 527-533

79 Gronthos, S. *et al*. (2001) Integrin-mediated interactions between human bone marrow stromal precursor cells and the extracellular matrix. *Bone* 28, 174-181

80 Bennett, J.H. *et al*. (2001) Cell adhesion molecules in human osteoblasts: structure and function. *Histol Histopathol* 16, 603-611

81 Moursi, A.M. *et al*. (1997) Interactions between integrin receptors and fibronectin are required for calvarial osteoblast differentiation in vitro. *J. Cell. Sci.* 110 ( Pt 18), 2187-2196

82 Zimmerman, D. *et al*. (2000) Impaired bone formation in transgenic mice resulting from altered integrin function in osteoblasts. *Dev Biol* 220, 2-15

83 Damsky, C.H. (1999) Extracellular matrix-integrin interactions in osteoblast function and tissue remodeling. *Bone* 25, 95-96

84 Cacciari, B. and Spalluto, G. (2005) Non peptidic alphavbeta3 antagonists: recent developments. *Curr Med Chem* 12, 51-70

85 Lai, C.F. and Cheng, S.L. (2005) Alphavbeta integrins play an essential role in BMP-2 induction of osteoblast differentiation. *J Bone Miner Res* 20, 330-340

86 Cheng, S.L. *et al*. (2001) Bone mineralization and osteoblast differentiation are negatively modulated by integrin alpha(v)beta3. *J Bone Miner Res* 16, 277-288

87 Garcia, A.J. and Gallant, N.D. (2003) Stick and grip: measurement systems and quantitative analyses of integrin-mediated cell adhesion strength. *Cell Biochem Biophys* 39, 61-73

88 Gallant, N.D. and Garcia, A.J. (2007) Quantitative analyses of cell adhesion strength. *Methods Mol. Biol.* 370, 83-96

89 Das, T. *et al*. (2008) Traction force microscopy on-chip: shear deformation of fibroblast cells. *Lab. Chip* 8, 1308-1318

90 Shim, J. *et al*. (2008) Measurement of the tensile strength of cell-biomaterial interface using the laser spallation technique. *Acta Biomater.* 4, 1657-1668

91 Boettiger, D. (2007) Quantitative measurements of integrin-mediated adhesion to extracellular matrix. *Methods Enzymol.* 426, 1-25

92 Hammer, D.A. and Lauffenburger, D.A. (1987) A dynamical model for receptor-mediated cell adhesion to surfaces. *Biophys J* 52, 475-487

93 Ominsky, M.S. (2003) Effects of Hydrostatic Pressure, Biaxial Strain, and Fluid Shear on Osteoblastic Cells: Mechanotransduction via NF-kB, MAP Kinase, and AP-1 Pathways, University of Michigan, AAT 3096163

94 Garcia, A.J. *et al*. (1997) Quantification of cell adhesion using a spinning disc device and application to surface-reactive materials. *Biomaterials* 18, 1091-1098

95 Lotz, M.M. *et al*. (1989) Cell adhesion to fibronectin and tenascin: quantitative measurements of initial binding and subsequent strengthening response. *J Cell Biol* 109, 1795-1805

96 Balaban, N.Q. *et al*. (2001) Force and focal adhesion assembly: a close relationship studied using elastic micropatterned substrates. *Nat Cell Biol* 3, 466-472

97 Selhuber-Unkel, C. *et al*. (2008) Cooperativity in Adhesion Cluster Formation during Initial Cell Adhesion. *Biophys. J.* 95, 5424-5431

98 Gallant, N.D. and Garcia, A.J. (2007) Model of integrin-mediated cell adhesion strengthening. *J. Biomech.* 40, 1301-1309

99 Moursi, A.M. *et al*. (1996) Fibronectin regulates calvarial osteoblast differentiation. *J Cell Sci* 109, 1369-1380

100 Weiss, R.E. and Reddi, A.H. (1981) Role of fibronectin in collagenous matrix-induced mesenchymal cell proliferation and differentiation in vivo. *Exp Cell Res* 133, 247-254

101 Athanassiou, G. and Deligianni, D. (2001) Adhesion strength of individual human bone marrow cells to fibronectin. Integrin beta1-mediated adhesion. *J. Mater. Sci. Mater. Med.* 12, 965-970

102 Kong, H.J. *et al*. (2005) FRET measurements of cell-traction forces and nano-scale clustering of adhesion ligands varied by substrate stiffness. *Proc. Natl. Acad. Sci. U. S. A.* 102, 4300-4305

103 McBeath, R. *et al*. (2004) Cell shape, cytoskeletal tension, and RhoA regulate stem cell lineage commitment. *Dev. Cell.* 6, 483-495

104 Wang, N. *et al*. (2002) Micropatterning tractional forces in living cells. *Cell Motil Cytoskeleton* 52, 97-106

105 Parker, K.K. *et al*. (2002) Directional control of lamellipodia extension by constraining cell shape and orienting cell tractional forces. *Faseb Journal* 16, 1195-204

106 Chen, C.S. *et al*. (2003) Cell shape provides global control of focal adhesion assembly. *Biochem Biophys Res Commun* 307, 355-361

107 Burridge, K. and Wennerberg, K. (2004) Rho and Rac take center stage. *Cell* 116, 167-179

108 Toksoz, D. and Merdek, K.D. (2002) The Rho small GTPase: functions in health and disease. *Histol. Histopathol.* 17, 915-927

109 Kjoller, L. and Hall, A. (1999) Signaling to Rho GTPases. *Exp. Cell Res.* 253, 166-179

110 Ren, X.D. *et al*. (2000) Focal adhesion kinase suppresses Rho activity to promote focal adhesion turnover. *J. Cell. Sci.* 113 ( Pt 20), 3673-3678

111 Heasman, S.J. and Ridley, A.J. (2008) Mammalian Rho GTPases: new insights into their functions from in vivo studies. *Nat. Rev. Mol. Cell Biol.* 9, 690-701

112 Schwartz, M.A. and Shattil, S.J. (2000) Signaling networks linking integrins and rho family GTPases. *Trends Biochem. Sci.* 25, 388-391

113 Arthur, W.T. *et al*. (2002) Regulation of Rho family GTPases by cell-cell and cell-matrix adhesion. *Biol. Res.* 35, 239-246

114 Price, L.S. *et al*. (1998) Activation of Rac and Cdc42 by integrins mediates cell spreading. *Mol. Biol. Cell* 9, 1863-1871

115 Ren, X.D. *et al*. (1999) Regulation of the small GTP-binding protein Rho by cell adhesion and the cytoskeleton. *EMBO J.* 18, 578-585

116 DeMali, K.A. *et al*. (2003) Integrin signaling to the actin cytoskeleton. *Curr Opin Cell Biol* 15, 572-582

117 Graness, A. *et al*. (2006) Differential involvement of the integrin-linked kinase (ILK) in RhoA-dependent rearrangement of F-actin fibers and induction of connective tissue growth factor (CTGF). *Cell. Signal.* 18, 433-440

118 Sotobori, T. *et al*. (2006) Bone morphogenetic protein-2 promotes the haptotactic migration of murine osteoblastic and osteosarcoma cells by enhancing incorporation of integrin beta1 into lipid rafts. *Exp. Cell Res.* 312, 3927-3938

119 Danen, E.H. *et al*. (2002) The fibronectin-binding integrins alpha5beta1 and alphavbeta3 differentially modulate RhoA-GTP loading, organization of cell matrix adhesions, and fibronectin fibrillogenesis. *J. Cell Biol.* 159, 1071-1086

120 Miao, H. *et al*. (2002) Differential regulation of Rho GTPases by beta1 and beta3 integrins: the role of an extracellular domain of integrin in intracellular signaling. *J. Cell. Sci.* 115, 2199-2206

121 Sordella, R. *et al*. (2003) Modulation of Rho GTPase signaling regulates a switch between adipogenesis and myogenesis. *Cell* 113, 147-158

122 Harb, N. *et al*. (2008) The Rho-Rock-Myosin signaling axis determines cell-cell integrity of self-renewing pluripotent stem cells. *PLoS ONE* 3, e3001

123 Wozniak, M.A. *et al*. (2003) ROCK-generated contractility regulates breast epithelial cell differentiation in response to the physical properties of a three-dimensional collagen matrix. *J. Cell Biol.* 163, 583-595

124 Harmey, D. *et al*. (2004) Regulation of osteoblast differentiation by Pasteurella multocida toxin (PMT): a role for Rho GTPase in bone formation. *J. Bone Miner. Res.* 19, 661-670

125 Woods, A. and Beier, F. (2006) RhoA/ROCK signaling regulates chondrogenesis in a context-dependent manner. *J. Biol. Chem.* 281, 13134-13140

126 Woods, A. *et al*. (2005) RhoA/ROCK signaling regulates Sox9 expression and actin organization during chondrogenesis. *J. Biol. Chem.* 280, 11626-11634

127 Kim TJ *et al*. (2008) Substrate rigidity regulates Ca(2+) oscillation via RhoA pathway in stem cells. *J Cell Physiol.* 218, 285-293

128 Tsuchiya, K. *et al*. (2004) Custom-shaping system for bone regeneration by seeding marrow stromal cells onto a web-like biodegradable hybrid sheet. *Cell Tissue Res.* 316, 141-153

129 Woo, K.M. *et al*. (2003) Nano-fibrous scaffolding architecture selectively enhances protein adsorption contributing to cell attachment. *J. Biomed. Mater. Res. A.* 67, 531-537

130 Huang, M.H. *et al*. (2004) Degradation and cell culture studies on block copolymers prepared by ring opening polymerization of epsilon-caprolactone in the presence of poly(ethylene glycol). *J. Biomed. Mater. Res. A.* 69A, 417-427

131 Tan, J. *et al*. (2005) Improved cell adhesion and proliferation on synthetic phosphonic acid-containing hydrogels. *Biomaterials* 26, 3663-3671

132 Gabriel, M. *et al*. (2006) Direct grafting of RGD-motif-containing peptide on the surface of polycaprolactone films. *J. Biomater. Sci. Polym. Ed.* 17, 567-577

133 Kim, C.H. *et al*. (2006) An improved hydrophilicity via electrospinning for enhanced cell attachment and proliferation. *J. Biomed. Mater. Res. B. Appl. Biomater.* 78, 283-290

134 Wang, D.A. *et al*. (2005) Bioresponsive phosphoester hydrogels for bone tissue engineering. *Tissue Eng.* 11, 201-213

135 Siebers, M.C. *et al*. (2005) Integrins as linker proteins between osteoblasts and bone replacing materials. A critical review. *Biomaterials* 26, 137-146

136 Lieb, E. *et al*. (2003) Poly(D,L-lactic acid)-poly(ethylene glycol)-monomethyl ether diblock copolymers control adhesion and osteoblastic differentiation of marrow stromal cells. *Tissue Eng.* 9, 71-84

137 Gopferich, A. *et al*. (1999) Modulation of marrow stromal cell function using poly(D,L-lactic acid)-block-poly(ethylene glycol)-monomethyl ether surfaces. *J. Biomed. Mater. Res.* 46, 390-398

138 Lee, M.H. *et al*. (2007) Adhesion of MC3T3-E1 cells to RGD peptides of different flanking residues: detachment strength and correlation with long-term cellular function. *J. Biomed. Mater. Res. A.* 81, 150-160

139 Shin, H. *et al*. (2002) Modulation of marrow stromal osteoblast adhesion on biomimetic oligo[poly(ethylene glycol) fumarate] hydrogels modified with Arg-Gly-Asp peptides and a poly(ethyleneglycol) spacer. *J. Biomed. Mater. Res.* 61, 169-179

140 Alsberg, E. *et al*. (2001) Cell-interactive alginate hydrogels for bone tissue engineering. *J Dent Res* 80, 2025-2029

141 Ruiz, S.A. and Chen, C.S. (2008) Emergence of patterned stem cell differentiation within multicellular structures. *Stem Cells* 26, 2921-2927

142 Keselowsky, B.G. *et al*. (2003) Surface chemistry modulates fibronectin conformation and directs integrin binding and specificity to control cell adhesion. *J. Biomed. Mater. Res. A*. 66, 247-259

143 Salasznyk, R.M. *et al*. (2004) ERK signaling pathways regulate the osteogenic differentiation of human mesenchymal stem cells on collagen I and vitronectin. *Cell. Commun. Adhes.* 11, 137-153

144 Chastain, S.R. *et al*. (2006) Adhesion of mesenchymal stem cells to polymer scaffolds occurs via distinct ECM ligands and controls their osteogenic differentiation. *J. Biomed. Mater. Res. A.* 78, 73-85

145 Keselowsky, B.G. *et al*. (2004) Surface chemistry modulates focal adhesion composition and signaling through changes in integrin binding. *Biomaterials* 25, 5947-5954

146 Garcia, A.J. *et al*. (1998) Effect of surface reaction stage on fibronectin-mediated adhesion of osteoblast-like cells to bioactive glass. *J. Biomed. Mater. Res.* 40, 48-56

147 El-Amin, S.F. *et al*. (2002) Integrin expression by human osteoblasts cultured on degradable polymeric materials applicable for tissue engineered bone. *J Orthop Res* 20, 20-28

148 El-Amin, S.F. *et al*. (2003) Extracellular matrix production by human osteoblasts cultured on biodegradable polymers applicable for tissue engineering. *Biomaterials* 24, 1213-1221

149 El-Amin, S.F. *et al*. (2004) Molecular regulation of osteoblasts for tissue engineered bone repair. *Clin. Orthop. Relat. Res.* (427), 220-225

150 Lim, J.Y. *et al*. (2005) Integrin expression and osteopontin regulation in human fetal osteoblastic cells mediated by substratum surface characteristics. *Tissue Eng* 11, 19-29

151 Phillips, J.E. *et al*. (2006) Mineralization capacity of Runx2/Cbfa1-genetically engineered fibroblasts is scaffold dependent. *Biomaterials* 27, 5535-5545

152 Curran, J.M. *et al*. (2008) PLGA doping of PCL affects the plastic potential of human mesenchymal stem cells, both in the presence and absence of biological stimuli. *J. Biomed. Mater. Res. A. Epub*

153 Engler, A.J. *et al*. (2006) Matrix elasticity directs stem cell lineage specification. *Cell* 126, 677-689

154 Rowlands, A.S. *et al*. (2008) Directing osteogenic and myogenic differentiation of MSCs: interplay of stiffness and adhesive ligand presentation. *Am. J. Physiol. Cell. Physiol.* 295, C1037-44

155 Winer, J.P. *et al*. (2008) Bone Marrow-Derived Human Mesenchymal Stem Cells Become Quiescent on Soft Substrates but Remain Responsive to Chemical or Mechanical Stimuli. *Tissue Eng. Part A.* 15, 147-154

156 Soolaman, D.M. and Yu, H.Z. (2005) Water microdroplets on molecularly tailored surfaces: correlation between wetting hysteresis and evaporation mode switching. *J Phys Chem B* 109, 17967-17973

157 Schneider, G.B. *et al*. (2004) The effect of hydrogel charge density on cell attachment. *Biomaterials* 25, 3023-3028

158 Ciapetti, G. *et al*. (2006) Human bone marrow stromal cells: In vitro expansion and differentiation for bone engineering. *Biomaterials* 27, 6150-6160

159 Curran, J.M. *et al*. (2006) The guidance of human mesenchymal stem cell differentiation in vitro by controlled modifications to the cell substrate. *Biomaterials* 27, 4783-4793

160 Marletta, G. *et al*. (2007) Improved osteogenic differentiation of human marrow stromal cells cultured on ion-induced chemically structured poly-epsilon-caprolactone. *Biomaterials* 28, 1132-1140

161 Rohman, G. *et al*. (2007) Influence of the physical properties of two-dimensional polyester substrates on the growth of normal human urothelial and urinary smooth muscle cells in vitro. *Biomaterials* 28, 2264-2274

162 Santovena, A. *et al*. (2005) Structural properties of biodegradable polyesters and rheological behaviour of their dispersions and films. *Journal of Biomaterials Science-Polymer Edition* 16, 629-641

163 Cappella, B. and Silbernagl, D. (2008) Nanomechanical properties of polymer thin films measured by force-distance curves. *Thin Solid Films* 516, 1952-1960

164 Grinnell, F. (1986) Focal adhesion sites and the removal of substratum-bound fibronectin. *J. Cell Biol.* 103, 2697-2706

165 Garcia, A.J. *et al*. (1999) Modulation of cell proliferation and differentiation through substrate-dependent changes in fibronectin conformation. *Mol. Biol. Cell* 10, 785-798

166 Haas, R. and Culp, L.A. (1982) Properties and fate of plasma fibronectin bound to the tissue culture substratum. *J. Cell. Physiol.* 113, 289-297

167 Wilson, K. *et al*. (2004) A molecular modeling study of the effect of surface chemistry on the adsorption of a fibronectin fragment spanning the 7-10th type III repeats. *J. Biomed. Mater. Res. A.* 69, 686-698

168 Keselowsky, B.G. *et al*. (2003) Surface chemistry modulates fibronectin conformation and directs integrin binding and specificity to control cell adhesion. *J. Biomed. Mater. Res. A*. 66, 247-259

169 Garcia, A.J. *et al*. (1998) Two-stage activation for alpha5beta1 integrin binding to surface-adsorbed fibronectin. *J. Biol. Chem.* 273, 34710-34715

170 Woo, K.M. *et al*. (2007) Suppression of apoptosis by enhanced protein adsorption on polymer/hydroxyapatite composite scaffolds. *Biomaterials* 28, 2622-2630

171 Woods, A. *et al*. (1983) Stages in specialization of fibroblast adhesion and deposition of extracellular matrix. *Eur. J. Cell Biol.* 32, 108-116

172 Sugawara, Y. *et al*. (2008) The alteration of a mechanical property of bone cells during the process of changing from osteoblasts to osteocytes. *Bone* 43, 19-24

173 Kim, M.S. *et al*. (2007) Adhesion behavior of human bone marrow stromal cells on differentially wettable polymer surfaces. *Tissue Eng.* 13, 2095-2103

174 Dos Santos, E.A. *et al*. (2008) Chemical and topographical influence of hydroxyapatite and beta-tricalcium phosphate surfaces on human osteoblastic cell behavior. *J. Biomed. Mater. Res. A, Epub*

175 Leonova, E.V. *et al*. (2006) Substrate mineralization stimulates focal adhesion contact redistribution and cell motility of bone marrow stromal cells. *J. Biomed. Mater. Res. A.* 79, 263-270

176 Barrias, C.C. *et al*. (2009) The correlation between the adsorption of adhesive proteins and cell behaviour on hydroxyl-methyl mixed self-assembled monolayers. *Biomaterials* 30, 307-316

177 Shi, Q. and Boettiger, D. (2003) A novel mode for integrin-mediated signaling: tethering is required for phosphorylation of FAK Y397. *Mol. Biol. Cell* 14, 4306-4315

178 Salasznyk, R.M. *et al*. (2007) Focal adhesion kinase signaling pathways regulate the osteogenic differentiation of human mesenchymal stem cells. *Exp. Cell Res.* 313, 22-37

179 Chiellini, C. *et al*. (2008) Stathmin-like 2, a developmentally-associated neuronal marker, is expressed and modulated during osteogenesis of human mesenchymal stem cells. *Biochem. Biophys. Res. Commun.* 374, 64-68

180 Kundu, A.K. and Putnam, A.J. (2006) Vitronectin and collagen I differentially regulate osteogenesis in mesenchymal stem cells. *Biochem. Biophys. Res. Commun.* 347, 347-357

181 Hu, J. *et al*. (2008) Induction of osteoblast differentiation phenotype on poly(L-lactic acid) nanofibrous matrix. *Biomaterials* 29, 3815-3821

182 Wang, G. *et al*. (2004) RhoA/ROCK signaling suppresses hypertrophic chondrocyte differentiation. *J. Biol. Chem.* 279, 13205-13214

183 Ishizaki, T. *et al*. (2000) Pharmacological properties of Y-27632, a specific inhibitor of rho-associated kinases. *Mol. Pharmacol.* 57, 976-983

184 Richardson, A. and Parsons, T. (1996) A mechanism for regulation of the adhesion-associated proteintyrosine kinase pp125FAK. *Nature* 380, 538-540

185 Gallant, N.D. *et al*. (2005) Cell adhesion strengthening: contributions of adhesive area, integrin binding, and focal adhesion assembly. *Mol. Biol. Cell* 16, 4329-4340

186 Baksh, D. *et al*. (2007) Cross-talk between Wnt signaling pathways in human mesenchymal stem cells leads to functional antagonism during osteogenic differentiation. *J. Cell. Biochem.* 101, 1109-1124

187 Chang, F. *et al*. (2007) FAK potentiates Rac1 activation and localization to matrix adhesion sites: a role for betaPIX. *Mol. Biol. Cell* 18, 253-264

188 Zhou, H.Y. (2007) Proteomic analysis of hydroxyapatite interaction proteins in bone. *Ann. N. Y. Acad. Sci.* 1116, 323-326

189 Wendel, M. *et al*. (1998) Bone matrix proteins: isolation and characterization of a novel cell-binding keratan sulfate proteoglycan (osteoadherin) from bovine bone. *J. Cell Biol.* 141, 839-847

190 Hamidouche, Z. *et al*. (2008) FHL2 mediates dexamethasone-induced mesenchymal cell differentiation into osteoblasts by activating Wnt/beta-catenin signaling-dependent Runx2 expression. *FASEB J.* 22, 3813-3822

191 Park, J. *et al*. (2008) Deficiency in the LIM-only protein FHL2 impairs assembly of extracellular matrix proteins. *FASEB J.* 22, 2508-2520

192 Lai, C.F. *et al*. (2006) Four and half lim protein 2 (FHL2) stimulates osteoblast differentiation. *J. Bone Miner. Res.* 21, 17-28

193 Kundu, A.K. *et al*. (2008) Extracellular Matrix Remodeling, Integrin Expression, and Downstream Signaling Pathways Influence the Osteogenic Differentiation of Mesenchymal Stem Cells on Poly(Lactide-Co-Glycolide) Substrates. *Tissue Eng. Part A*, Epub

194 Nagamatsu, Y. *et al*. (2008) Roles of Necl-5/poliovirus receptor and Rho-associated kinase (ROCK) in the regulation of transformation of integrin alpha(V)beta(3)-based focal complexes into focal adhesions. *J. Biol. Chem.* 283, 14532-14541

195 Endlich, N. *et al*. (2007) Movement of stress fibers away from focal adhesions identifies focal adhesions as sites of stress fiber assembly in stationary cells. *Cell Motil. Cytoskeleton* 64, 966-976

196 Katoh, K. *et al*. (2007) Rho-kinase dependent organization of stress fibers and focal adhesions in cultured fibroblasts. *Genes Cells* 12, 623-638

197 Friedman, M.S. *et al*. (2006) Osteogenic differentiation of human mesenchymal stem cells is regulated by bone morphogenetic protein-6. *J. Cell. Biochem.* 98, 538-554

198 Macpherson, P.C. *et al*. (2004) Activity-dependent gene regulation in conditionally-immortalized muscle precursor cell lines. *J. Cell. Biochem.* 91, 821-839

199 Calvert, J.W. *et al*. (2000) Characterization of osteoblast-like behavior of cultured bone marrow stromal cells on various polymer surfaces. *J. Biomed. Mater. Res.* 52, 279-284

200 Hosoya, K. *et al*. (2004) A novel covalently crosslinked gel of alginate and silane with the ability to form bone-like apatite. *J Biomed Mater Res A* 71, 596-601

201 Garcia, A.J. *et al*. (1997) Quantification of cell adhesion using a spinning disc device and application to surface-reactive materials. *Biomaterials* 18, 1091-1098

202 Pfaffl, M.W. (2001) A new mathematical model for relative quantification in real-time RT-PCR. *Nucleic Acids Res.* 29, e45

203 Tichopad, A. *et al*. (2003) Standardized determination of real-time PCR efficiency from a single reaction set-up. *Nucleic Acids Res.* 31, e122

204 Quissell, D.O. *et al.* (1986) Short-term primary culture of acinar-intercalated duct complexes from rat submandibular glands. *In Vitro Cell Dev Biol*. 22, 469-480